Office of Naval Research

Contract N00014-67-A-0298-0020

NR-031-732

A SECOND REPORT ON DEFORMATION MECHANISM MAPS

By

H. J. Frost and M. F. Ashby

Final Report

August 1973

The research reported in this document was made possible through support extended the Division of Engineering and Applied Physics, Harvard University, by the Office of Naval Research, under Contract N00014-67-A-0298-0020.

Division of Engineering and Applied Physics

Harvard University · Cambridge, Massachusetts

Unclassified
Security Classification

AD-769821

DOCUMENT CONTROL DATA - R & D

(Security classification of title, body of abstract and indexing annotation must be entered when the overall report is classified)

1. ORIGINATING ACTIVITY (Corporate author)
Division of Engineering and Applied Physics
Harvard University
Cambridge, Massachusetts 02138

2a. REPORT SECURITY CLASSIFICATION
Unclassified

2b. GROUP

3. REPORT TITLE
A SECOND REPORT ON DEFORMATION MECHANISM MAPS

4. DESCRIPTIVE NOTES (Type of report and, inclusive dates)
Final Report

5. AUTHOR(S) (First name, middle initial, last name)
H. J. Frost
M. F. Ashby

6. REPORT DATE	7a. TOTAL NO. OF PAGES	7b. NO. OF REFS
August 1973	113	88

8a. CONTRACT OR GRANT NO.	9a. ORIGINATOR'S REPORT NUMBER(S)
N00014-67-A-0298-0020 b. PROJECT NO. NR-031-732 c. d.	Final Report 9b. OTHER REPORT NO(S) (Any other numbers that may be assigned this report)

10. DISTRIBUTION STATEMENT
This document has been approved for public release and sale; its distribution is unlimited. Reproduction in whole or in part is permitted by the U. S. Government.

11. SUPPLEMENTARY NOTES	12. SPONSORING MILITARY ACTIVITY
	Office of Naval Research

13. ABSTRACT

A crystalline solid can deform plastically in a number of ways. Deformation mechanism diagrams can be constructed which show the fields of stress and temperature in which a given mechanism is dominant and the strain-rate that it yields. This second report presents detailed maps for five pure f. c. c. metals (Ni, Cu, Ag, Al and Pb), six pure b. c. c. metals (V, Cr, Nb, Mo, Ta and W) and a recrystallized Ni – 1 vol% ThO_2 alloy, which are based on direct comparison to available experimental data. It also presents further discussion of the various deformation mechanisms, with refinements of their rate equations.

Various applications of the diagrams are illustrated. They provide a convenient means for the normalized comparison of the behavior of different metals. They also demonstrate the effects of various changes in materials in a manner useful for qualitative engineering design.

DD FORM 1 NOV 65 1473 (PAGE 1)
S/N 0102-014-6700

Unclassified
Security Classification

D-23822

14. KEY WORDS	LINK A		LINK B		LINK C	
	ROLE	WT	ROLE	WT	ROLE	WT
Deformation Mechanism Maps						
Dislocation Glide						
Creep						
Diffusional Flow						
Rate-Equations for Plastic Flow						
Plastic Properties of Metals						

ERRATA:

Title should read as follows:

A SECOND REPORT ON DEFORMATION MECHANISM MAPS

A SECOND REPORT ON DEFORMATION MECHANICS MAPS

By

H. J. Frost and M. F. Ashby*

Division of Engineering and Applied Physics

Harvard University, Cambridge, Massachusetts

ABSTRACT

A crystalline solid can deform plastically in a number of ways. Deformation mechanism diagrams can be constructed which show the fields of stress and temperature in which a given mechanism is dominant and the strain-rate that it yields. This second report presents detailed maps for five pure f. c. c. metals (Ni, Cu, Ag, Al and Pb), six pure b. c. c. metals (V, Cr, Nb, Mo, Ta and W) and a recrystallized Ni – 1 vol% ThO_2 alloy, which are based on direct comparison to available experimental data. It also present further discussion of the various deformation mechanisms, with refinements of their rate equations.

Various applications of the diagrams are illustrated. They provide a convenient means for the normalized comparison of the behavior of different metals. They also demonstrate the effects of various changes in materials in a manner useful for qualitative engineering design.

*University Engineering Laboratories, The University of Cambridge, Cambridge, England

V

A SECOND REPORT ON DEFORMATION MECHANISM MAPS

I. INTRODUCTION

Plastic flow is a *kinetic process*. Although it is often convenient to think of a solid as having a well defined yield stress, below which it does not flow, this is inaccurate. Above absolute zero, any stress will cause a polycrystalline solid to flow — although the *rate* at which it does so may be indetectably small on the time scale of a laboratory experiment or an engineering application. This rate depends on the *mechanisms of flow*. A polycrystal may deform plastically by one, or a combination of, the following *atomistic processes*: defect-less shear of atom layers, dislocation glide, dislocation climb, diffusive flow of individual atoms, displacement of grains by grain boundary sliding, and mechanical twinning. It is the kinetics of these processes that determine the rate of flow.

Although these are the only atomistic processes available, it is more convenient to describe the plastic behavior in terms of mechanisms which describe the different manners in which the atomistic processes may operate. We therefore consider the following *deformation mechanisms*, divided into five groups:

1) *Defect-less flow* (flow when the ideal shear strength is exceeded).
2) *Flow by dislocation glide alone.*
    a) Limited by a lattice resistance (Peierls stress).
    b) Limited by discrete obstacles.
    c) Limited by phonon or other drag.

3) *Twinning.*

4) *Flow involving dislocation climb.*

   a) Glide plus lattice-diffusion controlled climb ("High temperature creep")

   b) Glide plus core-diffusion controlled climb ("Low temperature creep")

   c) Harper-Dorn creep.

   d) Power-law breakdown.

5) *Diffusional flow* (involving the motion of single ions only).

   a) Lattice-diffusion controlled flow (Nabarro-Herring creep).

   b) Grain-boundary-diffusion controlled flow (Coble creep).

   c) Interface-reaction controlled diffusional flow.

Certain *other mechanisms* (e.g. superplastic flow) may exist, but are insufficiently well understood to include them in the calculations presented below. Equally important are a number of *coupled mechanisms* (e.g. grain boundary sliding accommodated by dislocation creep).

For each mechanism a *rate-equation* exists. In its simplest form, this is an equation linking shear-strain rate ($\dot{\gamma}$) to the shear stress (σ), temperature (T) and to structure:

$$\dot{\gamma} = \dot{\gamma} \ (\sigma, \ T, \ \text{structure})$$

or, more generally

$$\dot{\varepsilon}_{ij} = \dot{\varepsilon}(\sigma_{ij}, \ T, \ \text{structure})$$

(where $\dot{\varepsilon}_{ij}$ is the strain rate tensor, and σ_{ij} the stress tensor). "Structure" includes all the internal characteristics of the deforming polycrystal;

first, its atomic structure: the crystal class and type of bonding; and second, its defect structure: grain size, solute or precipitate concentration, dislocation density and arrangement, and so on. In more complete form, the rate-equation mechanism may be described by a set of coupled differential equations that explicitly consider the time dependent changes in a number of structural parameters, S_1, S_2, S_3, etc:

$$\begin{aligned} \dot{\varepsilon}_{ij} &= f(\sigma_{ij}, T, S_1, S_2, S_3 \ldots) \\ dS_1 &= f_1(\sigma_{ij}, T, S_1, S_2, S_3 \ldots) \\ dS_2 &= f_2(\sigma_{ij}, T, S_1, S_2, S_3 \ldots)dt \end{aligned} \tag{2}$$

where dt is an increment of time.

In order to conveniently present the relation between $\dot{\gamma}$, T and σ in three dimensions, it is necessary to make certain assumptions about the internal structure. Two formulations may be used to simplify the internal structure dependence. The first assumes *steady-state* flow. In this case the internal variables of dislocation density and arrangement no longer appear explicitly in the rate-equations because they are uniquely determined by the external variables of stress and temperature. This is the condition that $0 = dS_1 = dS_2 = dS_3$ etc., and it implies that we can solve for S_1, S_2, etc. in terms of σ and T. The second formulation assumes *constant internal structure*, particularly dislocation structure. This case can be used to

represent the strain-rate and temperature dependence of the flow stress for a given initial internal structure. It requires that the parameters S_1, S_2, S_3 . . . be known or specified. High temperature deformation is usually described by the steady-state formulation. Low temperature deformation is commonly characterized by constant structure yield stress. In fact, a steady-state deformation is rarely measured at low temperatures because of work-hardening effects. We have attempted to use the steady-state formulation as far as possible, but have been forced to use a constant structure formulation for the dislocation glide mechanisms which dominate at low temperatures: the equation describes the yield stress at a given structure, not the steady-state flow stress.

This rather complicated behavior can be presented on a map with axes of stress and temperature. The map is divided into fields which indicate regions of stress and temperature where each of the various mechanisms are dominant, as shown in Fig. 1 (maps for pure nickel of grain size 1mm and 10μm). Superimposed on the fields are contours of constant strain-rate: these show the net strain-rate (due to appropriate superposition of all the mechanisms) that a given combination of stress and temperature will produce. The map depicts the relationship between three variables: stress, temperature, and strain-rate. If any two of these variables are specified, the map can be used to determine the third. There are, of course, other methods of presenting this relationship. Fig. 2 is a plot for nickel (grain size = 0.1mm), showing various con-

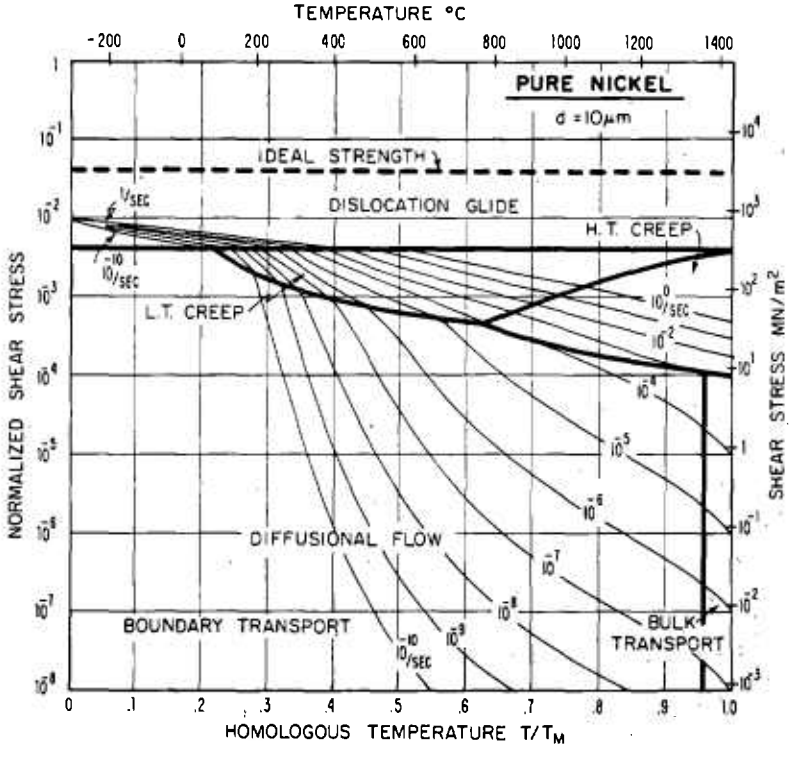

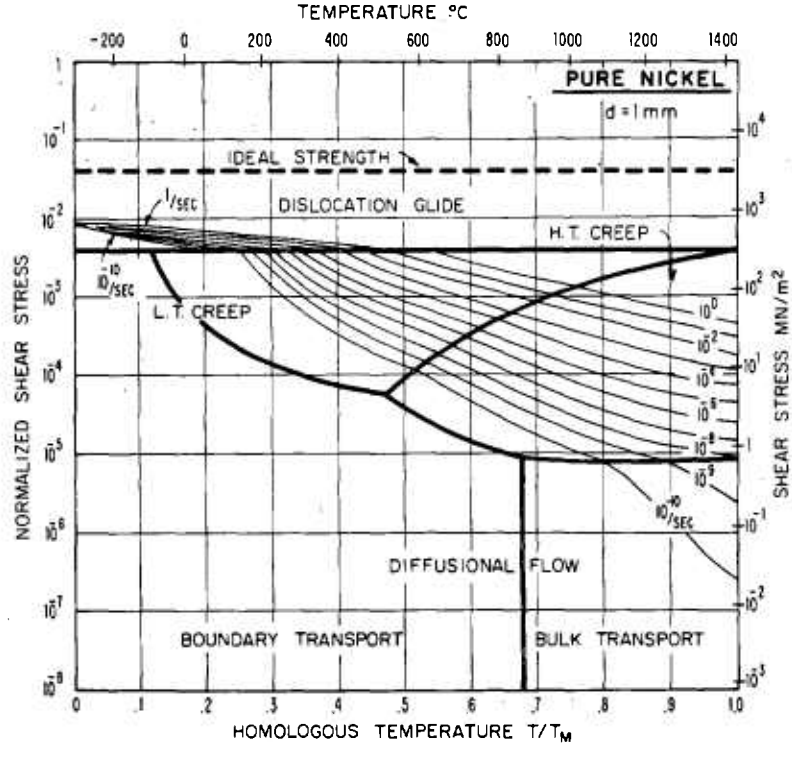

Fig. 1) Deformation maps for pure nickel of grain size 10μm and 1mm.

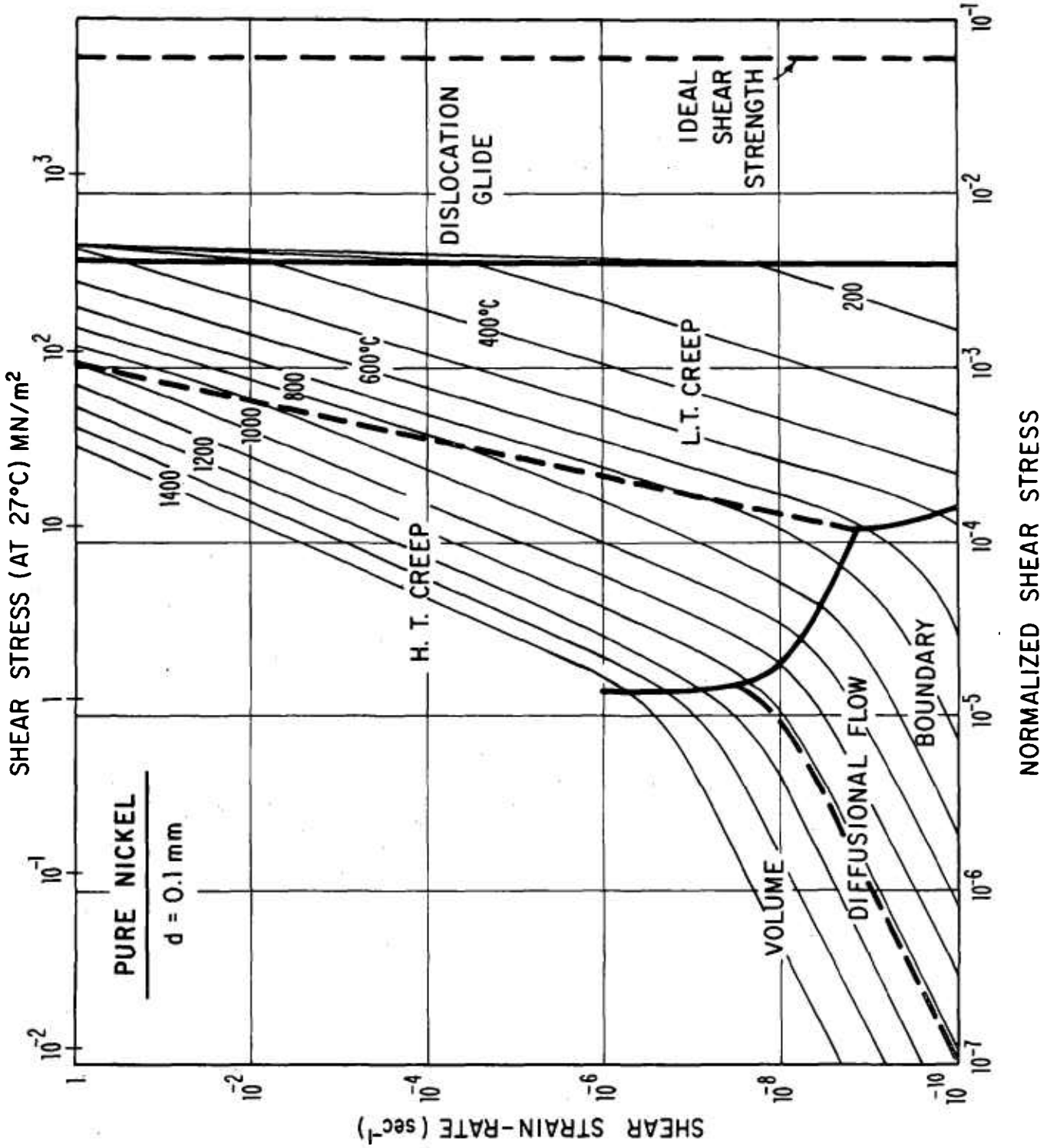

Fig. 2) Deformation map for pure nickel of grain size 0.1mm, showing contours of constant temperature on axes of stress versus strain-rate.

tours of constant temperature on axes of strain-rate versus normalized shear stress, showing the same mechanism fields. This type of plot is useful for comparisons to isothermal tests. A third type of plot showing various contours of constant stress (or constant normalized stress) on axes of strain-rate versus temperature (or reciprocal temperature) can be used for comparison to tests at constant stress. This third type is not shown in this paper.

Such maps are constructed from the rate-equations. In doing so, one has to make assumptions about the way in which the mechanisms superimpose. The simplest supposition is that the five classes of mechanisms operate independently so that the strain-rates produced by each add to give the total resultant strain-rate: the *dominant* mechanism is the one which contributes most to this total. Although this is a gross oversimplification, it works surprisingly well — because at any given point on the diagram one mechanism usually dominates overwhelmingly. Nevertheless, in constructing the maps shown here, we have used a somewhat more sophisticated set of assumptions which we discuss in section 2.

Once the rate-equations and method of superposition are specified, the maps can be constructed most easily by numerical computation. This paper reports further progress in developing the maps, presenting them for five f.c.c. and six b.c.c. metals. The principal differences between

this and our first report (Ashby, 1972a) are:

a) A change from *tensile* strain-rate and stress to equivalent *shear* strain-rate and stress. The equivalent shear stress is defined as:

$$\bar{\sigma}_s = (\tfrac{1}{2} S_{ij} S_{ij})^{1/2}$$

where

$$S_{ij} = \sigma_{ij} - \frac{1}{3} \delta_{ij} \sigma_{kk}$$

and the equivalent shear strain-rate as:

$$\dot{\bar{\gamma}} = (2\dot{\varepsilon}_{ij} \dot{\varepsilon}_{ij})^{1/2}$$

These values are equal to the simple shear stress or strain-rate, and are related to the tensile stress, σ_{11}, and tensile strain-rate, $\dot{\varepsilon}_{11}$, as

$$\bar{\sigma}_s = \frac{\sigma_{11}}{\sqrt{3}} ; \qquad \dot{\bar{\gamma}} = \sqrt{3}\, \dot{\varepsilon}_{11} .$$

b) The introduction of new or improved rate-equations. One of these appears as a field on all the maps shown here: it is a core-diffusion controlled creep mechanism ("Low temperature creep").

c) An improved computational method.

d) A much more thorough selection and optimization of the data used to construct the maps.

In spite of these improvements, one must be careful not to attribute too much precision to the diagrams. Although they are the best we can do at present, they are far from perfect or complete. *Both the equations in the following sections, and the maps constructed from them, must be regarded as a first approximation only.*

2. RATE-EQUATIONS

In this section we list, with a brief explanation, the equations used to construct the maps. These equations differ in detail from those of our earlier report. The approach we have used is to select an equation which is based on a physically sound microscopic model, or family of models. Frequently this leads to a rate-equation containing one or more coefficients or exponents for which only *bounds* are known; the model is too imprecise, or the family of models too broad, to predict exact values. Theory gives the form of the equation; we have to resort to experimental data to set the constants which enter it. This approach of "model inspired phenomenology" is a powerful one in dealing with phenomena too complicated to model exactly. In particular, an equation obtained in this way can be used to extrapolate outside the range for which data is available; a purely

empirical equation cannot.

In accordance with this approach we have set our accuracy aims in line with the general accuracy of experiments, which is generally about $\pm$ 10% for yield stress: the error being somewhat greater for strain-rate at a given stress and temperature. Thus, for example, we have not considered the temperature dependence of the atomic volume or Burgers' vector, but have considered the temperature dependence of the shear modulus.

The symbols which appear in the rate-equations have the following meaning:

$\dot{\gamma}$	Shear strain-rate
σ, σ_s	Shear stress
T	Absolute temperature
k	Boltzmann's constant
Ω	Atomic or molecular volume
b	Burgers' vector
T_M	Absolute melting temperature
μ	An appropriate, temperature dependent, shear modulus
D_v	Lattice-diffusion coefficient
D_B	Grain-boundary diffusion coefficient
D_c	Dislocation-core-diffusion coefficient
δ	Thickness of the high-diffusivity boundary path
a_c	Area of the high-diffusivity core path
n	A dimensionless constant
A_1, A_2	Dimensionless constants for dislocation creep
τ_{TH}	Ideal shear strength

$\hat{\tau}_p$	Peierls stress at 0°K
$\hat{\tau}$	Flow stress for obstacle cutting in absence of thermal activation
ν	Debye frequency (taken as 10^{12}/sec)
$\dot{\gamma}_p, \dot{\gamma}_0$	Constants with the dimensions of strain-rate
$\Delta F_k, \Delta F$	Helmholtz free-energies of activation for kink-pair formation, and for obstacle cutting respectively
d	Grain size
ρ	Dislocation density
ρ_m	Mobile dislocation density
α, β, p, q	Dimensionless constants for dislocation glide
ℓ	Obstacle spacing
β', α'	Dimensionless constants for power-law breakdown

2.1 Defect-less Flow

The *ideal shear strength* defines a stress level above which flow of a defect-free crystal (or of one in which all defects are pinned) becomes catastrophic: the structure becomes mechanically unstable. Simple interatomic force models can be used to compute this onset of this instability (Tyson, 1966; Kelly, 1966) and hence the ideal strength at 0°K, which we call τ_{TH}. Above 0°K the problem is a kinetic one: with what frequency do stable dislocation loops appear in an initially defect-free crystal? In this paper, we have not solved this kinetic problem; the temperature dependence of the ideal shear strength is assumed to be the same as the

shear modulus. We have used the same equation that was used earlier:

$$\dot{\gamma} = \infty \quad \text{when } \sigma \geq \tau_{TH}$$

$$\dot{\gamma} = 0 \text{ when } \sigma < \tau_{TH} \tag{3}$$

There have been several theoretical calculations of τ_{TH}, generally yielding $\mu/20$ to $\mu/10$. The exact value is expected to depend on the crystal structure. For f.c.c. metals we have used $\tau_{TH} = 0.0606$, taken from the computer calculations of Tyson (1966) based on a Lennard-Jones interatomic potential. For b.c.c. metals we have used $\tau_{TH} = 0.11$, taken from an analytical calculation of MacKenzie (1949).

2.2 Dislocation Glide

Below the ideal shear strength, flow by the *conservative motion of dislocations* is possible — provided (since we are here concerned with polycrystals) an adequate number of independent slip systems are available. This motion is almost always *obstacle-limited*: it is the interaction of mobile dislocations with other dislocations, with solute or precipitates, with grain boundaries, or with the lattice itself which determines the rate of flow.

Dislocation glide is responsible for the yielding of most laboratory and engineering materials. The yield-strength of many polycrystalline materials does not depend strongly on the rate of straining — a fact which

has lead to models for yielding which ignore the effect of strain-rate (and of temperature) entirely. This is misleading: dislocation glide is a kinetic process. A density ρ_m of mobile dislocations, moving through a field of obstacles with an average velocity $\bar{v}$ (determined almost entirely by their waiting time at obstacles) produces a strain-rate

$$\dot{\gamma} = \rho_m b \bar{v} \tag{4}$$

At steady-state, ρ_m is a function of stress and temperature only. The simplest function, and one broadly consistent with both theory (Argon, 1970) and experiment is

$$\rho_m = \alpha \left(\frac{\sigma}{\mu b}\right)^2 \tag{5}$$

where α is a constant of order unity. Then

$$\dot{\gamma} = \frac{\alpha}{b} \left(\frac{\sigma}{\mu}\right)^2 v \tag{6}$$

The kinetic problem is to calculate v. In the most interesting range of stress, it is determined by the rate at which a dislocation segment is thermally activated through, or round obstacles. (Above a sufficiently high stress — the "mechanical flow stress", $\hat{\tau}$ — the segment can overcome an average obstacle without any help from thermal energy. Its velocity is then determined by energy-dissipating processes such as phonon drag).

In developing rate-equations for v (for reviews see Evans and Rawlings, 1969; Kocks et al, 1974; de Meester et al, 1973) one immediately encounters a difficulty: the velocity is always an exponential function of stress, but the details of the expression depend on the shape and nature of the obstacles, their density, and the statistics of their distribution. There are as many rate-equations as there are obstacle types. On closer examination, obstacle types fall into three broad classes: discrete, point-like obstacles which can be cut or surrounded by a moving dislocation; and extended, or diffuse obstacles such as a concentrated solid solution. Rate-equations for obstacles of one class differ in details, but have certain features in common. Our approach here has been to select the rate-equation which most nearly describes all classes of obstacles, and to treat certain of the parameters which appear in it as adjustable, to be matched with experiment. This approach utilizes the most that model-based theory has to offer, while still ensuring an accurate description of experimental data.

2.2a Glide limited by discrete obstacles

If the Gibbs free-energy of activation for the cutting or by-passing of an obstacle is $G(\sigma)$, the velocity of a dislocation segment, v, is given by (see reviews listed above):

$$v = \beta b \nu \exp - \frac{\Delta G(\sigma)}{kT} \qquad (7)$$

where β is a dimensionless constant. $\Delta G(\sigma)$ depends on the distribution

and shape of obstacles. ("Shape" refers to the distribution of internal stress which characterizes an obstacle). A regular array of box shaped obstacles (each one viewed as a circular patch of constant, adverse, internal stress) leads to the simple result:

$$\Delta G(\sigma) = \Delta F(1 - \frac{\sigma}{\hat{\tau}})$$

where ΔF is the total free energy required to overcome the obstacle without aid from external stress. $\hat{\tau}$ is the stress which reduces ΔG to zero: roughly, the flow stress at 0°K times a factor to account for modulus temperature dependence.

But obstacles are seldom box shaped and regularly spaced. If other obstacle shapes are considered, or allowance for a random, rather than a regular distribution, all the results can be described in the general equation (Kocks et al, 1974):

$$\Delta G(\sigma) = \Delta F[1 - (\frac{\sigma}{\hat{\tau}})^p]^q \qquad (8)$$

The quantities, p, q and ΔF are bounded: all logical models lead to values of:

$$0 \leq p \leq 1$$

$$1 \leq q \leq 2.$$

The choice of p and q will influence the exact shape of the strain-rate contours. For the case of pure f.c.c. metals, however, the influence is not great; it would not appear on maps of the scale presented here. We

have therefore used the box shaped obstacle, with the rate-equation:

$$\dot{\gamma}_2 = \dot{\gamma}_0 \exp\left[-\frac{\Delta F}{kT}\left(1 - \frac{\sigma}{\hat{\tau}}\right)\right]. \tag{9}$$

For the pre-exponential,

$$\dot{\gamma}_0 = \frac{\alpha}{b}\left(\frac{\tau}{\mu}\right)^2 \beta b \nu, \tag{10}$$

we have used $\dot{\gamma}_0 = 10^6/\text{sec}$. Neglecting the pre-exponential stress dependence also has little effect on the f.c.c. maps.

The strain-rate does depend sensitively on ΔF and $\hat{\tau}$. The value of ΔF depends on the strength of the obstacles, which may be classed as follows:

Obstacle strength	ΔF	Example
Weak	$< 0.2\mu b^3$	Isolated solute atoms; Peierls barriers.
Medium	$\approx 0.5\mu b^3$	Forest dislocations; Radiation damage.
Strong	$> \mu b^3$	Dispersions; Most precipitates.

For pure f.c.c. metals in a work-hardened state, the important obstacles are forest dislocations. Accordingly we have used $\Delta F = 0.5\mu b^3$ for all the f.c.c. maps.

The value of $\hat{\tau}$ is the flow stress in the absence of thermal activation. For localized obstacles it is proportional to $\frac{\mu b}{\ell}$ where ℓ is the obstacle spacing. The constant of proportionality is complicated, depending on the strength of the obstacles and on the statistics of their distributions. We have simply used $\hat{\tau} = \frac{\mu b}{\ell}$. This can also be expressed in terms of the dislocation density, ρ, as $\hat{\tau} = \mu b\sqrt{\rho}$. In the maps presented here, we have specified ℓ, thereby specifying the degree of work-hardening.

2.2b Glide limited by lattice friction

The velocity of a dislocation in most polycrystalline solids* is limited by an additional sort of barrier: that due to its interaction with the atomic structure itself. This *Peierls resistance* or *lattice resistance* reflects the fact that the energy of the dislocation fluctuates with position with an amplitude and wavelength dictated by the nature of the interatomic or intermolecular bonding, and the lattice parameter. The crystal lattice presents an array of infinitely long straight barriers to the motion of the dislocation; it advances by throwing forward (with help from the applied stress and thermal energy) kink pairs, which subsequently spread apart. (For a review, see Guyot and Dorn, 1967).

It is usually the nucleation-rate of kink-pairs which limits dislocation velocity. The Gibbs free energy of activation for this event depends on the detailed way in which the dislocation energy fluctuates with distance,

*Examples are: elements with the diamond cubic structure, most covalent, and many ionic compounds, interstitial compounds such as carbides, borides and nitrides, some pure metals (notably those with a b.c.c. structure), alloys and intermetallic compounds, and (probably) most organic compounds.

and on the applied stress and temperature. Like those for overcoming discrete obstacles, the activation energies for all reasonable forms of energy fluctuation, and temperatures, form a family described (as before) by:

$$\Delta G(\sigma) = \Delta F_k [1 - (\frac{\sigma}{\hat{\tau}_p})^p]^q$$

where ΔF_k is the Helmholtz free energy of an isolated pair of kinks, and τ_p is, to a sufficient approximation, the flow stress at 0°K. (The equation of Guyot and Dorn, used in our earlier report* will be recognized as the special case of p = 1, q = 2). Kocks et al (1974) have reviewed various calculations for ΔG and have concluded that an adequate description of all such barriers is

$$\Delta G(\sigma) = \Delta F_k [1 - (\frac{\sigma}{\hat{\tau}_p})^{3/4}]^{4/3} \qquad (11)$$

though it should be emphasized that the result is not sensitive to small changes in exponents. Combining this with eqs. 6 and 7 leads to an optimum, model-based rate-equation for glide limited by a lattice friction:

$$\dot{\gamma}_3 = \dot{\gamma}_p (\frac{\sigma}{\mu})^2 \exp -\{ \frac{\Delta F_k}{k T} [1 - (\sigma/\tau_p)^{3/4}]^{4/3} \} \qquad (12)$$

To demonstrate that this equation is insensitive to p and q, we have calculated constant strain-rate contours for several sets of p and q, as

*This equation was misprinted as $(1 - \sigma_p/\sigma)^2$ instead of $(1 - \sigma/\sigma_p)^2$.

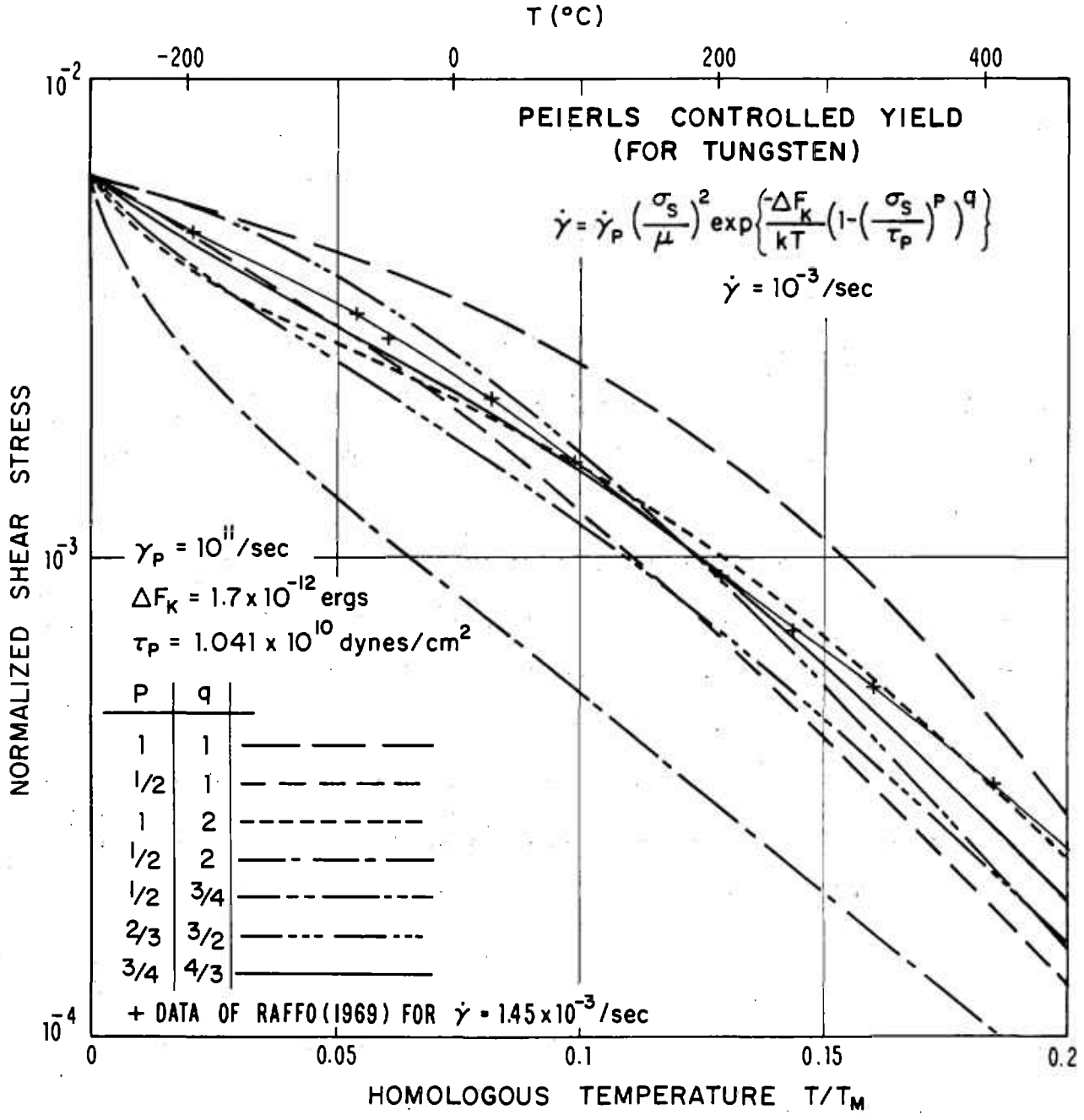

Fig. 3) Contours for $\dot{\gamma} = 10^{-4}$/sec for various formulations of the Peierls-controlled glide equation.

shown (on an expanded scale) in figure 3. Although these contours do not exactly overlap, the shapes are similar, and they could be made to overlap well if the parameters $\dot{\gamma}_p$, ΔF_k and τ_p were adjusted appropriately.

The *atomic structure* enters the equations via ΔF_k (typically 0.1 to $1\mu b^3$) and $\hat{\tau}_p$ (typically 10^{-3} to $10^{-1}\mu$), which directly reflect the nature and strength of the interatomic forces: these, too, are to be determined by fitting equation (12) to experiment. Note that the pre-exponential contains a factor of stress squared, representing the variation of mobile dislocation density with stress. This is a simplification because it neglects the way in which the steady-state kink density varies with stress, which is a complicated and only partly resolved problem (Hirth and Lothe, 1968; and Kocks et al, 1974). If experimental data were to permit it, the pre-exponential stress power should be treated as adjustable. Changing this power would not substantially change the maps shown in this paper. It would however require changing the value of $\dot{\gamma}_p$. With the stress-squared pre-exponential we have used $\dot{\gamma}_p = 10^{11}$.

It should be noted that the value of $\hat{\tau}_p$ in the rate-equation will differ by some appropriate Taylor factor between single crystal and polycrystalline samples. The proper value should depend on the crystal structure and slip systems involved. Various calculations of the Taylor factor, $\bar{M}$, have been discussed by Kocks (1970), who finds that $\bar{M} = 2.9 \pm 5\%$ is most appropriate for b.c.c. metals, converting critical resolved shear stress to tensile stress. Using our conversion to effective shear stress ($\sigma_s = \sigma_{11}/\sqrt{3}$), we have a factor of about 1.67. This factor can be directly applied to τ_p in

equation 12 to find the polycrystalline rate-equation from experimental critical resolved shear stress data.

2.2c Glide limited by phonon or other drags

Under conditions of explosive or shock loading, and in certain metal-forming operations, the strain-rate can be large ($>10^2$/sec). Then the interaction of a moving dislocation with electrons and phonons can limit its velocity. (Under special conditions — when solute atoms are mobile, for example — other drag mechanisms may become important at lower strain-rates). The strength of the interaction is measured by the *drag coefficient*, B, defined by

$$v = \frac{\sigma b}{B} \tag{13}$$

leading to the rate-equation for purely drag-limited glide:

$$\dot{\gamma} = \frac{\alpha \rho_m \mu}{B} \left(\frac{\sigma}{\mu}\right). \tag{14}$$

For pure f.c.c. metals the important drag is that due to phonons, although electron viscosity may become important at very low temperatures. B has values which typically lie between 10^{-3} and 10^{-4} dyne sec/cm^2 for most metals and ionic crystals (see Klahn et al, 1970). The value of B for phonon drag should depend on the phonon density, and should therefore be approximately linear with temperature below the Debye temperature:

$$B \approx \frac{kT}{\nu\Omega} .$$

This is found experimentally for single dislocations (e.g. Jassby and Vreeland, 1970). For the polycrystalline rate-equation the important

parameter is ρ_m/B. Experimentally, this has been found to be constant, or even increasing, with temperature (Kumar et al, 1968; Kumar and Kumble, 1969). This indicates that ρ_m increases with temperature sufficiently to offset the increase in B. The same studies found that σ increased linearly with $\dot{\gamma}$, indicating that ρ_m remains constant with respect to change of σ. (For other types of drag the usual $\rho_m \propto \sigma^2$ may be more accurate). Although there are experimental values available for ρ_m/B for some metals, we have not yet included this mechanism in our maps; it would not appear on most of the maps presented here, which show $\dot{\gamma}$ = 1/sec as the maximum strain-rate contour.

2.2d Superposition of glide-limiting processes

The rate-equations of this section describe the strain-rate when each strengthening mechanism — discrete obstacles or a lattice friction — operates alone. At the lowest level of approximation they can be treated as *alternatives*:

$$\dot{\gamma}_{Glide} = \text{Least of } \{\dot{\gamma}_2, \dot{\gamma}_3\} \tag{16}$$

This is the level of approximation adopted here. It is equivalent to assuming that the strongest obstacles control the flow stress, and is entirely adequate for our purposes.

A better approximation is to recognize that, when several strengthening mechanisms (drag, obstacles, lattice resistance)operate at once, their contributions to the flow stress superimpose in a roughly linear way. Even this is an approximation: the superposition is seldom truly linear. The

highest precision is possible only by modelling the detailed way in which a given pair of mechanisms interact (see Evans and Rawlings, 1969; Kocks et al, 1974; Frost and Ashby, 1971).

2.3 Twinning

Mechanical twinning may be an important deformation mechanism at low temperatures in h.c.p. and b.c.c. metals. It is less important in f.c.c. metals, only occuring at very low temperatures. Twinning does not appear on the maps presented here because no reliable rate-equation is available to describe it. Strictly speaking, twinning is a variety of dislocation glide which involves partial dislocations instead of complete dislocations. The kinetics of the process, however, are not identical to those of dislocation glide described in the previous section. The process involves the nucleation of twins which then grow very rapidly. If twin nucleation is the rate-controlling process, the rate-equation could be expressed as a stress assisted, thermally activated rate process:

$$\dot{\gamma} = \dot{\gamma}_t \exp\left[-\frac{\Delta G_N(\sigma,T)}{kT}\right] \approx \dot{\gamma}_t \exp\left[-\frac{\Delta F_N}{kT}\left(1 - \frac{\sigma}{\tau_t(T)}\right)\right]$$

where $\Delta G_N(\sigma,T)$ is the Gibbs free energy to nucleate a twin; ΔF_N is the free energy to nucleate a twin without the aid of external stress; $\dot{\gamma}_t$ is a constant with dimensions of strain-rate which includes the density of available nucleation sites and the strain produced per successful nucleation; and τ_t is the stress required to nucleate twinning in the absence of thermal activation. The temperature dependence of ΔG_N must be included to explain

the observation that the twinning stress may decrease with decreasing temperature (Bolling and Richman, 1965). The observation of a slight inverse strain-rate dependence of the twinning stress cannot be explained by this rate-equation.

Although we have not used a rate-equation for twinning, we have plotted a few experimental points where twinning is observed, particularly for f.c.c. metals. (All the b.c.c. metals discussed here show some twinning at low temperatures). The tendency for f.c.c. twinning increases with decreasing stacking fault energy, being a maximum in silver and not observed in aluminum. This is in accordance with a twinning mechanism involving partial dislocations.

2.4 Flow Involving Climb

Above 0.3 T_M dislocations acquire a new degree of freedom: they can *climb* as well as glide. If a gliding dislocation is held up by discrete obstacles, a little climb may release it, allowing it to glide to the next set of obstacles where the process is repeated (see, for example, the work of Weertman). The glide step in its motion is responsible for almost all the strain, although its average velocity is determined by the climb step. Mechanisms which are based on this climb-plus-glide sequence we refer to as *climb-controlled creep* (Weertman, 1963).

The important feature which distinguishes these mechanisms from those of earlier sections is that the rate-controlling process, at an atomic level, is *the diffusive motion of single ions or vacancies* to or from the climbing dislocation, rather than the activated glide of the dislocation itself.

2.4a Climb-controlled creep: Lattice and core diffusion

Above 0.6 T_M climb is generally *lattice-diffusion controlled.* The velocity v_c at which a dislocation climbs under a local normal stress σ_n is (Hirth and Lothe, 1968):

$$v_c \simeq \frac{D_v \sigma_n \Omega}{b\ kT} \tag{17}$$

We obtain the basic climb-controlled creep equation by supposing that σ_n is proportional to the applied stress σ, and the average velocity of the dislocation v is proportional to the rate at which it climbs, v_c. Then (combining eqs. 6 and 17)

$$\dot{\gamma} = A_1 \frac{D_v \mu b}{kT} \left(\frac{\sigma}{\mu}\right)^3 \tag{18}$$

where we have approximated Ω by b^3, and incorporated all the constants of proportionality into the dimensionless constant, A_1.

Some materials obey this equation: they exhibit power-law creep with a power of 3 and a constant A_1 of about unity, as we would expect (see, for example, Stocker and Ashby, 1973). But they are the exception rather than the rule. It would appear that the local normal stress, σ_n, is not necessarily proportional to σ (implying that dislocations may be moving in a cooperative manner) or that the average dislocation velocity or mobile density varies in a more complicated way than we assumed here. Over a limited range of stress, up to roughly $10^{-3}\mu$, experiments are well described by a modification of equation 18 (Mukherjee, Bird and Dorn, 1969) with an exponent, n, which varies from 3 to about 8:

$$\dot{\gamma} = A_2 \frac{D_v \mu b}{kT} \left(\frac{\sigma_s}{\mu}\right)^n \qquad (19)$$

Present theoretical models for this behavior are unsatisfactory. None can convincingly explain the observed values of n, and the large values of the dimensionless constant* A_2 (up to 10^{15}) strongly suggest that some important physical quantity is missing from the equation in its present form (Stocker and Ashby, 1973). But it *does* provide a good description of experimental observations, and in so far as it is a generalization of eq. 18, it has some basis in a physical model.

This was the only climb-creep equation incorporated into our earlier report. We have found it incapable of explaining certain experimental facts. To do so it is necessary to assume that transport of matter via *dislocation core diffusion* contributes significantly to the overall diffusive transport of matter, and — under certain circumstances — becomes the dominant transport mechanism. Robinson and Sherby (1969) have suggested, rightly, we believe, that this might explain the lower activation energy for creep at lower temperatures. We have incorporated the *contribution of core diffusion* by defining an effective diffusion coefficient (following Hart, 1957 and Robinson and Sherby, 1969):

$$D_{eff} = D_v f_v + D_c f_c$$

---

*Eq. 19 is usually written in terms of tensile stress and strain-rate. Our constant A_2 (which relates shear stress to shear strain-rate) is related to the equivalent constant A which appears in tensile forms of this equation by $A_2 = (\sqrt{3})^{n+1} A$. For further discussion see section 4.

where D_c is the core diffusion coefficient, and f_v and f_c are the fractions of atom sites associated with each type of diffusion. The value of f_v is essentially unity. The value of f_c is determined by the dislocation density, ρ, as $f_c = a_c\rho$, where a_c is the cross-sectional area of the dislocation core in which fast diffusion is taking place. Experimentally it is only possible to measure the quantity $a_c D_c$. The rather sparse measurements of it have recently been reviewed by Balluffi (1970): the diffusion enhancement varies with dislocation orientation (being perhaps 10 times larger for edges than for screws), and with the degree of dissociation and therefore the arrangement of the dislocations. Even the activation energy is not constant. In general, D_c is about equal to D_b, the grain boundary diffusion coefficient, if a_c is taken as about $5b^2$. By using the common experimental observation* that $\rho \approx \frac{10}{b^2}(\sigma/\mu)^2$ (eq. 5), our effective diffusion coefficient becomes:

$$\boxed{D_{eff} = D_v\left[1 + \frac{10a_c}{b^2}(\sigma/\mu)^2 \frac{D_c}{D_v}\right]} \qquad (20)$$

which, when inserted into eq. 19, yields the rate-equation for dislocation creep:

$$\boxed{\dot{\gamma}_4 = \frac{A_2 D_{eff}\,\mu b}{kT}(\sigma/\mu)^n} \qquad (21)$$

Equation 21 is really two rate-equations. At high temperatures and low stresses lattice diffusion is dominant; we have called the resulting field

*The observations of Vandervoort (1970), for example, indicate $\rho \approx \beta/b^2(\sigma/\mu)^2$ for tungsten in the creep regime.

high temperature creep ("H.T. creep"). At lower temperatures, or higher stresses, core diffusion becomes dominant, and the strain-rate varies as σ^{n+2} instead of σ^n; this field appears on the maps as *low temperature creep* ("L.T. creep").

2.4b Harper-Dorn creep

There is some experimental evidence that at sufficiently low stresses dislocation creep operates with $\dot{\gamma}$ linearly proportional to σ. The effect was first reported by Harper and Dorn (1957) and Harper et al (1958) in pure aluminum. For $\sigma/\mu \leq 5 \times 10^{-6}$ they found linear viscous creep at rates much higher than the diffusional creep predictions. Similar behavior has recently been found for lead and tin by Mohamed et al (1973). Some theoretical discussion of the mechanism has been summarized by Mohammed et al (1972). The most plausible mechanism is the diffusion-controlled climb of dislocations under conditions in which the dislocation density does not change with stress. Mohammed et al (1972) summarize data showing a constant low dislocation density in the Harper-Dorn range ($\rho \approx 10^4/cm^2$). Given this constant density, we may formulate a rate-equation: $\dot{\gamma} = \rho b v$, using eq. 17 for v:

$$\dot{\gamma} = \rho \frac{D_v \mu \Omega}{kT} (\sigma/\mu) \tag{22}$$

This may be expressed as:

$$\boxed{\dot{\gamma}_5 = A_{HD} \frac{D_v \mu b}{kT} (\sigma/\mu)} \tag{23}$$

with:

$$A_{HD} = \frac{\rho\,\Omega}{b} \quad . \tag{24}$$

We have included Harper-Dorn creep in our maps for aluminum and lead, using the following experimental values for A_{HD}:

Aluminum: 5×10^{-11} (Harper et al, 1958)

Lead: 1.2×10^{-9} (Mohammed et al, 1972).

These experimental values of A_{HD} agree well with our simplified theory if $\rho = 10^4 - 10^5/cm^2$. We have not used this field for other metals because of the lack of experimental verification. The field only appears when the diffusional creep fields are suppressed by the large grain size.

2.4c Power-law breakdown

At sufficiently high stresses (usually about $10^{-3}\mu$) it is observed that the simple power-law (eq. 19) breaks down; the strain-rate exceeds that of the simple power-law prediction. Part of this is explained by the low-temperature creep field where the power rises from n to (approximately) n + 2. (For a series of tests within a particular strain-rate range, those done at low temperatures will be done at higher stresses). There is, however, a more dramatic breakdown at higher stresses, both at high temperatures where the L.T. creep field is not predicted to have any effect, and at low temperatures at the high stress end of the L.T. creep

field. The process is evidently a transition from the climb-controlled power-law creep to glide-controlled flow which varies exponentially with stress. This glide behavior, however, is not identical to the low temperature glide behavior of yield because the diffusion available at elevated temperatures allows the dislocation structure to recover as rapidly as the deformation proceeds, thereby allowing steady-state deformation to be measured. It should also be noted that in many cases dynamic recrystallization has been shown to be the recover mechanism resulting in a steady-state.

Although there is no firm theoretical model for the power-law breakdown behavior, there have been various attempts to develop empirical equations. The review by Jonas, Sellars and Tegart (1969) discusses the various experimental data. The exponential dependence of strain-rate on stress provides a relationship:

$$\dot{\gamma} \propto \exp(\beta'\sigma). \tag{25}$$

Sellars and Tegart (1966) have proposed an equation to include both the low stress power-law behavior and the high stress exponential behavior:

$$\dot{\gamma} \propto A(\sinh \alpha'\sigma)^{n'} \tag{26}$$

At low stresses ($\alpha'\sigma \leq 0.8$) this reduces to:

$$\dot{\gamma} \propto A\alpha'^{n'}\sigma^{n'} .$$

At high stresses ($\alpha'\sigma \geq 1.2$) this reduces to:

$$\dot{\gamma} \propto \frac{1}{2} A \exp(n'\alpha'\sigma).$$

Equation 26 has been shown to describe deformation over a wide range of stresses (e.g. Wong and Jonas, 1968).

The temperature dependence for this rate-equation has been included as a simple activation energy:

$$\dot{\gamma} = A[\sinh\ (\alpha'\sigma)\ ]^{n'} \exp(\frac{-Q}{kT}).$$

Measured values of the apparent activation energy, Q, typically exceed that of self-diffusion, Q_v. This is taken as an indication that the recovery process is different from that of climb-controlled power-law creep. Some of the difference, however, may be accounted for by considering the temperature dependence of the shear modulus, which has greater effect when the stress dependence is greater (as in the exponential region). A closer approximation may then be found with:

$$\dot{\varepsilon} = A[\sinh\ (\frac{\alpha'\sigma}{\mu})\ ]^{n'} \exp(\frac{-Q}{kT}).$$

In order to have an exact correspondence of this equation with our power-law creep (eq. 19) we propose:

$$\boxed{\dot{\gamma}_6 = A_2' \frac{D_{eff}\mu b}{kT} [\sinh\ (\alpha'\frac{\sigma}{\mu})]^n} \qquad (27)$$

where

$$A_2'\ \alpha'^n = A_2.$$

We have, however, found some difficulty with this equation. The problem

stems from the use of only two parameters, n' and α', to describe three quantities: n' describes the low stress power-law; α prescribes the stress level at which the power-law breaks down ($\sigma \approx 1/\alpha'$); and $n'\alpha'$ describes the strength of the exponential stress dependence. Lacking any physical model, it must be considered fortuitous that any set of n' and α' can correctly describe the behavior over a wide range of stresses.

In spite of these reservations, however, we have attempted to fit this equation to hot working (power-law breakdown) data for copper and aluminum. Because we retain our fit to power-law creep, the value of n' is prescribed, and the only new adjustable parameter is α'. This will be discussed further in section 4.

2.5 Diffusional Flow

A stress can induce a *diffusional flux of matter* through, or around the surfaces of grains in a polycrystal. This trans- or circum-granular flux leads to strain, provided it is coupled with sliding displacements in the plane of the boundaries themselves. The simple models of the process (Nabarro, 1948; Herring, 1950; Coble, 1963; Lifshitz, 1963; Gibbs, 1965; Raj and Ashby, 1971) assume that it is *diffusion-controlled.* They are in substantial agreement in predicting a rate-equation: if both lattice and grain boundary diffusion are permitted, the result is:

$$\dot{\gamma}_7 = \frac{42\tau\Omega}{kTd^2} D_{eff} \tag{28}$$

where

$$D_{eff} = D_v[1 + \frac{\pi\delta}{d} \frac{D_B}{D_v}] \tag{29}$$

This was the eauation in our earlier report. Like the equation for climb-controlled creep, it is really two equations. At high temperatures *lattice diffusion* controls the rate; the resulting flow is known as Nabarro-Herring creep. At lower temperatures *grain boundary diffusion* takes over; the flow is then called Coble creep. Eq. 28 predicts Newtonian-viscous flow, at a rate which depends strongly on grain size.

This equation is an oversimplification; it neglects the kinetics involved in detaching vacancies from grain boundary sites and re-attaching them again, which may be important under certain conditions (Ashby, 1969, 1972b). Lacking a precise model at this time, we have not included this in our present maps.

3. CONSTRUCTION OF THE MAPS

Climb-controlled creep ($\dot{\gamma}_{climb}$) and diffusional flow ($\dot{\gamma}_{Diff\ flow}$) are independent flow mechanisms involving different defects. At a first approximation, their strain-rates add. Climb creep ($\dot{\gamma}_{climb}$) and glide ($\dot{\gamma}_{glide}$) do not. Both precesses involve the same defect; they describe the different behavior of dislocations under different conditions. As the stress is raised, the gliding part of the motion of a dislocation becomes more important, and the climbing part less important, until, when the boundary between the two fields is reached, climb is not necessary at all. We have solved the problem by treating dislocation creep and glide as alternative mechanisms, choosing always the faster one. This is actually a convenient method of dividing the map into two regions, one depicting

steady-state flow (dislocation creep) and one depicting constant structure yield (dislocation glide). We resort to this because our glide equations do not accurately describe steady-state flow. If we did have an accurate steady-state glide equation (containing a temperature dependent recovery term) the treatment as alternative mechanisms would still be the most accurate simple method of describing the transition from dislocation creep to glide.

The problem of the superposition of strengthening mechanisms for $\dot{\gamma}_{glide}$ (mechanisms 2 and 3) was discussed earlier: as a first approximation, the slowest one is rate-controlling. Finally, if the ideal strength is exceeded, flow becomes catastrophic ($\dot{\gamma}_1$). (We have made the special case of Harper-Dorn creep ($\dot{\gamma}_5$) an alternative mechanism to diffusional flow. This is not entirely accurate when both mechanisms give equal contributions, but is sufficiently accurate to demonstrate the new mechanism. The special case of the power-law breakdown equation ($\dot{\gamma}_6$) is used as alternative to climb-controlled creep).

In summary, the net strain-rate of a polycrystal subject to a stress σ at a temperature T is:

$$\dot{\gamma}_{net} = \dot{\gamma}_1 + \dot{\gamma}_{Diff} + \text{Greatest of } (\dot{\gamma}_{glide}, \dot{\gamma}_{climb}) \qquad (30)$$

Within a field, one contribution to this equation is larger than any other. (Remember that $\dot{\gamma}_{climb}$ and $\dot{\gamma}_{Diff\ flow}$ each describe the sum of two additive contributions). A *field boundary* is defined as the set of values of σ and T at which a switch of dominant mechanism occurs. The *contours of constant*

strain-rate are obtained by solving eq. 30 for σ as a function of T at constant $\dot{\gamma}$.

The actual construction of the maps is done by a computer program which searches incrementally over the stress-temperature field to find the strain-rate contours and field boundaries. The main program contains the search algorithm and the plotting routine. The calculations are done primarily within a subroutine that evaluates the rate-equations (for a prescribed stress and temperature), forms a sum of the contributions to the strain-rate of participating mechanisms, and identified the dominant contribution. This method provides for easy changes in rate-equations or their form of interaction. The method is also amenable to changes in the axes of the maps, such as is shown in the log $\dot{\gamma}$ versus log (σ/μ) plot in Fig.2.

4. EXPERIMENTAL CORRELATIONS

To demonstrate the use of deformation maps we have constructed maps for five common f.c.c. metals and six refractory b.c.c. metals, as shown in Figs. 4-14. The data used to construct these maps is given in Table 1. The accuracy of the maps reflects that of the experiments. Different experimenters may report strain-rates that differ by up to two orders of magnitude at a given σ and T. It is therefore necessary to make judgements, as to which experiments more accurately reflect the true material behavior. These judgements are largely subjective because of the large number of parameters involved — parameters which include purity, testing atmosphere, grain size, thermomechanical history, recrystallization effects, and type of tests.

We have characterized the behavior of pure materials. This causes some confusion because even small amounts of impurity may dramatically change the behavior. As little as 0.1% impurity has been shown to lower the creep rate of Ni by more than an order of magnitude (Dennison et al, 1966). The low temperature yield stress of b.c.c. metals is raised substantially by even smaller amounts of interstitial impurities.

One general problem in high temperature measurements is dynamic recrystallization, which may result in oscillations in strain-rate at constant stress (of an order of magnitude or more) — or oscillations in the flow stress at constant strain-rate. This behavior will cause difficulty in defining steady-state behavior. If recrystallization occurs only once during a test, it may be neglected in evaluating steady-state behavior. If the test produces repeated recrystallization, as is common in hot torsion tests taken to large strains, the successive waves of recrystallization may overlap to produce another type of steady-state behavior. Recrystallization behavior depends dramatically on purity, directly implying that the mechanical behavior depends on purity.

The maps presented in this section are constructed by direct comparison to experimental data. The experimental data is plotted on the same axes, and the parameters are adjusted until the map matches experiment (within the accuracy of experiment). Most of the adjustment involves the dislocation creep parameters, n and A. The Peierls yield parameters for the b.c.c. metals and in some cases the dislocation core diffusion coefficients, have also been adjusted. On the experimental plots shown

here, the numbers for the points represent $\log_{10}\dot{\gamma}$. Points attached by solid lines have the same strain-rate. A dashed line between points indicates a series of intermediate experimental points. Included on the plots are creep, tension, compression, torsion and extrusion tests. All are converted to shear stress for plotting. Some confusion is possible for torsion and extrusion data because the stress and strain-rate are not constant throughout the specimen; they must be derived from the tests according to some mechanical assumption. We have plotted shear stress data from torsion as reported by the experimenters. The data for single crystals is plotted as critical resolved shear stress whenever possible, and with the standard conversion from tensile to shear stress otherwise. To compare it with the polycrystal data shown on the same map, the reader must multiply the single-crystal stresses by the Taylor factor: $3.06/\sqrt{3}$ for f.c.c. and $2.9/\sqrt{3}$ for b.c.c. In arriving at the optimized data of Table 1, single-crystal data was treated in this way.

4.1 F.C.C. metals

For the common f.c.c. metals, there is extensive data on the low temperature yield and work-hardening behavior. The yield stress depends on the obstacle density (or dislocation density) and will therefore be different for different states of annealing and work-hardening. Direct comparison with experiment is therefore inappropriate. Unless otherwise noted, we have used a dislocation density of $\rho = 6.25 \times 10^{10}/cm^2$ (or an obstacle spacing of $\ell = 4 \times 10^{-6}$cm) for the f.c.c. maps. This represents a well work-hardened state, though it is not the maximum density observable and is therefore not a saturation or steady-state density. We have used $\Delta F = 0.5\mu b^3$ for the following maps, which is slightly greater than the expected proper value for forest dislocation cutting; the effect of this difference is very small on the scale of the following maps.

The elastic moduli and volume diffusion coefficients of f.c.c. metals have been well studied. For the shear modulus, μ, we have used the geometric mean of the two shear moduli of a cubic crystal:

$$\mu = \sqrt{C_{44} \cdot \frac{(C_{11} - C_{12})}{2}}$$

This is the value that enters the anisotropic calculation of the elastic energy of a $\frac{1}{2}$ <110> screw dislocation in the f.c.c. structure. We have incorporated a linear temperature dependence of the modulus — a reasonably accurate approximation. We have chosen volume diffusion coefficients which are generally intermediate among the many reported values. Modulus and diffusion coefficients are listed in Table 1.

The following is a brief summary of the experimental data used for each map:

NICKEL (Figure 4)

The high temperature creep parameters are based on Weertman and Shahinian (1956) who reported creep tests on 99.75% Ni, with n = 4.6 in the high temperature region. It has been shown, however, (Dennison et al, 1966) that small amounts of impurites (~0.1%) may lower the creep rate of nickel by up to an order of magnitude. We have therefore used an A value (3.0×10^6) almost an order of magnitude greater than would be derived from Weertman and Shahinian. This value provides a much closer correspondence to the peak flow stress in torsion data of Luton and Sellars (1969), and other various data near the H.T. creep—L.T. creep boundary. In

general, our A value for nickel is only approximate.

For low temperature creep, we have used the core diffusion coefficient given by Canon and Stark (1969) for edge dislocations in a symmetric tilt boundary. The activation energy for this (Q = 40.6 kcal/mole) matches the findings of Norman and Duran (1970) in the L.T. creep region. In addition, Norman and Duran find $n \tilde{=} 7.0$, which they believe verifies the low temperature creep field. Their strain-rates accurately match our numerical prediction (using $A = 3.0 \times 10^6$). Weertman and Shahinian also find a low temperature increase in the stress exponent, although their strain-rates are lower. We have not chosen a power-law breakdown parameter for nickel.

COPPER (Figure 5)

The primary references for the high temperature creep of copper are Feltham and Meakin (1959) and Barrett and Sherby (1964). For the low temperature creep field we have used a core diffusion activation energy of 28.0 kcal/mole. This is chosen to match the activation energy for low temperature creep found by Barrett and Sherby (1964). We have found no experimental determination of core or boundary diffusion coefficients. We have used the power-law breakdown equation for one map, using $\alpha' = 7.94 \times 10^2$. This is in general agreement with the dynamic compression data of Alder and Phillips (1954) and Samanta (1969,1971).

SILVER (Figure 6)

There has been less work on the creep of silver than on the other common f.c.c. metals. The high temperature creep parameters are based on Leverant et al, (1966). For the low temperature creep field, the average dislocation core diffusion coefficient given by Turnbull and Hoffman (1954)

has been used. Using these values, and considering diffusional creep, we have obtained good agreement with the data of Carreker and Guard (1955) and Shröder et al (1968).

ALUMINUM (Figure 7)

The high temperature creep parameters for aluminum are based on Weertman (1956) and Servi and Grant (1951). At high temperatures, these studies show an activation energy in agreement with the diffusion coefficient of Lundy and Murdock (1962): Q_v = 34.0 kcal/mole. For low temperature creep, the dislocation core diffusion coefficient cited by Balluffi (1970): Q_c = 19.6 kcal/mole, which provides good agreement with low temperature creep experiments, has been used. The Harper-Dorn creep field is based on Harper et al (1958). It appears on the map for d = 1mm, but is suppressed by diffusional creep at d = 10μm.

The power-law breakdown region of aluminum has been extensively studied; experimental data has been correlated according to a sinh equation by Wong and Jonas (1968). Data for commercial purity aluminum — dynamic compression (Alder and Phillips, 1954; Samanta, 1969, 1971 and Hockett, 1967) and for extrusion (Wong and Jonas, 1968) — show much lower strain-rates than data for high purity aluminum — torsion (Sellars and Tegart, 1966) and for extrapolation of creep (Servi and Grant, 1951). Both sets of data cannot be matched by the same power-law breakdown parameter. The value used for both maps ($\alpha' = 1 \times 10^3$) provides an intermediate approximation. The field appears here as a general demonstration, not as an exact representation of experiment.

LEAD (Figure 8)

Our high temperature creep parameters are based on Mohamed et al (1973): $n = 5.0$, $A = 2.5 \times 10^8$. These differ from those that could be derived from the single crystal creep experiments of Weertman (1960), which show a slightly lower n at high temperatures. We have used a diffusion activation energy of 26.1 kcal/mole (Resing and Nachtrieb, 1961) which is higher than the value found by Mohamed et al and lower than the value derived from Weertman.

Low temperature creep behavior is indicated by a number of studies. Weertman's low temperature data shows a higher stress exponent and a lower activation energy. Data of Feltham (1956) shows an apparent $Q \approx 22$ kcal/mole, with $n \geq 7$. Room temperature data of Gifkins (1952, 1959) and Nichols and McCormick (1970) show $n \approx 8$. The dislocation core diffusion coefficient is taken to match the boundary diffusion data of Okkerse (1954): $Q_c = 15.6$ kcal/mole. The Harper-Dorn creep field is based on Mohamed et al (1973). It appears for d = 1mm, but not for d = 10μm.

4.2 B.C.C. Metals

We have prepared maps for the refractory metals in groups Va and VIa: V, Cr, Nb, Mo, Ta, and W. These maps use the same mechanism equation as the f.c.c. maps (without Harper-Dorn creep or power-law breakdown) plus a Peierls barrier controlled glide equation.

For these b.c.c. metals it is important to specify the choice of shear modulus and its temperature dependence. Some of these metals show fairly large anisotropy, so different averages of the single crystal elastic

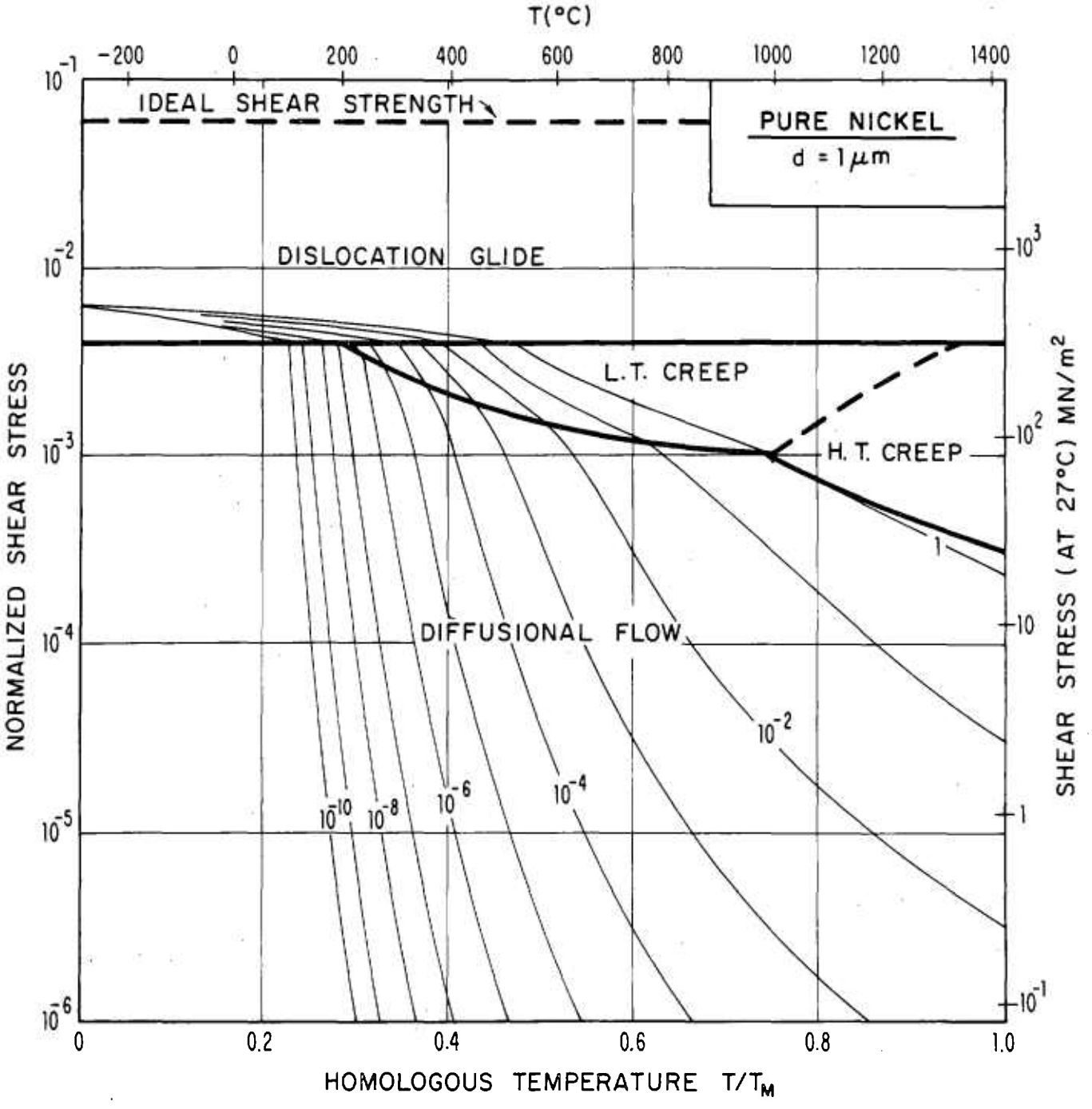

Fig. 4a) Pure nickel of grain size 1μm.

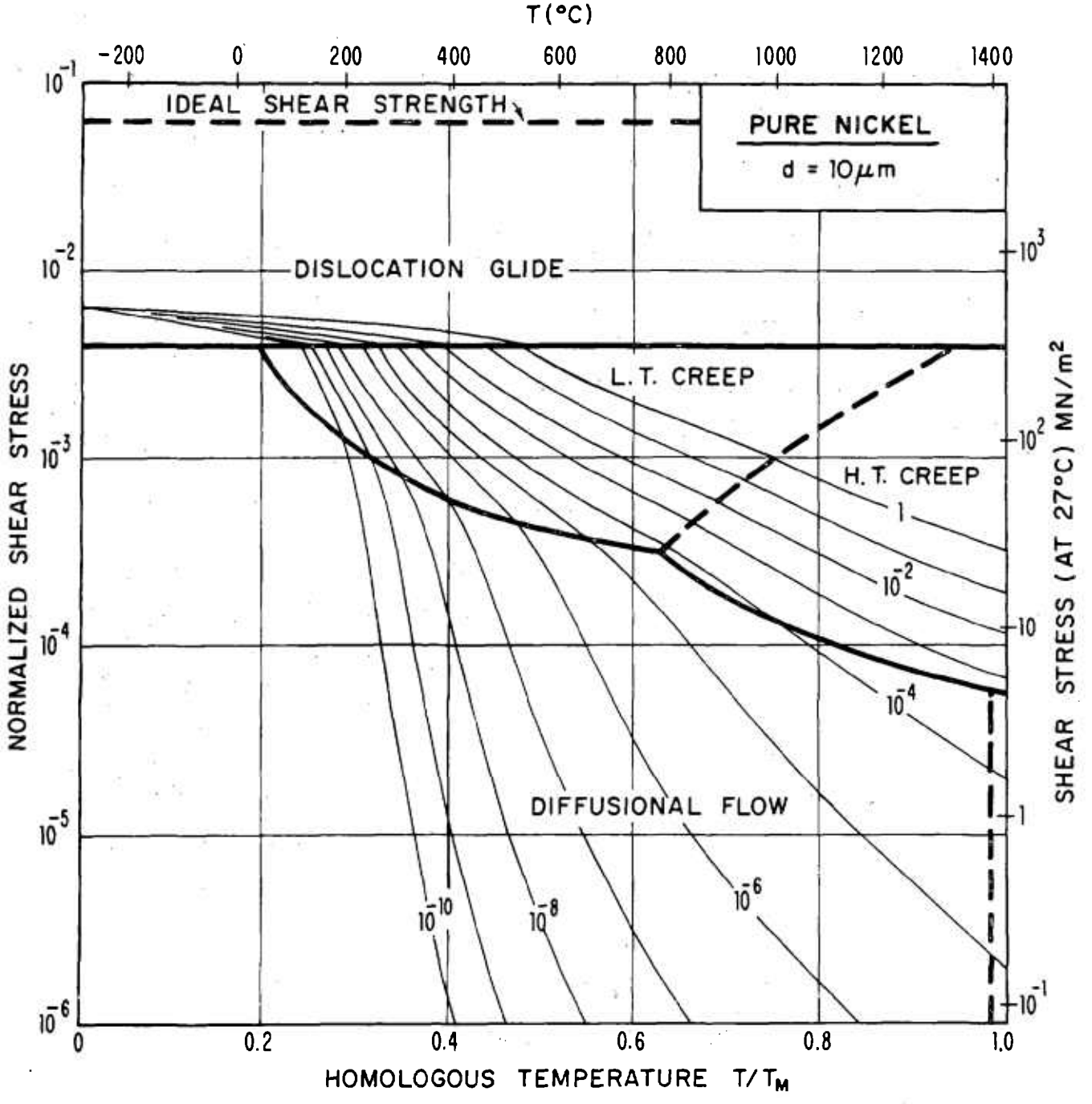

Fig. 4b) Pure nickel of grain size 10μm.

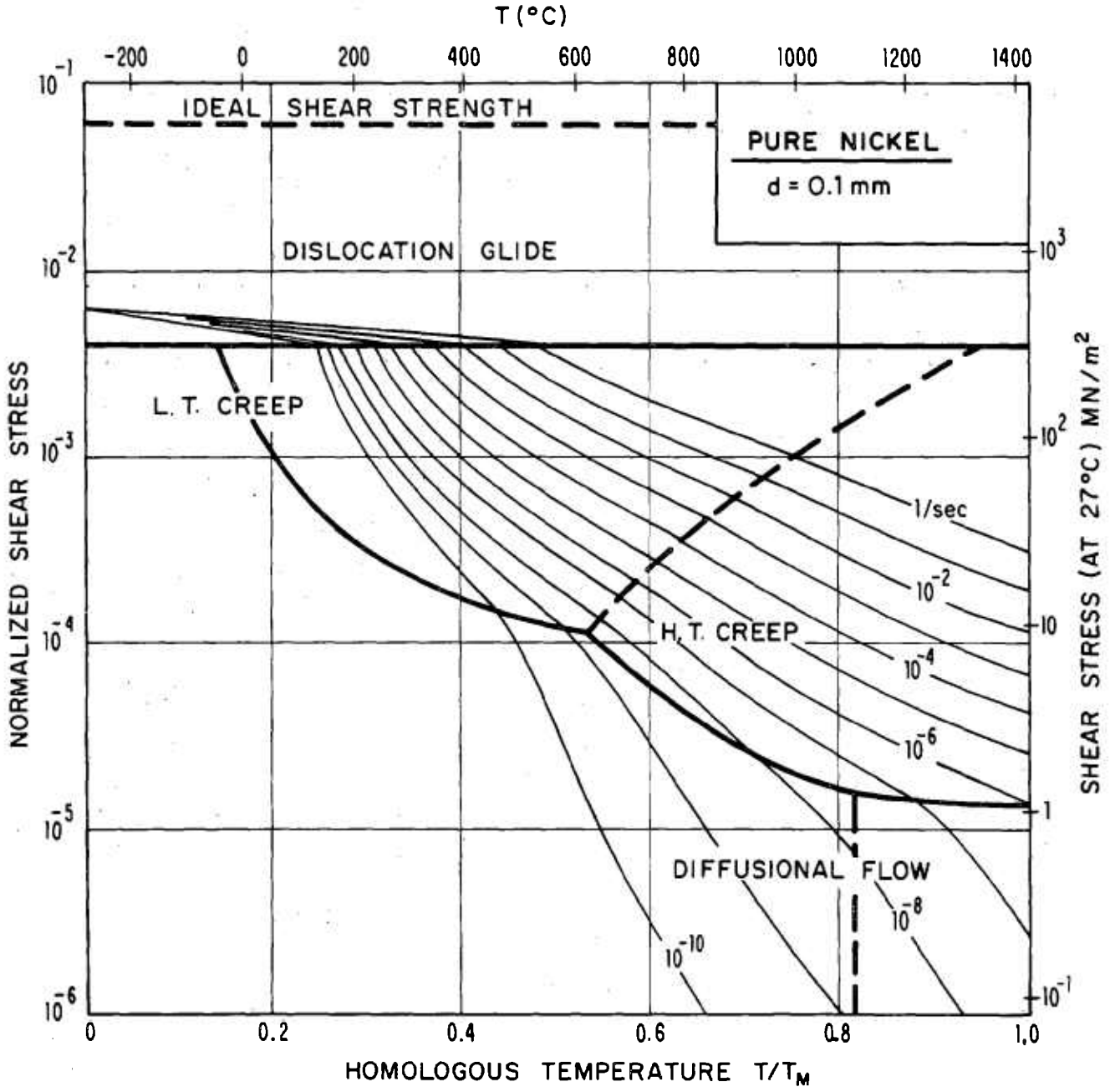

Fig. 4c) Pure nickel of grain size 100μm.

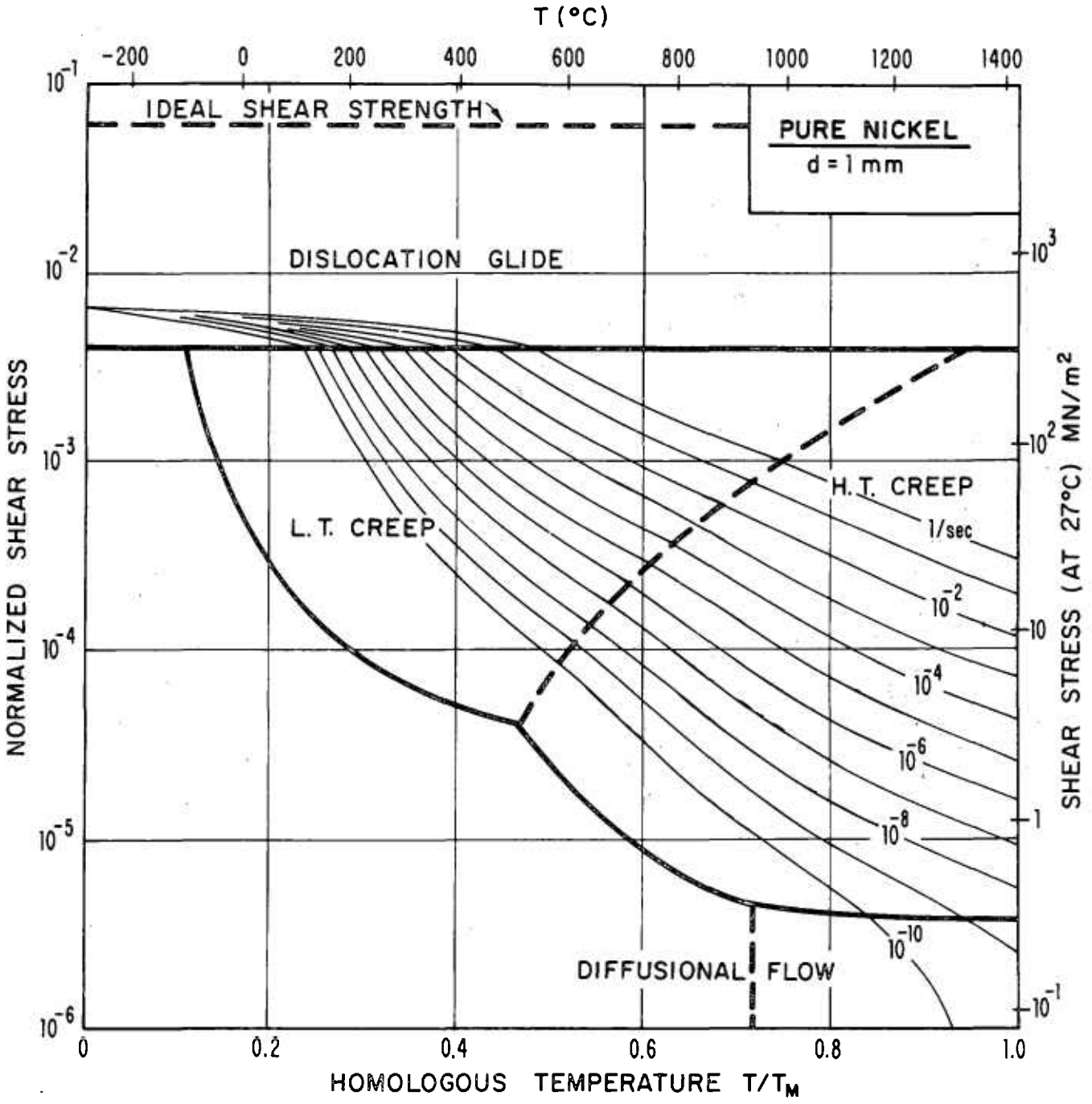

Fig. 4d) Pure nickel of grain size 1mm.

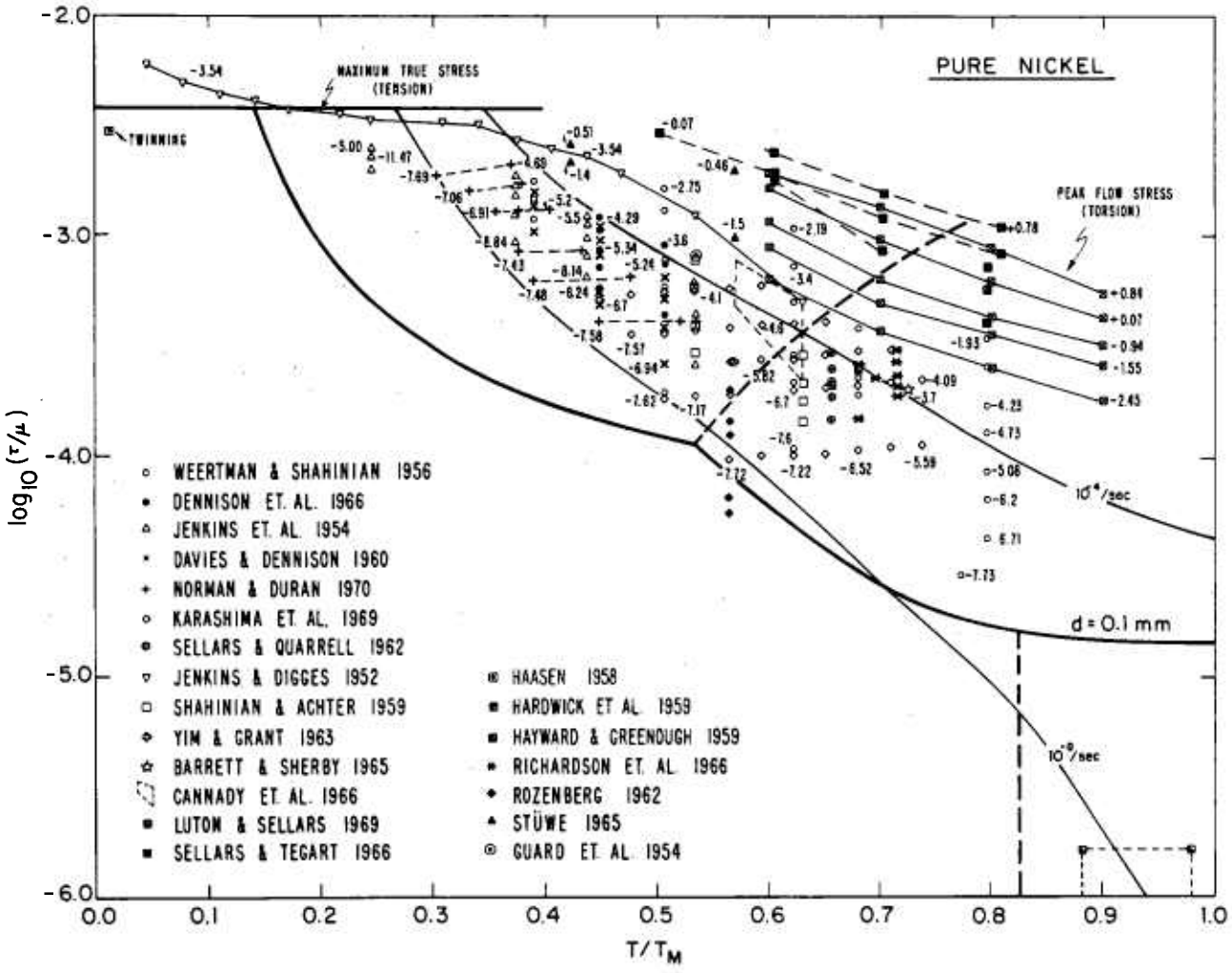

Fig. 4e) Pure nickel experimental data.

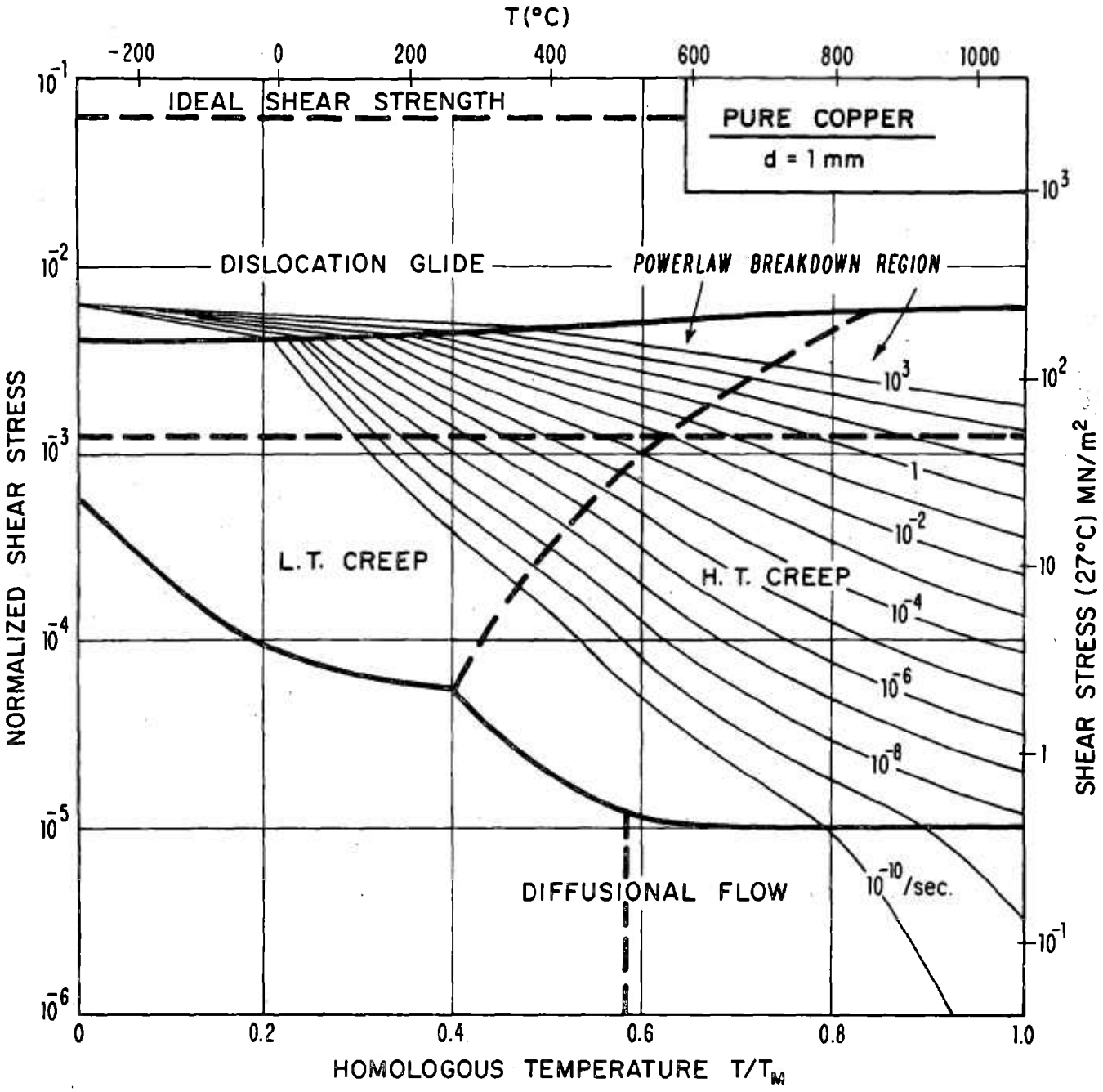

Fig. 5a) Pure copper of grain size 1mm, including the power-law breakdown region.

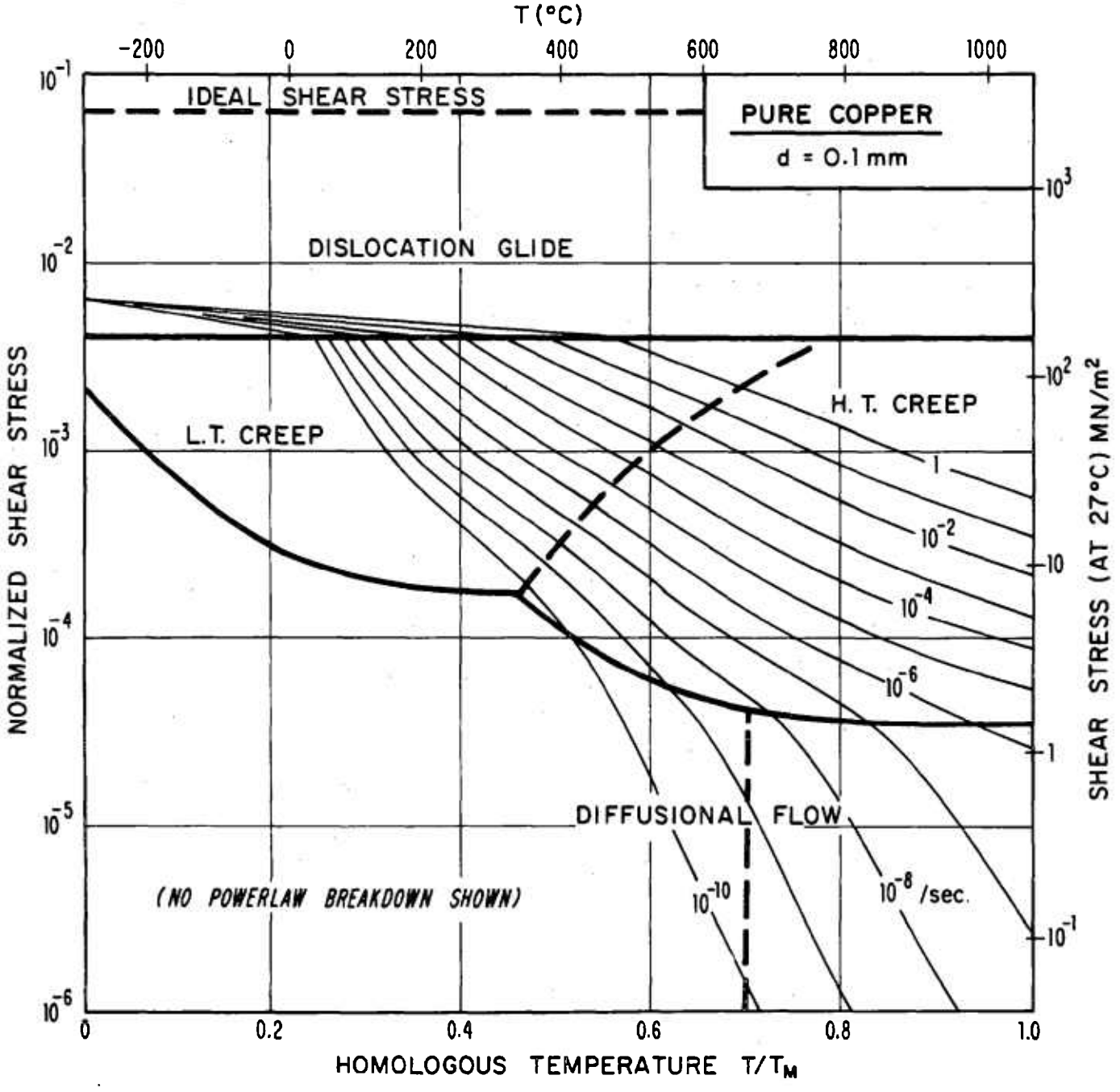

Fig. 5b) Pure copper of grain size 0.1mm, not including the power-law breakdown region.

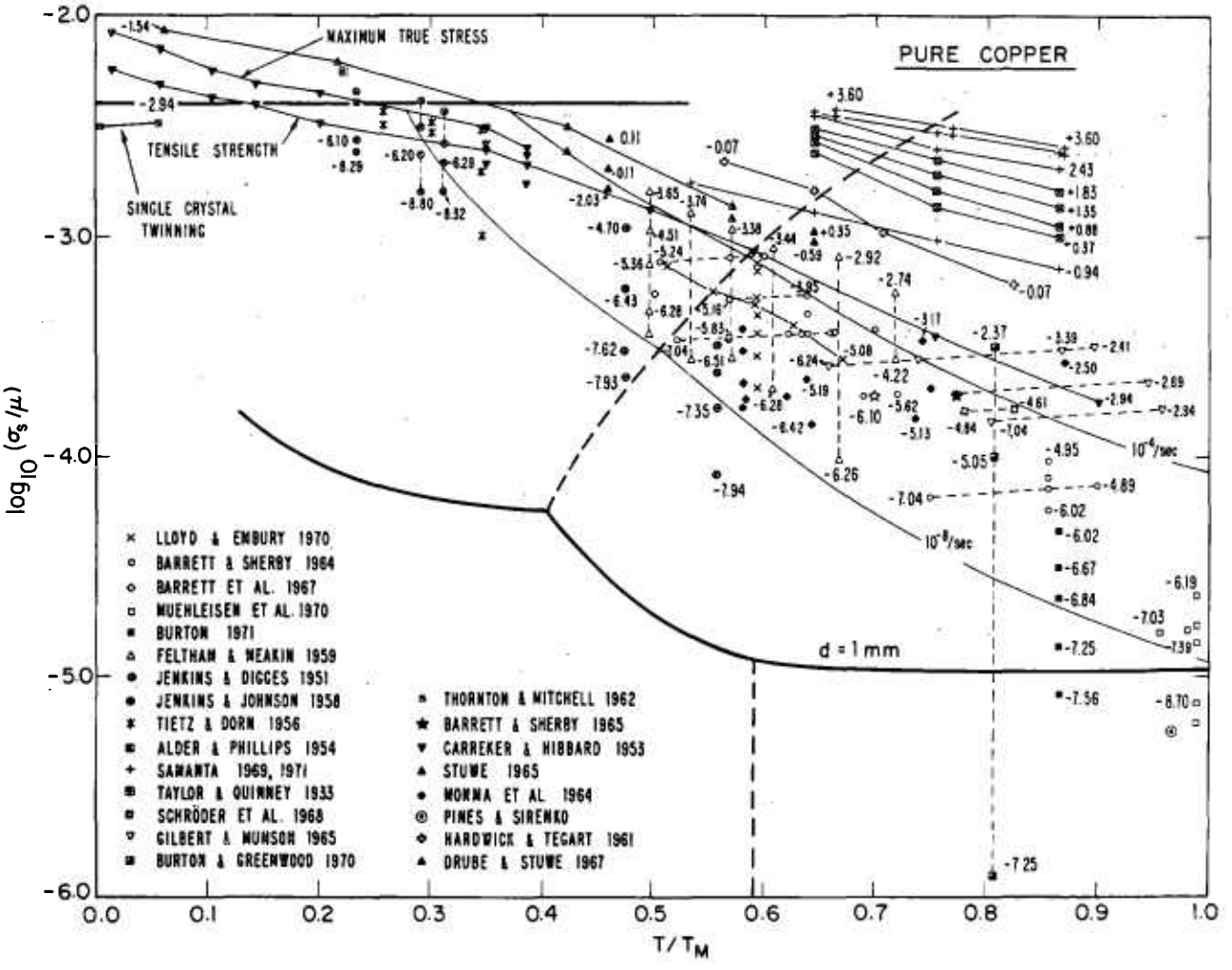

Fig. 5c) Pure copper experimental data.

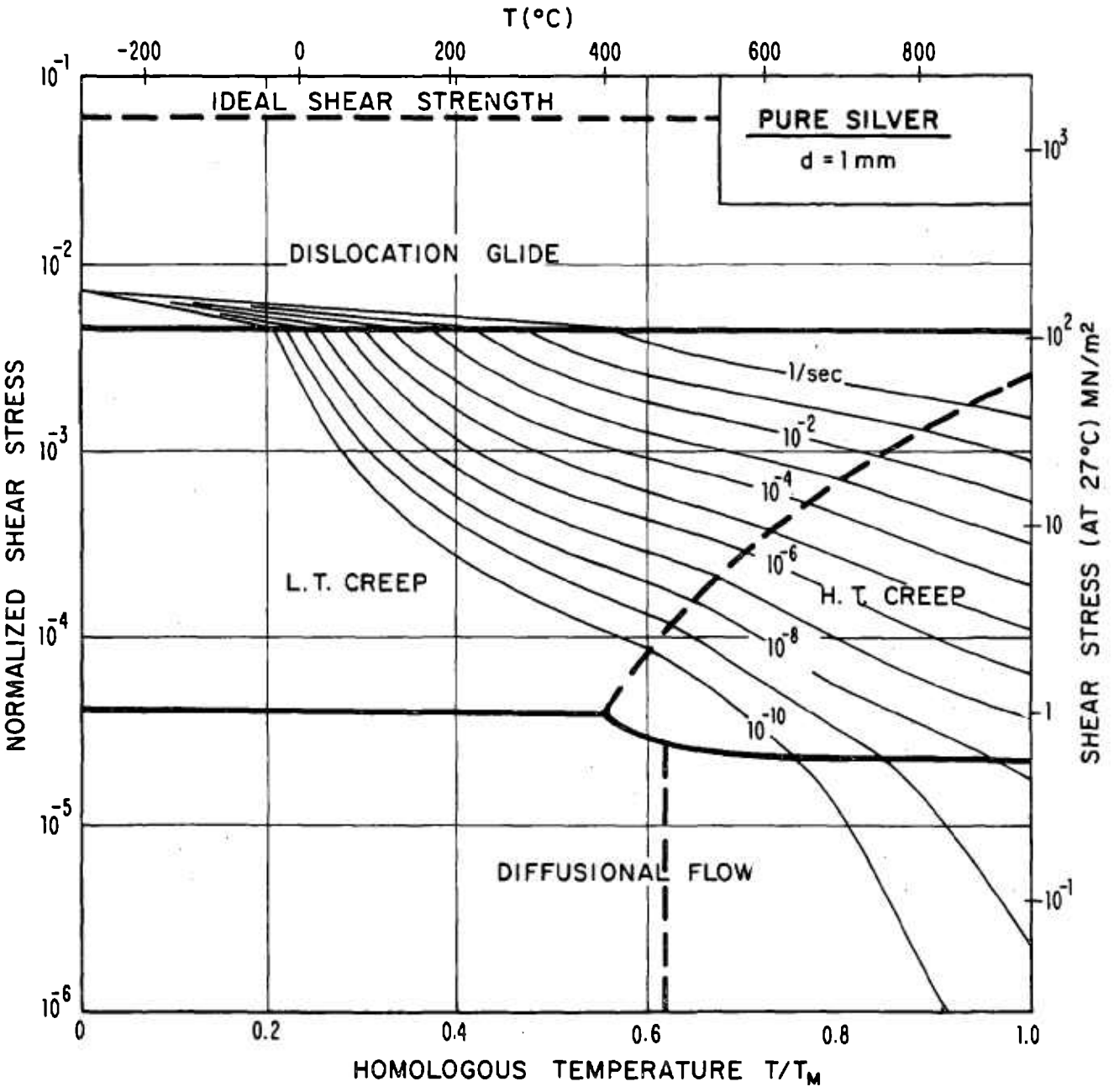

Fig. 6a) Pure silver of grain size 1mm.

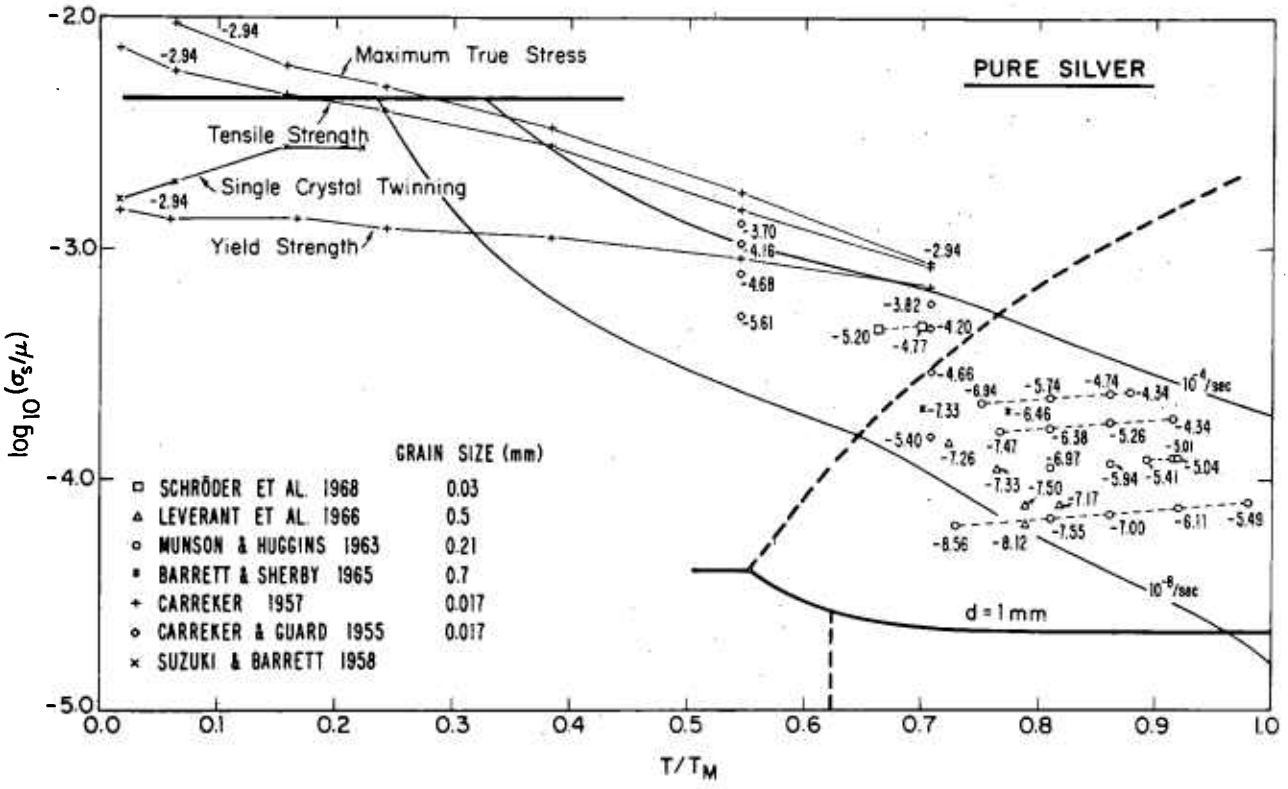

Fig. 6b) Pure silver experimental data.

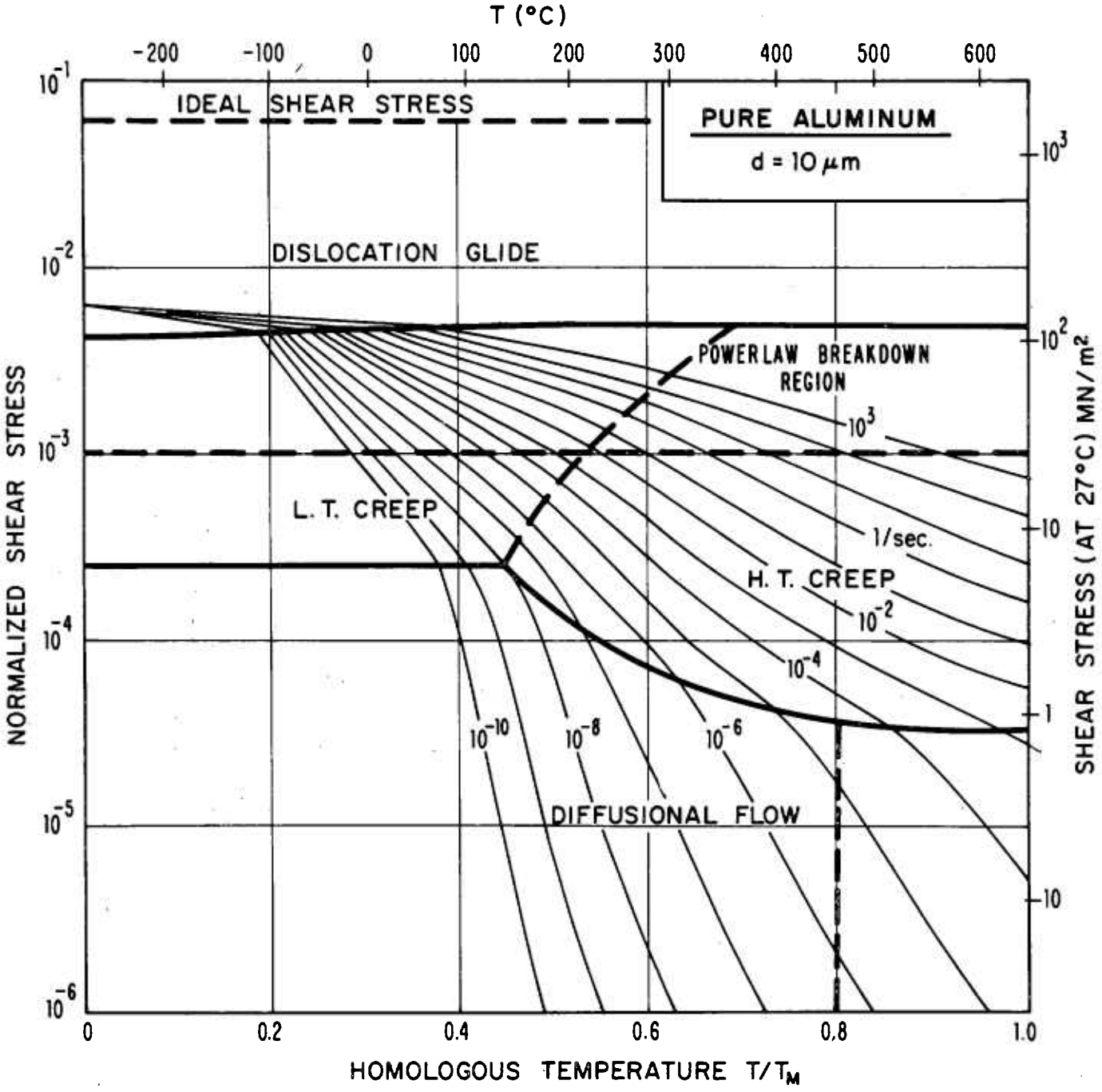

Fig. 7a) Pure aluminum of grain size 10μm, including the power-law breakdown region.

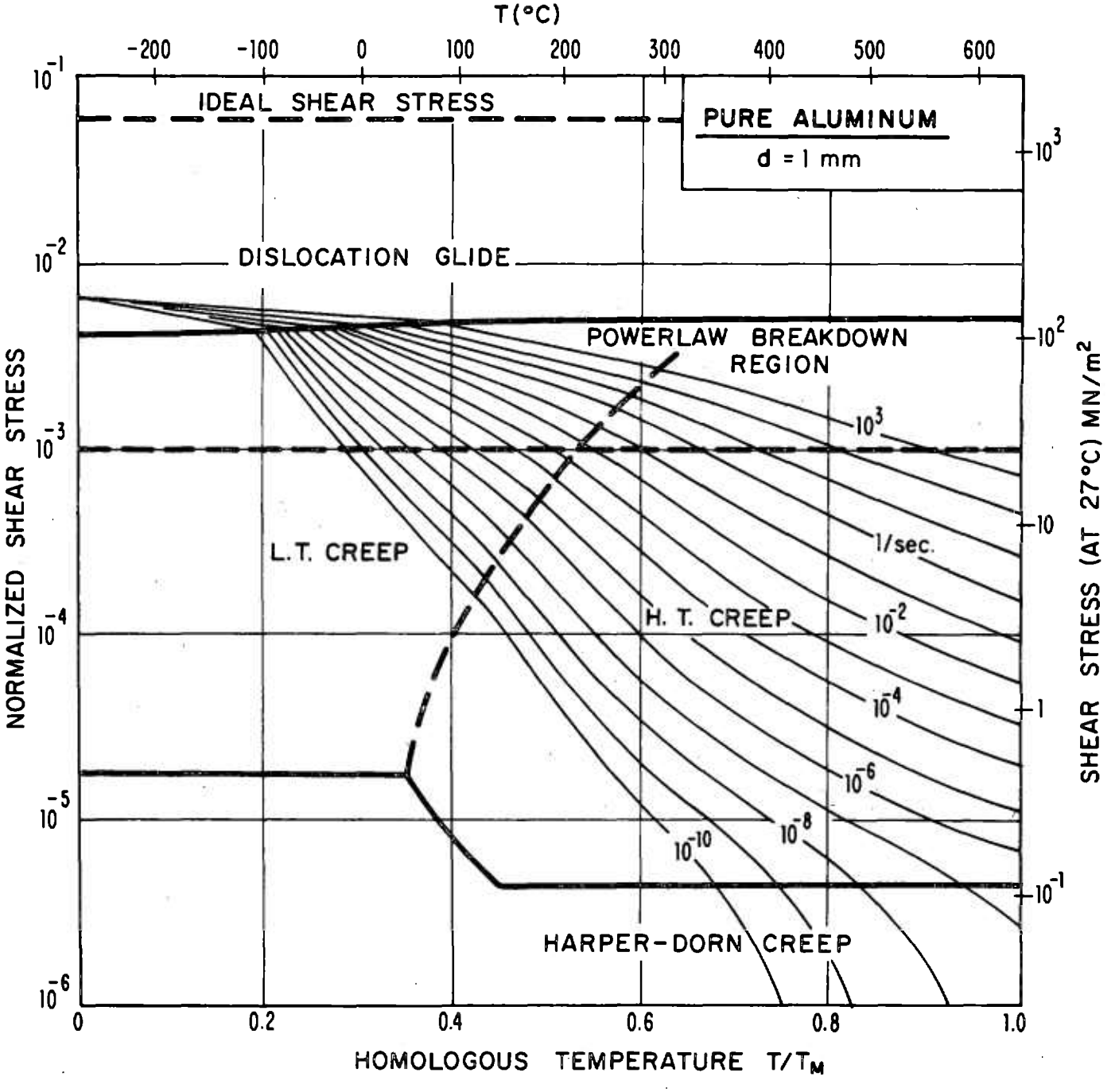

Fig. 7b) Pure aluminum of grain size 1mm, including the power-law breakdown region, and showing the Harper-Dorn creep region.

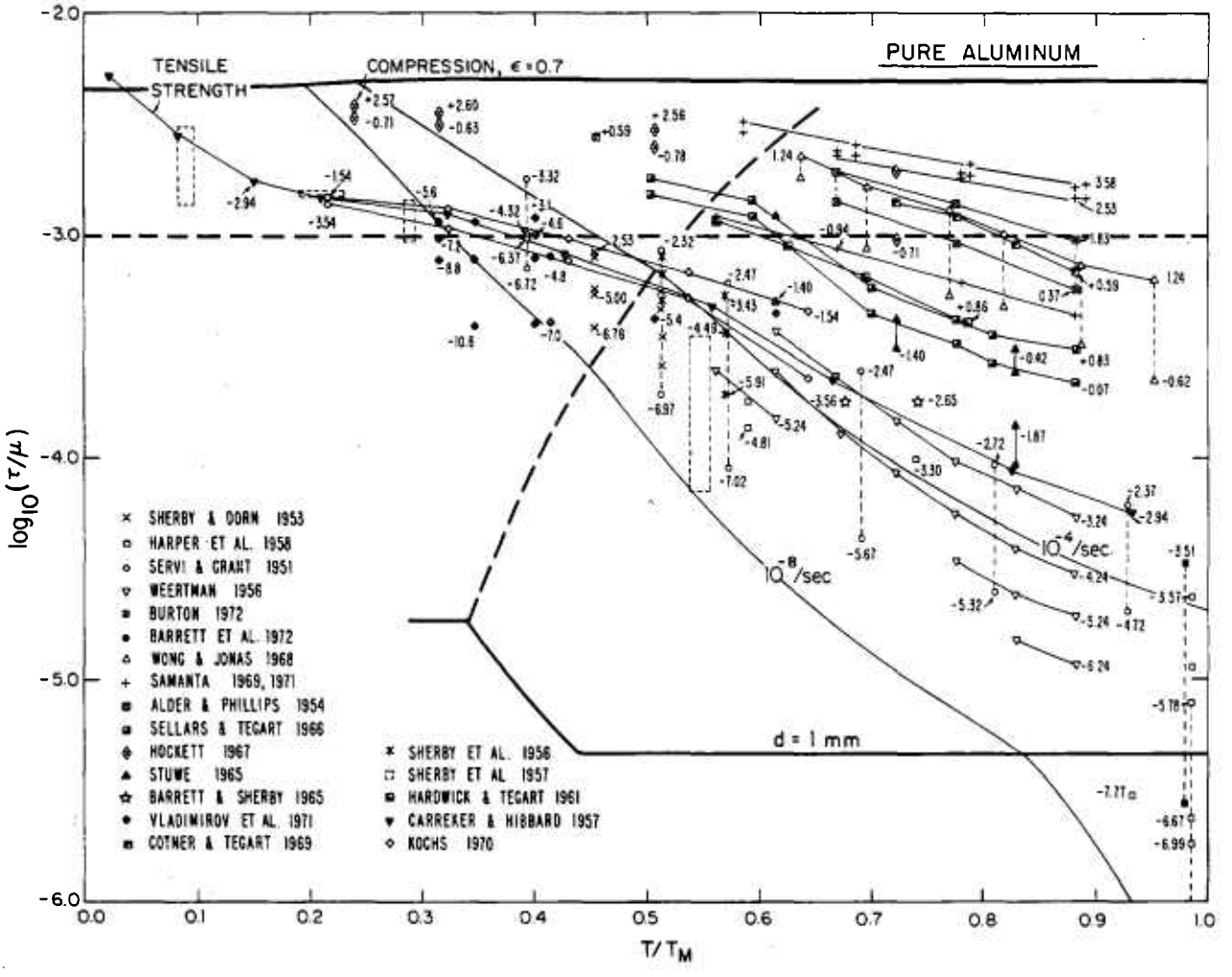

Fig. 7c) Pure aluminum experimental data.

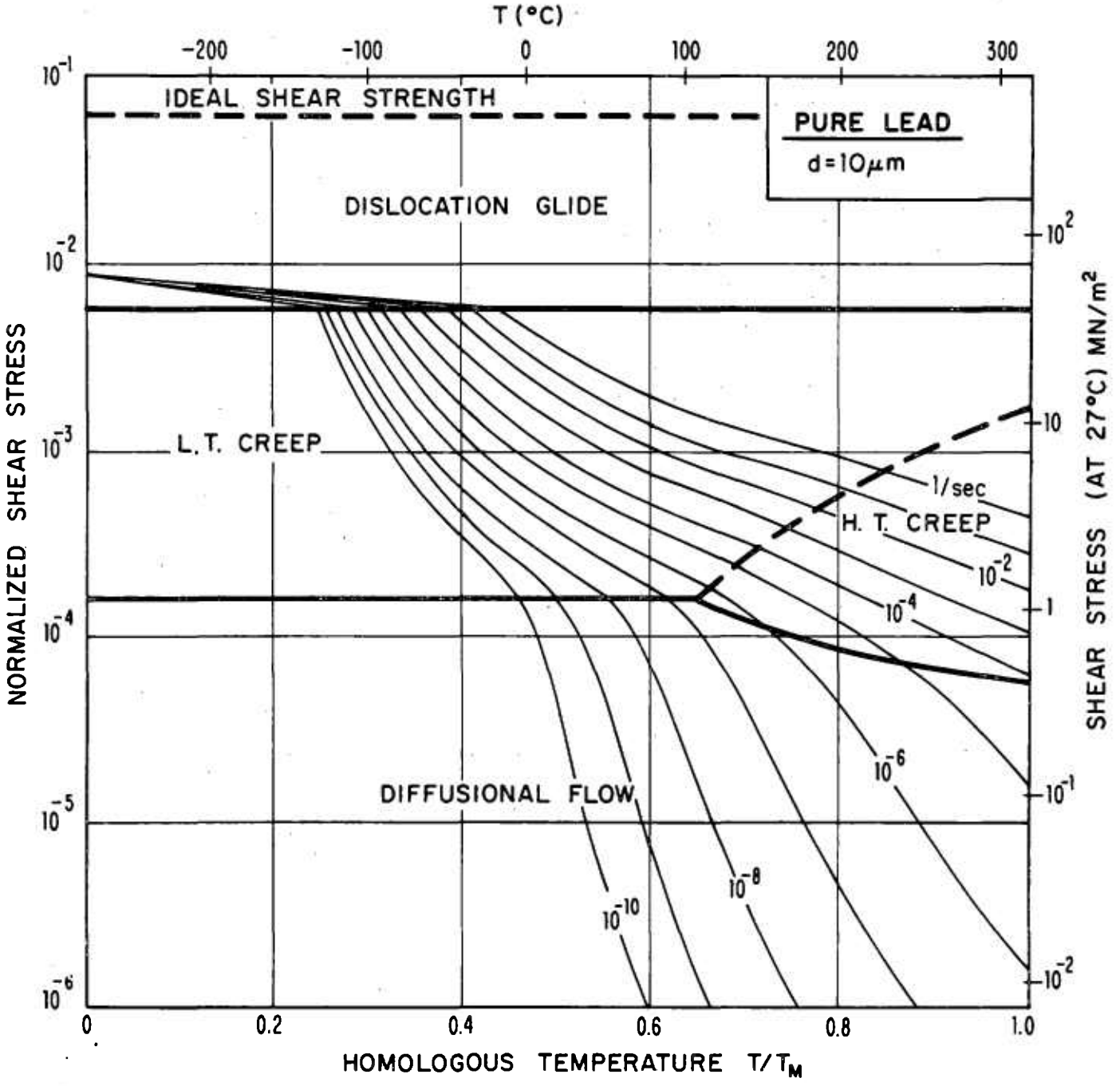

Fig. 8a) Pure lead of grain size 10μm; Harper-Dorn creep does not appear.

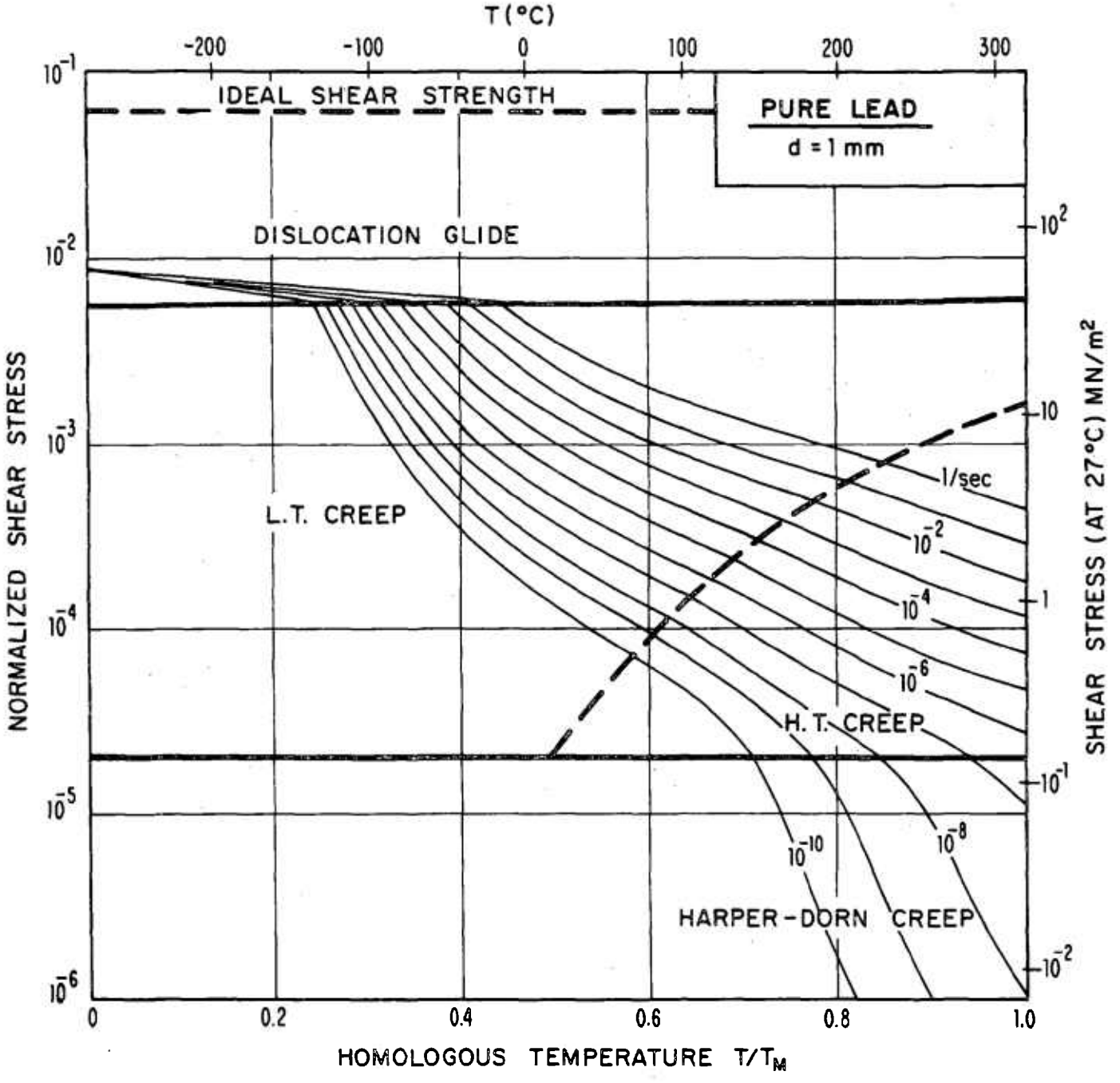

Fig. 8b) Pure lead of grain size 1mm, showing Harper-Dorn creep which has supplanted diffusional flow.

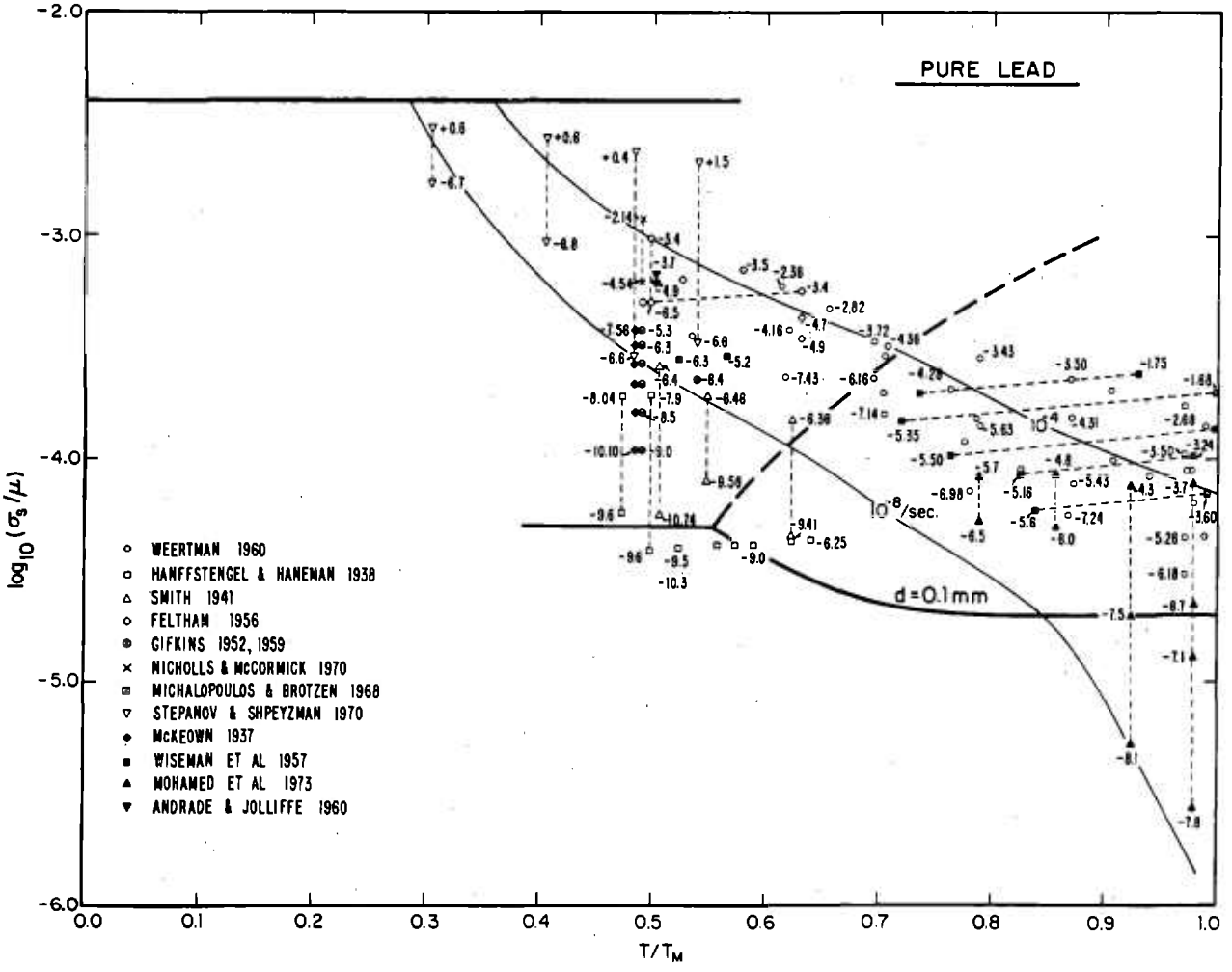

Fig. 8c) Pure lead experimental data.

constants will have different values. We have used room temperature modulus values that are derived from the anisotropic calculation of the energy of a 1/2 <111> screw dislocation (see Hirth and Lothe, 1968, p.435). These values are listed in Table I. For the temperature dependence we have made estimates from the temperature dependence of other single crystal or polycrystal moduli. In all cases we have used the approximation of a linear temperature dependence. This is fairly accurate for all these metals except niobium which shows anomalous behavior (see Armstrong, et al, 1966).

The volume self-diffusion for these metals is fairly well known. For some there is evidence that the activation energy increases with temperature. In particular, we have used a dual expression for the volume diffusion coefficient of vanadium, as given in Table 1. Similar behavior has been demonstrated for tantalum (Pawel and Lundy, 1965) but can be well approximated by one simple Arrhenius relationship.

We have found complete data for grain boundary and dislocation core self-diffusion only for tungsten. For chromium, an activation energy for core diffusion has been reported. All other core and boundary diffusion coefficients have been estimated using the approach, $Q_c \simeq Q_B \simeq \frac{2Q_v}{3}$.

For all the b.c.c. metals the parameters we have used for Peierls barrier controlled yielding are only approximate. We have found our rate-equation to be a good but not perfect match to experiment. The parameters ΔF_k and τ_p would, however, be different were a different form of ΔG used.

In any approximate fit to experimental data the chosen values of ΔF_k, τ_p and $\dot{\gamma}_p$ are all interdependent; changing any one slightly would be acceptable, but would require changing the others.

It is difficult to find $\dot{\gamma}_p$ experimentally unless the flow stress is known for different strain-rates. From the Briggs and Campbell (1972) data on molybdenum, we have derived $\dot{\gamma}_p = 10^{11}$/sec and have used this for all the b.c.c. metals. This is the appropriate value for equation 12 (with stress-squared pre-exponential) and would differ for other pre-exponential stress dependencies.

Given the $\dot{\gamma}_p$ value, the ΔF_k value can easily be found from the temperature dependence of the flow stress. The yield stress of b.c.c. metals is substantially lowered by increased purity. In fact, there has been debate as to whether the Peierls stress results from an intrinsic lattice resistance or from small concentrations of interstitial impurities. The question does not concern us here, except that it must be recognized that the yield parameters refer to a particular level of purity.

Much of the recent work on b.c.c. metals has measured the single crystal critical resolved shear stress. This is related to the polycrystalline tensile flow stress by an appropriate Taylor factor, ~1.67, as discussed in section 2.2b. On our experimental plots it can be seen that polycrystalline data and single crystal critical resolved shear stress data (for comparable purities) differ by about this factor, at all temperatures. The Taylor factor can then be included in the value of τ_p; the

τ_p values in Table 1 are for polycrystalline yield. As discussed in section 2.2d, we have used the approximation that Peierls-controlled and obstacle-controlled glide are alternative mechanisms: the slowest strain-rate is controlling. This results in the sharp corner in the strain-rate contours. A more complete model of the mechanism interaction would smooth the transition, as shown for the plotted experiments. We have arbitrarily chosen an obstacle spacing of $\ell = 2 \times 10^{-5}$cm (or a dislocation density of $\rho = 2.5 \times 10^{9}/cm^{2}$). This value is lower than that used for f.c.c. maps, and represents a lower state of work-hardening. It is not necessarily that of the samples used for the plotted yield stress experiments.

Let us briefly review the experimental data for each metal.

VANADIUM (Figure 9)

The dislocation creep parameters are based on Wheeler et al (1971). As mentioned above, the activation energy for volume diffusion decreased from ~94 kcal/mole at above 1350°C to ~74 below. Wheeler et al find that the activation for creep also decreased (from 113 to 94 to 76 kcal/mole) with decreasing temperature, though the decrease occurs at a lower temperature. At their lowest temperatures, the activation energy drops to 54 kcal/mole, which they ascribe to core diffusion. The stress exponent, n, increases from 5 at high temperatures to ~8 at low temperatures which is also in accord with the low temperature creep behavior.

The Peierls stress parameters are derived from the high purity polycrystalline data of Wang and Bainbridge (1972), which is probably the highest purity reported. This data agrees with their single crystal data and with the single crystal data of Mitchell et al (1970) when the Taylor factor conversion is included.

CHROMIUM (Figure 10)

The dislocation creep parameters for chromium are derived from Stephens and Klopp (1972) who used high purity iodide chromium. Their data at 1316° and 1149°C shows a stress exponent of $n \simeq 4.5$; data at 816° and 982°C shows $n \simeq 6.5$. The lower temperature data, however, shows no tendency toward a lower activation energy. There is, therefore, no conclusive evidence for (or against) a low temperature creep field in chromium. The yield behavior of chromium is based on the Marcinkowski and Lipsitt (1962) data for polycrystals. We have not found any single crystal studies.

NIOBIUM (Figure 11)

The elastic constants of niobium have an anomalous temperature dependence (Armstrong et al, 1966). Because of this, we have neglected the temperature dependence of the modulus. We have not found any extensive creep studies at very high temperatures. We have used creep parameters based on Brinson and Argent (1962-1963) which are in agreement with Stoop and Shahinian (1966) but show greater strain-rate than Abramyon et al (1969). The creep field of niobium is the least accurate

among the metals discussed in this paper. The low temperature yield behavior of niobium has been extensively studied for both polycrystals and single crystals. We have used yield parameters based on Briggs and Campbell (1972), which also agree well with earlier studies.

MOLYBDENUM (Figure 12)

The high temperature creep of molybdenum has been well studied. We have based our high temperature creep parameters on data of Conrad and Flagella (1968), which is more than an order of magnitude faster in creep rate than Green, Smith and Olson (1959). The high temperature stress exponent is $n = 4.85$. There are several studies which generally support a low temperature creep field. Carvalhinos and Argent (1967), Pugh (1955) and Semchyshen and Barr (1955) all show $n = 6 - 8$ for $T = 0.4 - 0.53\ T_M$, and a lower activation energy than is found for volume diffusion. For the low temperature yield parameters, we have used Briggs and Campbell (1972). This data is not the lowest yield stress data available and therefore does not represent the highest purity. Lawley et al (1962-63) have found that the polycrystalline yield stress can be substantially lowered (nearly a factor of 2.0) by further zone refining, although the change in purity cannot be detected.

TANTALUM (Figure 13)

The high temperature creep parameters for tantalum are taken from W.V. Green (1965). His steady-state data does show an activation energy increasing with temperature, as pointed out by J.E. Flinn and E.R. Gilbert

(1966), but this may be explained by the fact that the highest temperature tests were done at higher temperature than the annealing temperature. The indicated stress exponent is $n \cong 4.2$. There is some indication of low temperature creep behavior. The data of Schmidt et al (1960) at 1200° and 1000°C shows $n \cong 6$. The yield parameters for tantalum are based on data of Wessel as cited by Bechtold, Wessel and France (1961), which is in good agreement with the single crystal data of Mitchell and Spitzig (1965), adjusted by the appropriate Taylor factor.

TUNGSTEN (Figure 14)

The high temperature creep of tungsten has been reviewed by Robinson and Sherby (1969), who demonstrated that most of the available data can be divided into high temperature creep above about 2000°C and low temperature creep below about 2000°C. The high temperature data is that of Flagella (1967) — for wrought arc-cast tungsten — and of King and Sell (1965). This data shows faster creep rates than that of Green (1959) and Flagella (1967) for powder metallurgy tungsten. The low temperature creep region is represented by the data of Gilbert, Flinn and Yaggee (1965) which shows $n \cong 7$ between 1300° and 1900°C with an apparent activation energy of about 90 kcal/mole, although it is nearly an order of magnitude slower than the Flagella data in the overlapping temperature range. This general behavior is also indicated by other papers. The low temperature yield parameters for tungsten are based on the polycrystalline yield data of Raffo (1969). This data is in general agreement with single crystal critical resolved shear stress data of Koo (1963) and Argon and Maloof (1966).

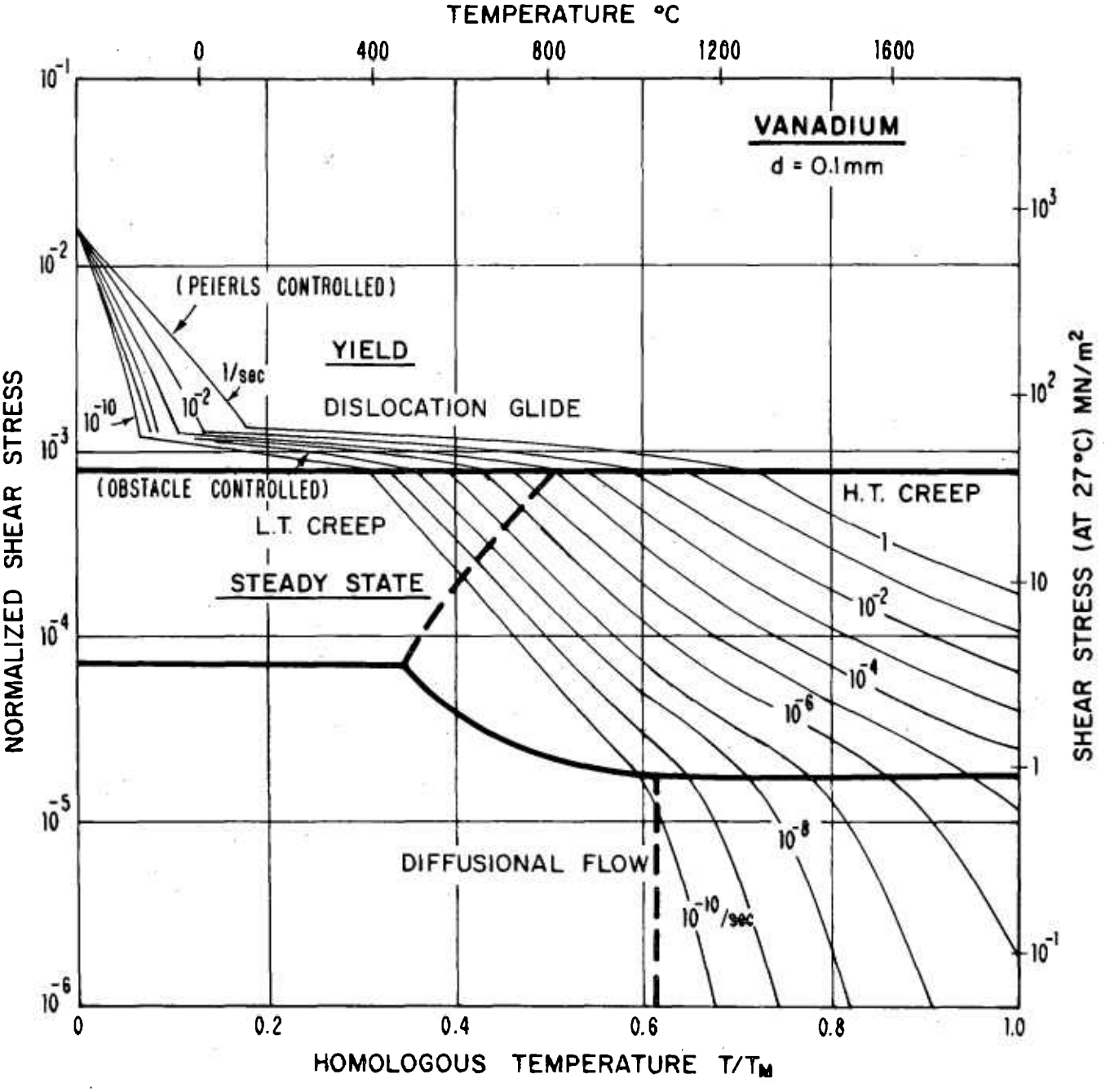

Fig. 9a) Vanadium of grain size 0.1mm.

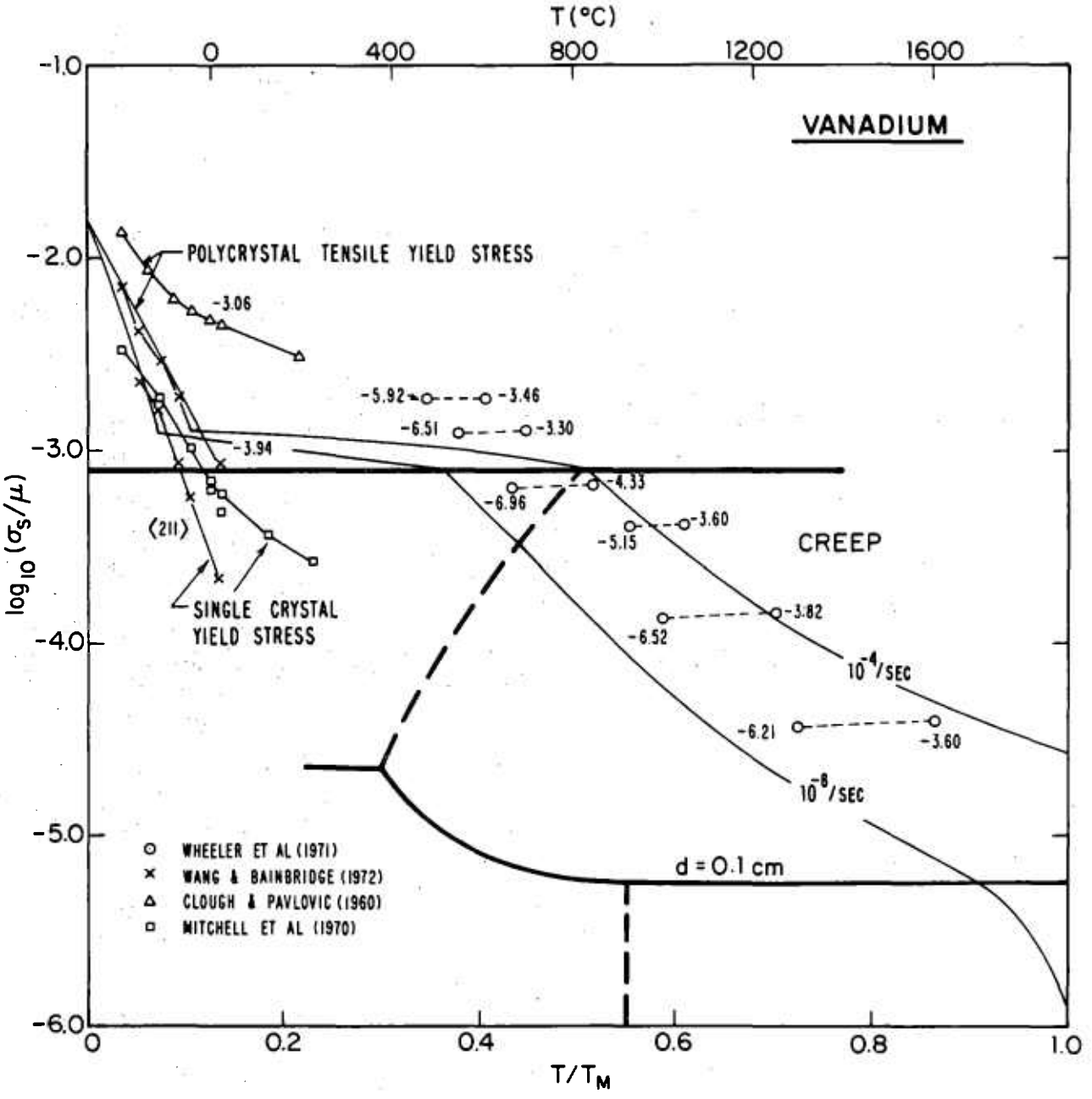

Fig. 9b) Vanadium experimental data.

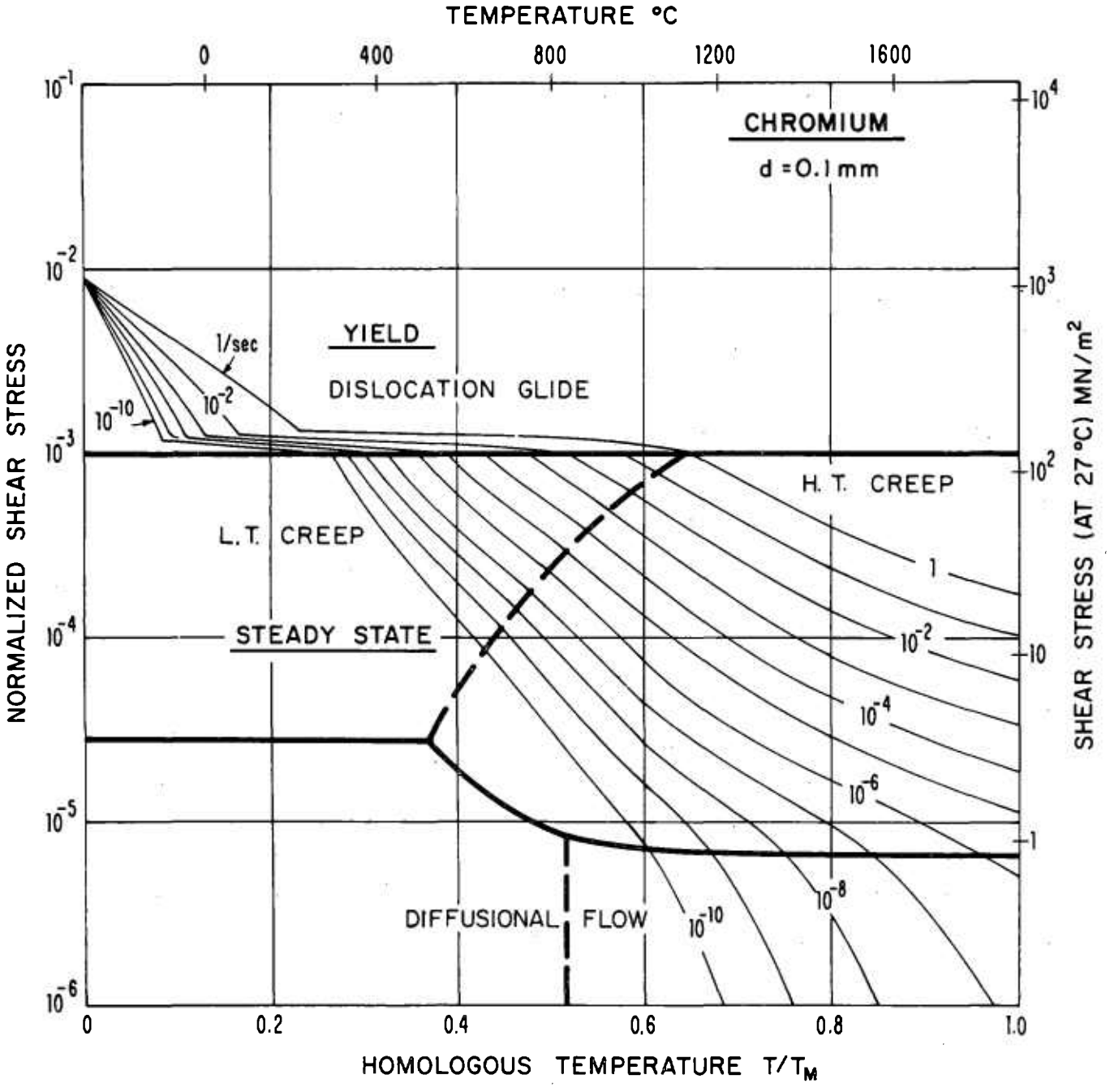

Fig. 10a) Chromium of grain size 0.1mm.

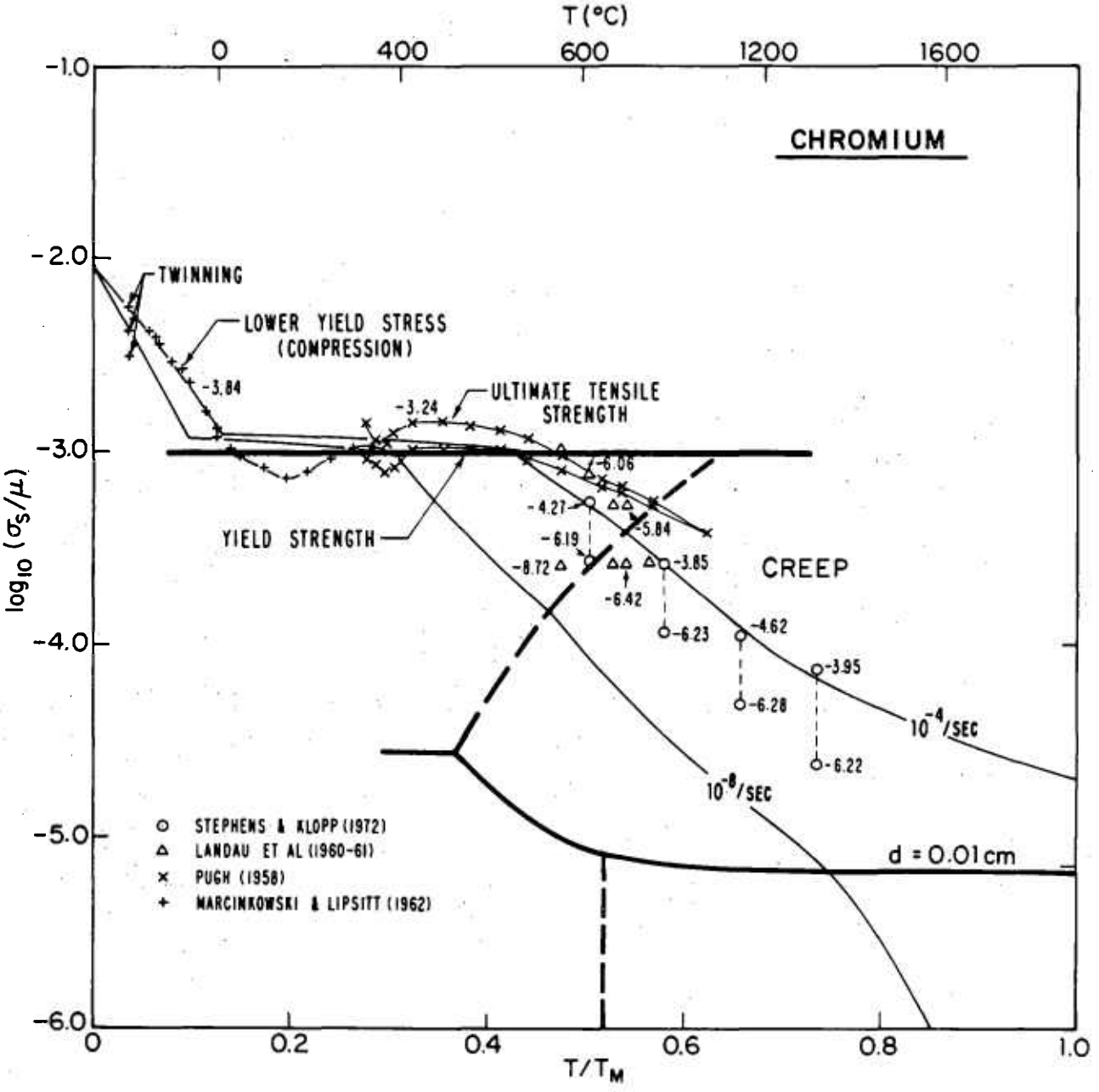

Fig. 10b) Chromium experimental data.

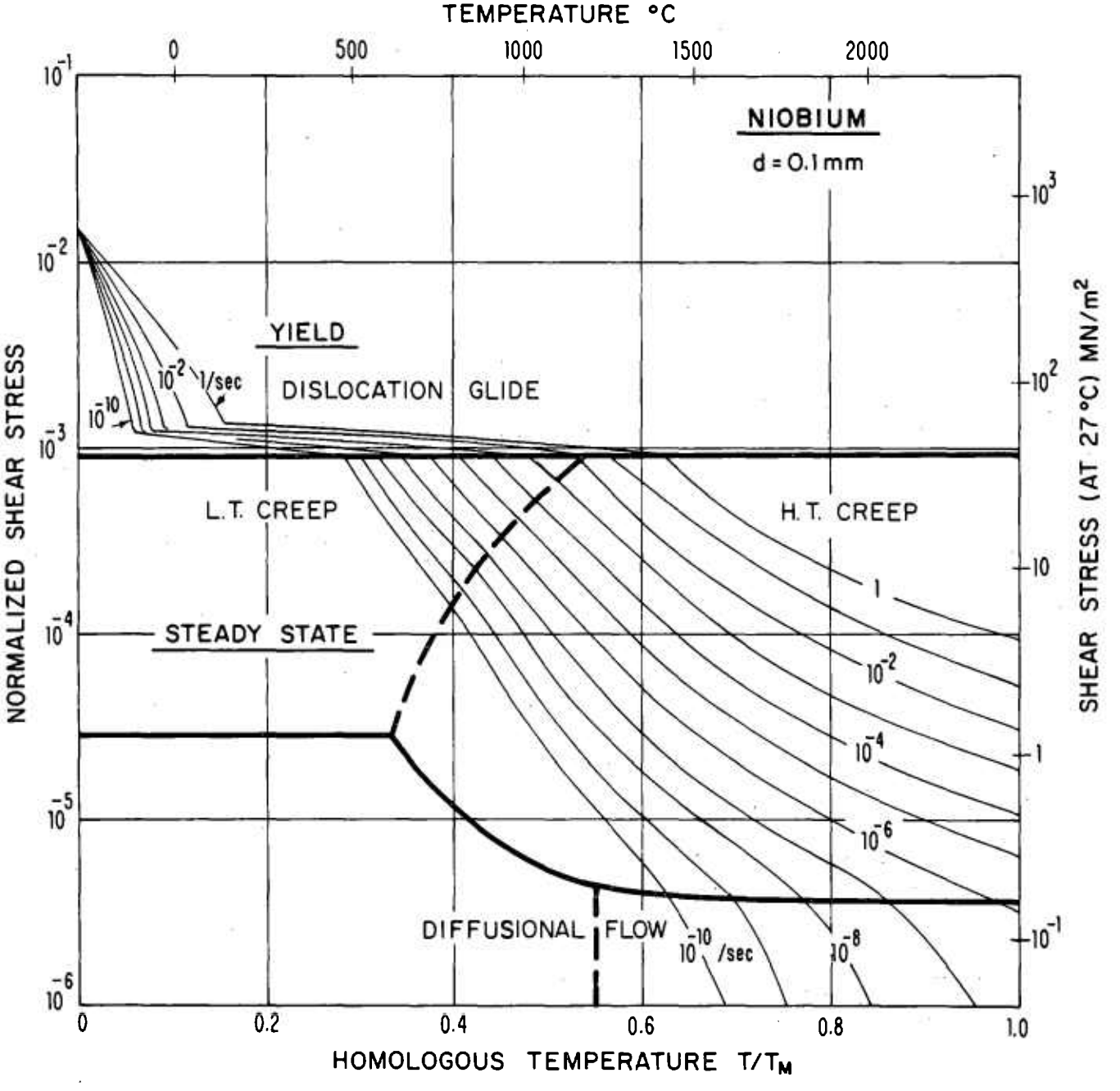

Fig. 11a) Niobium of grain size 0.1mm.

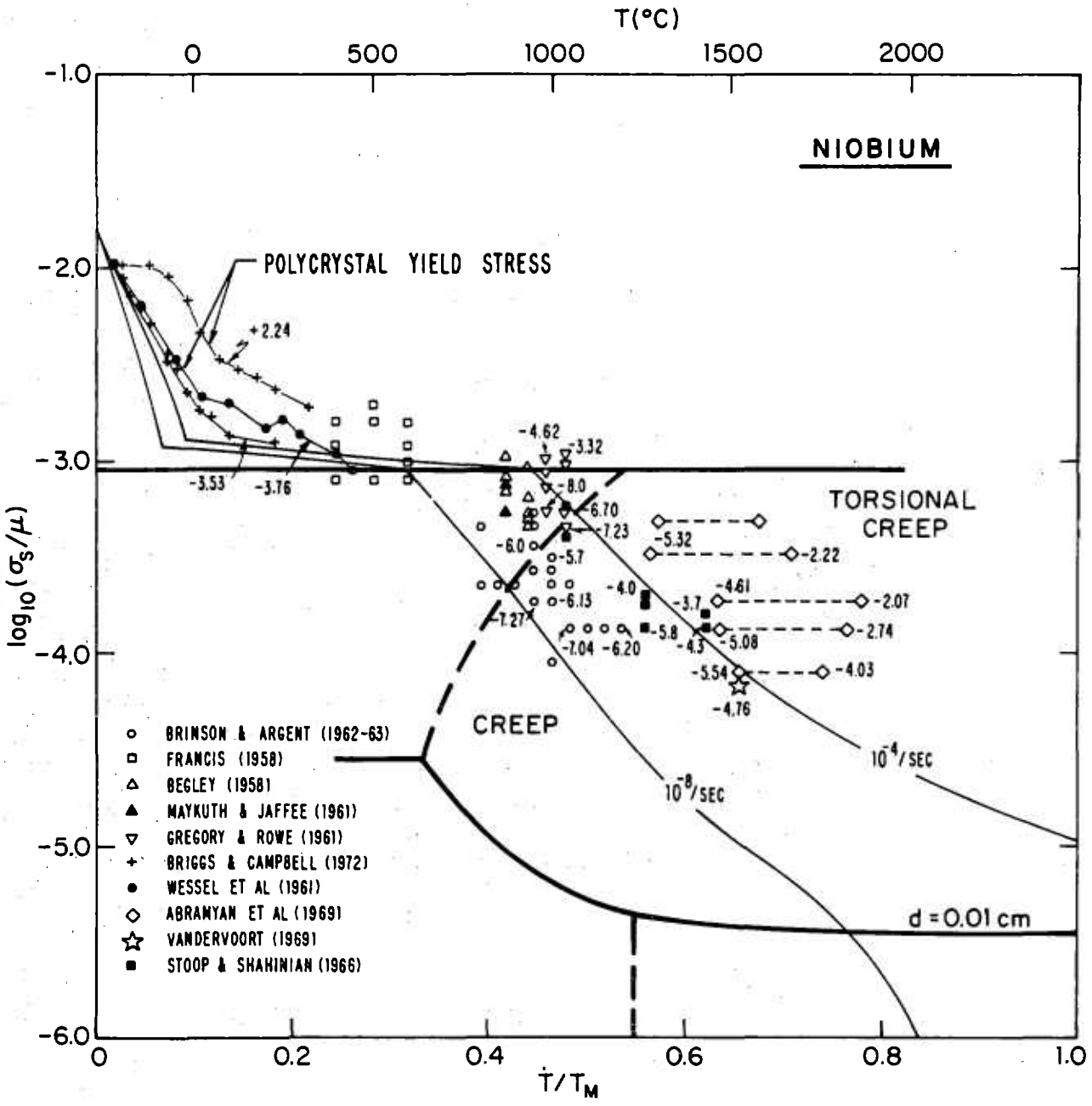

Fig. 11b) Niobium experimental data.

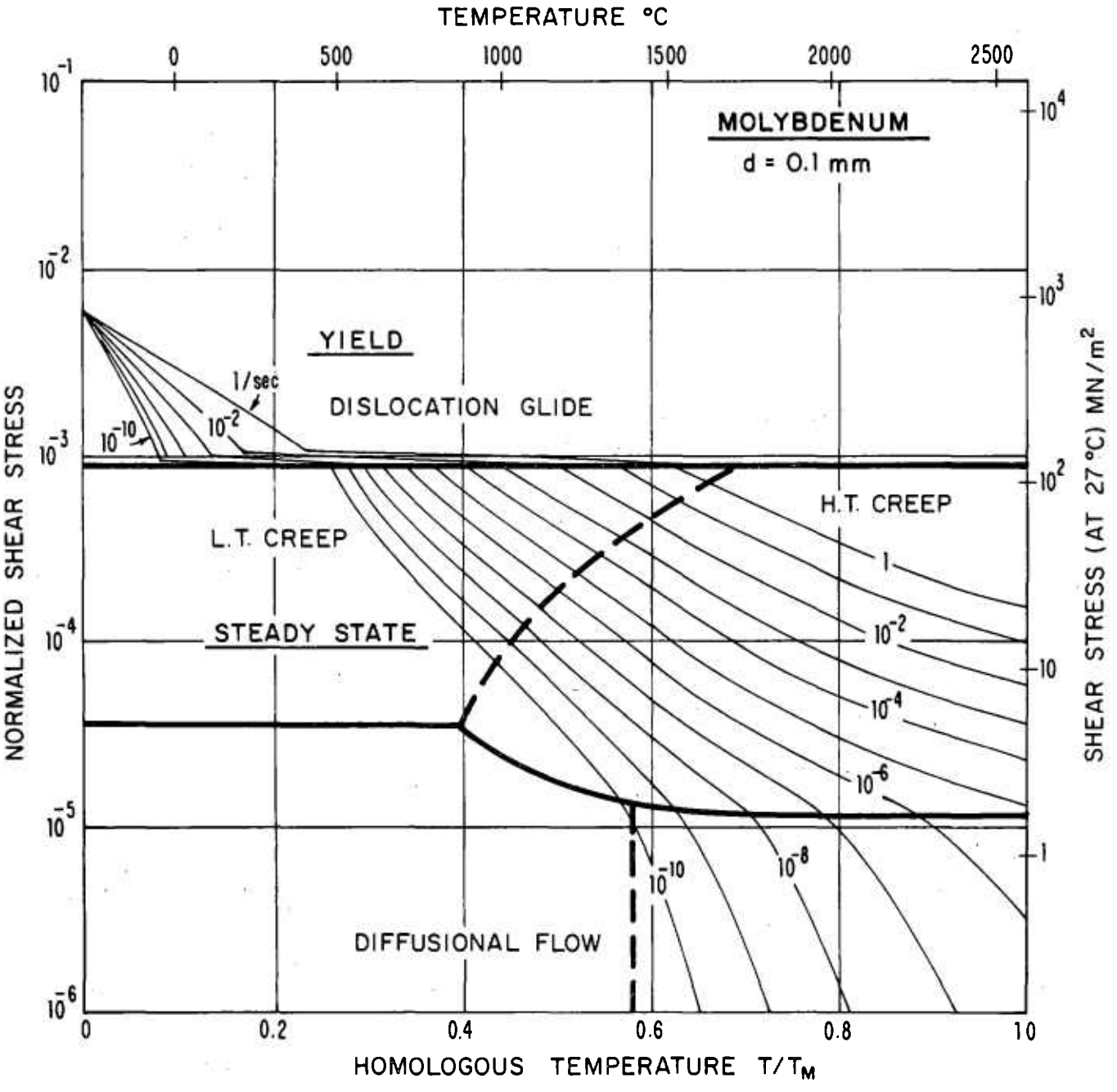

Fig. 12a) Molybdenum of grain size 0.1mm.

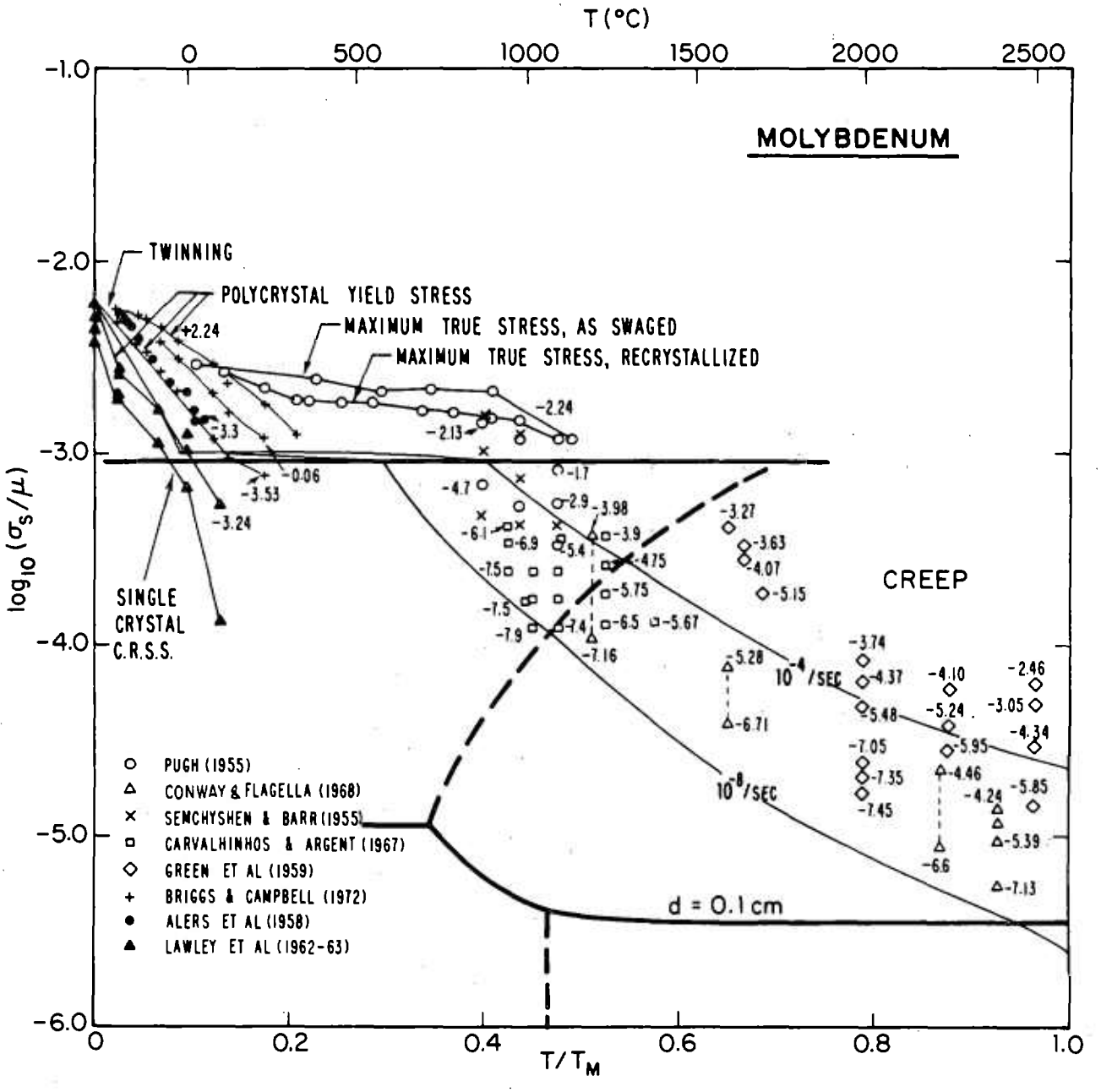

Fig. 12b) Molybdenum experimental data.

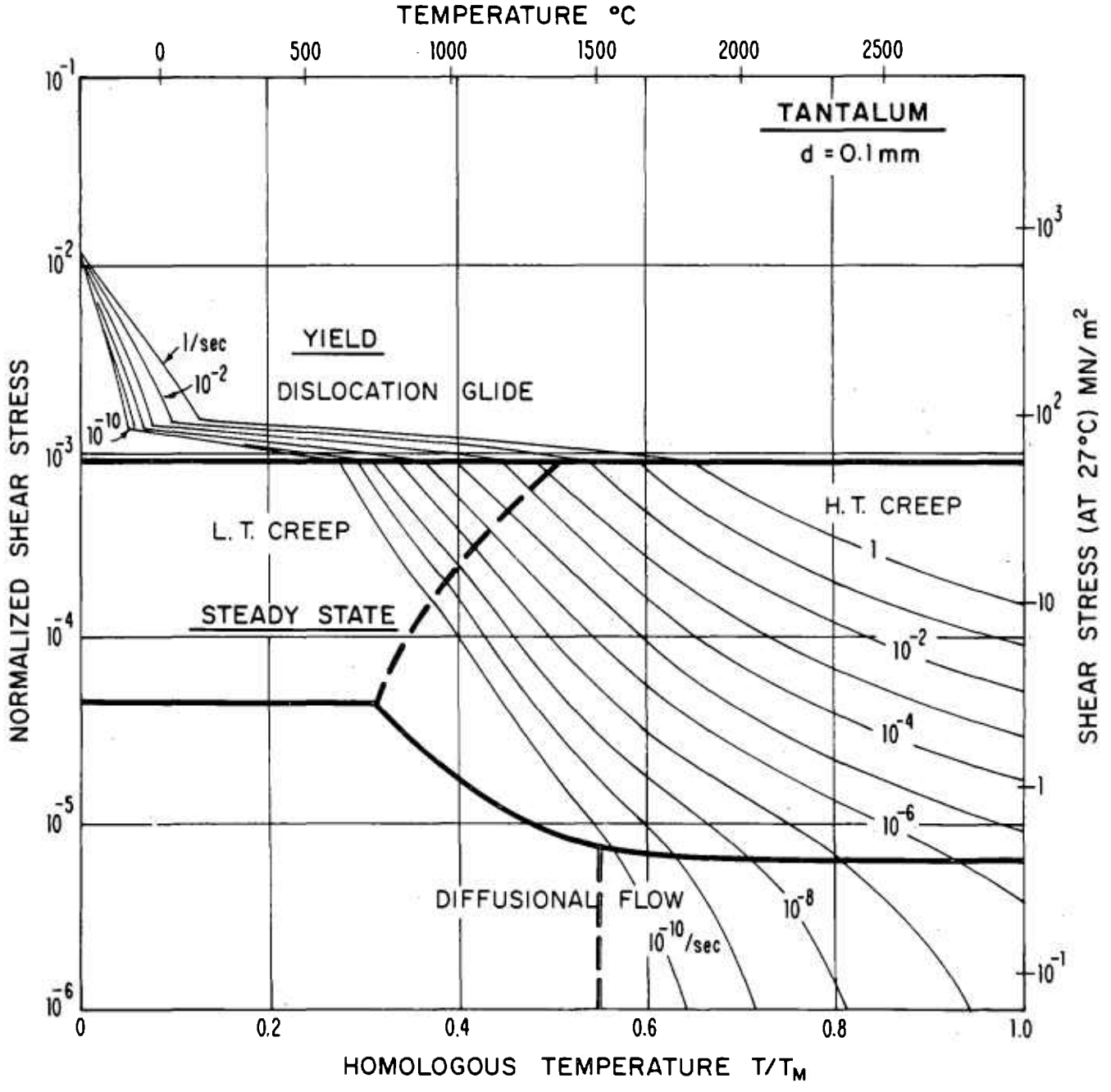

Fig. 13a) Tantalum of grain size 0.1mm.

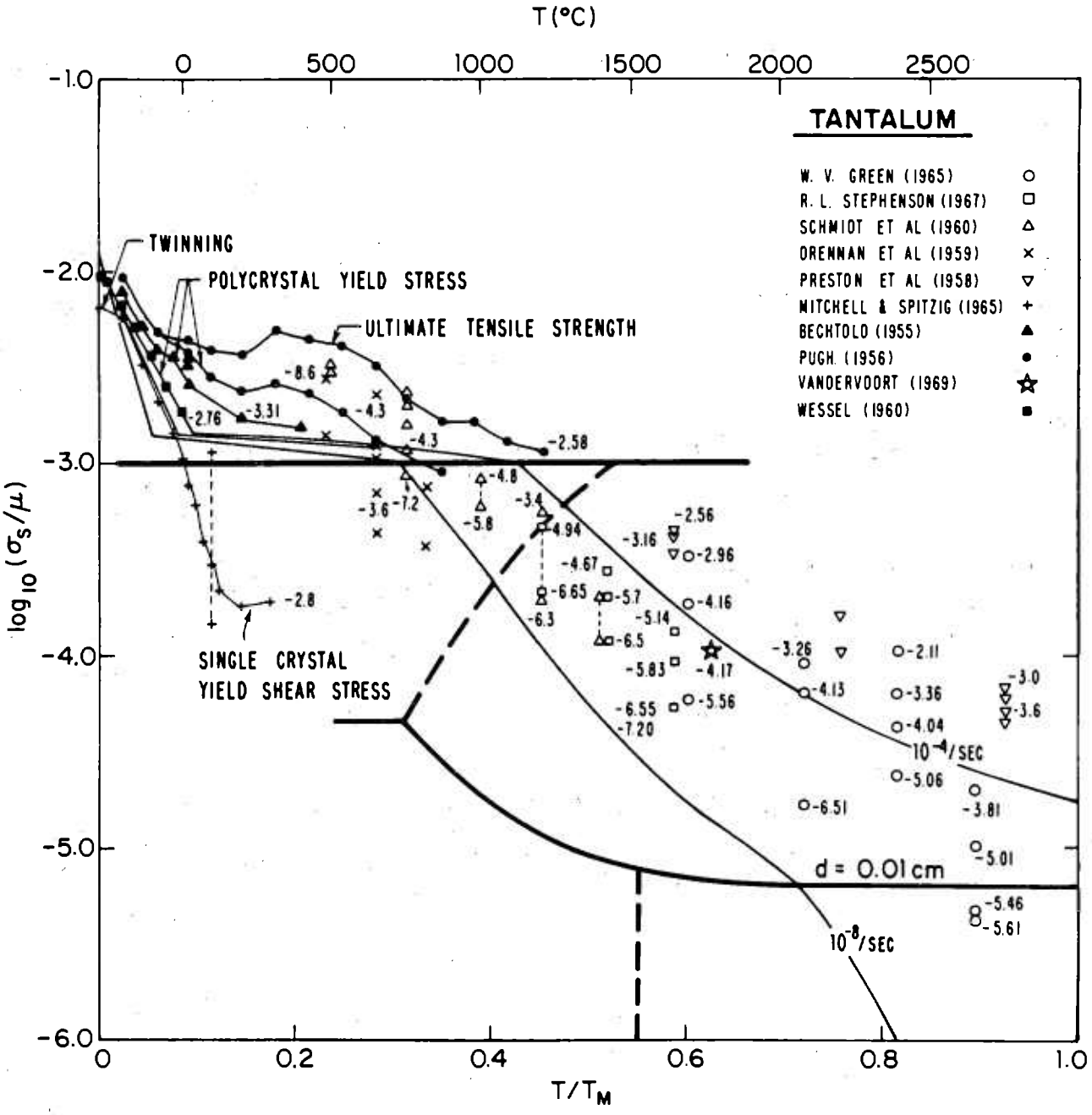

Fig. 13b) Tantalum experimental data.

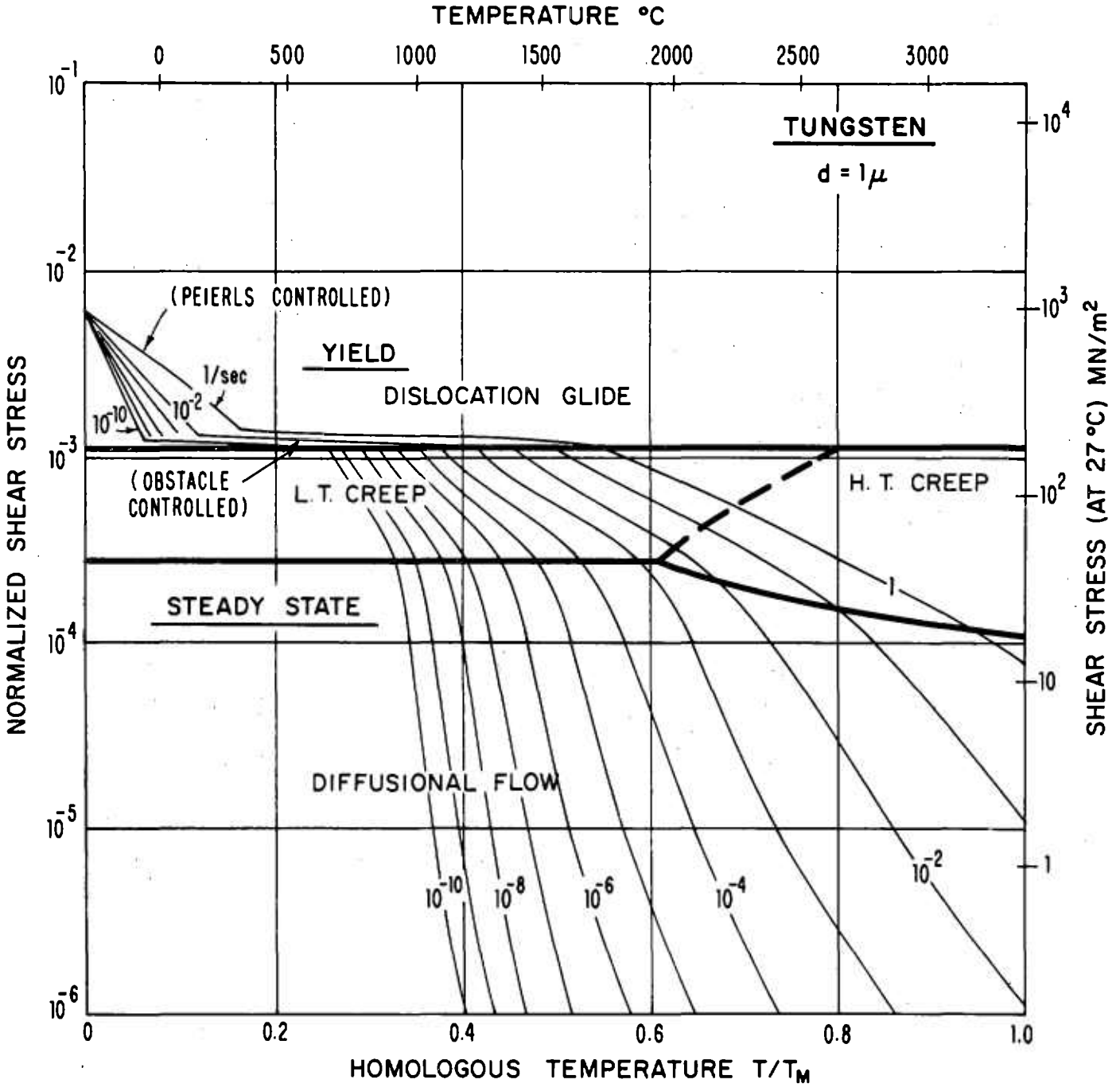

Fig. 14a) Tungsten of grain size 1μ.

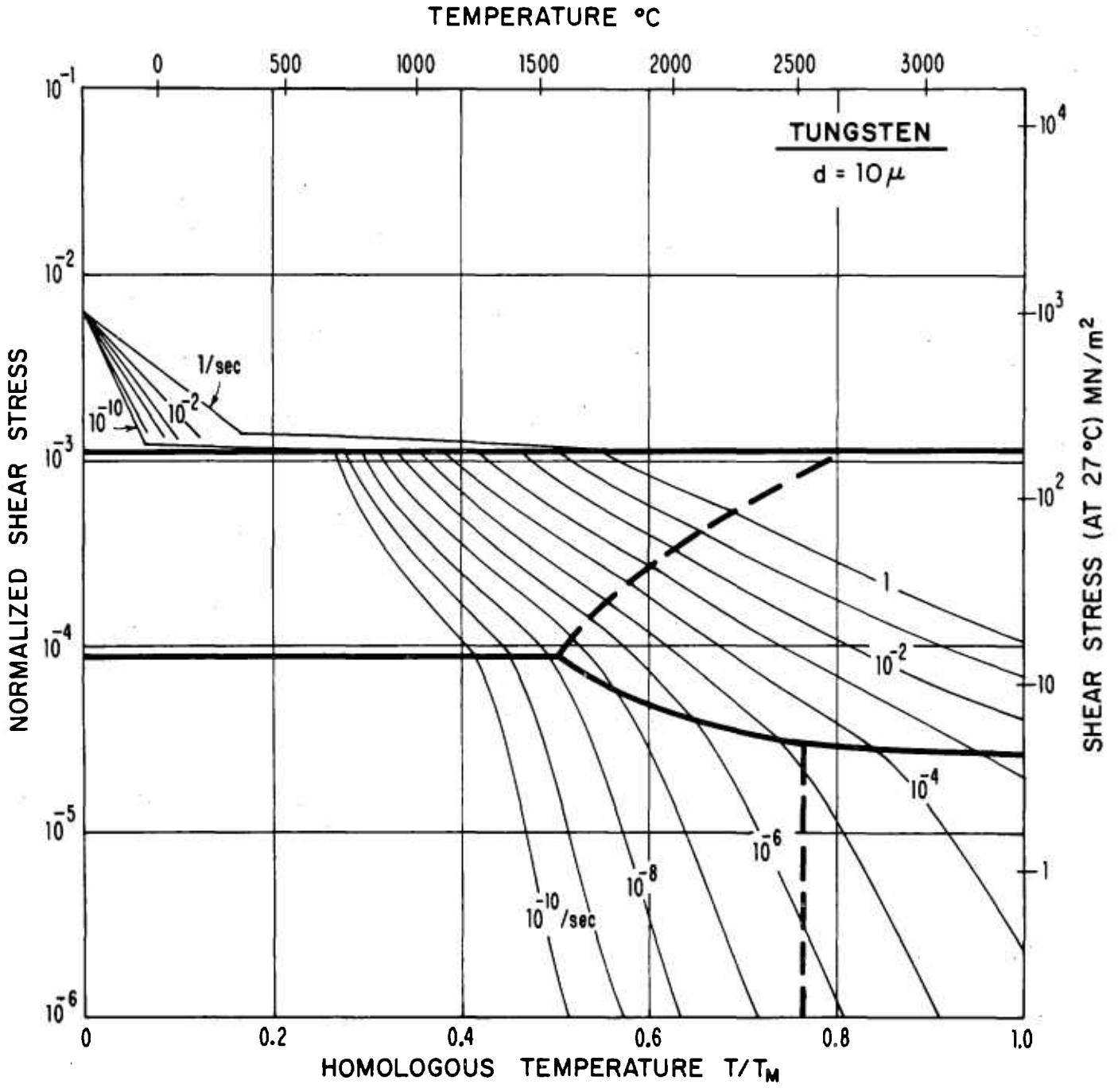

Fig. 14b) Tungsten of grain size 10μ.

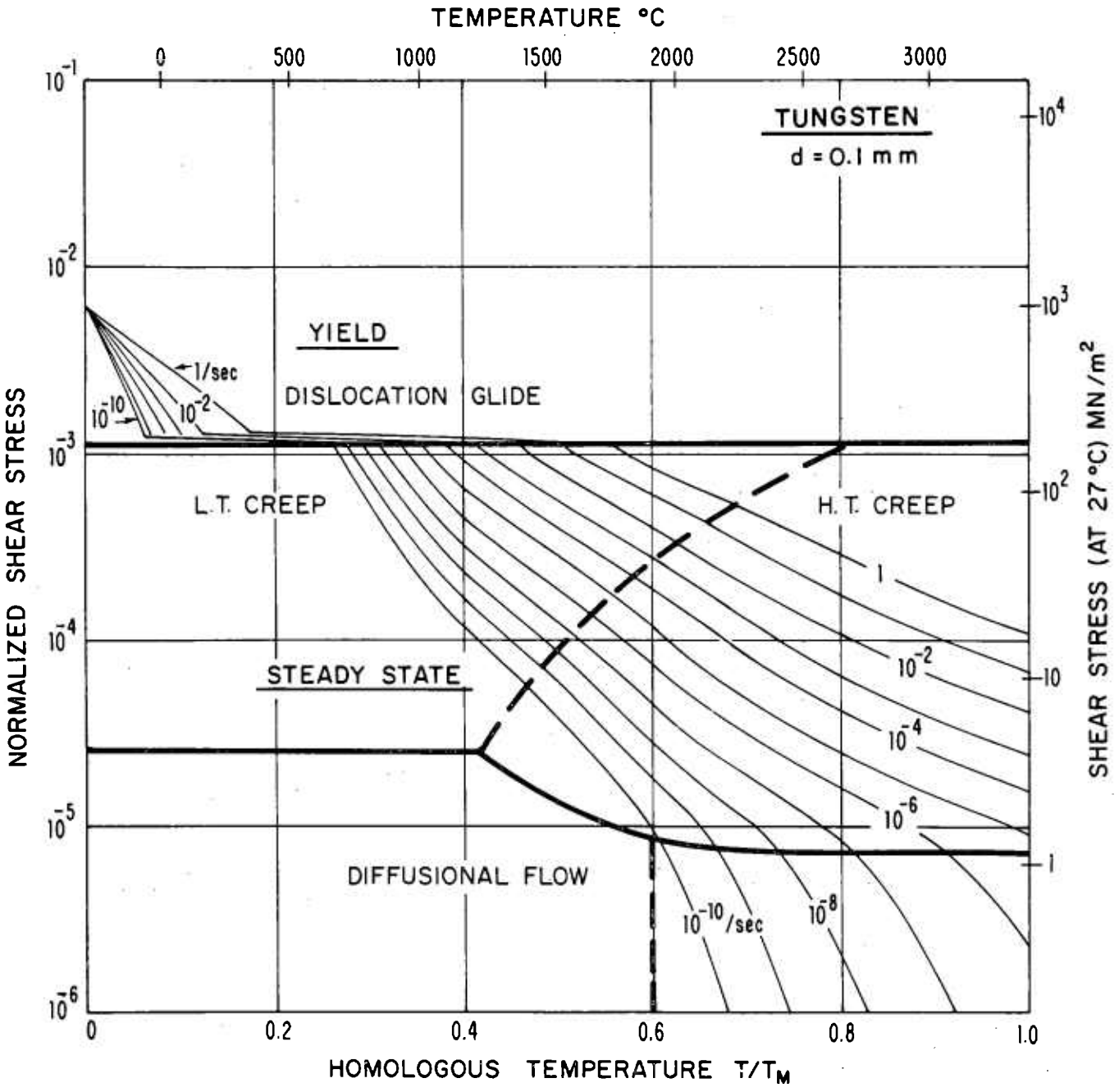

Fig. 14c) Tungsten of grain size 0.1mm.

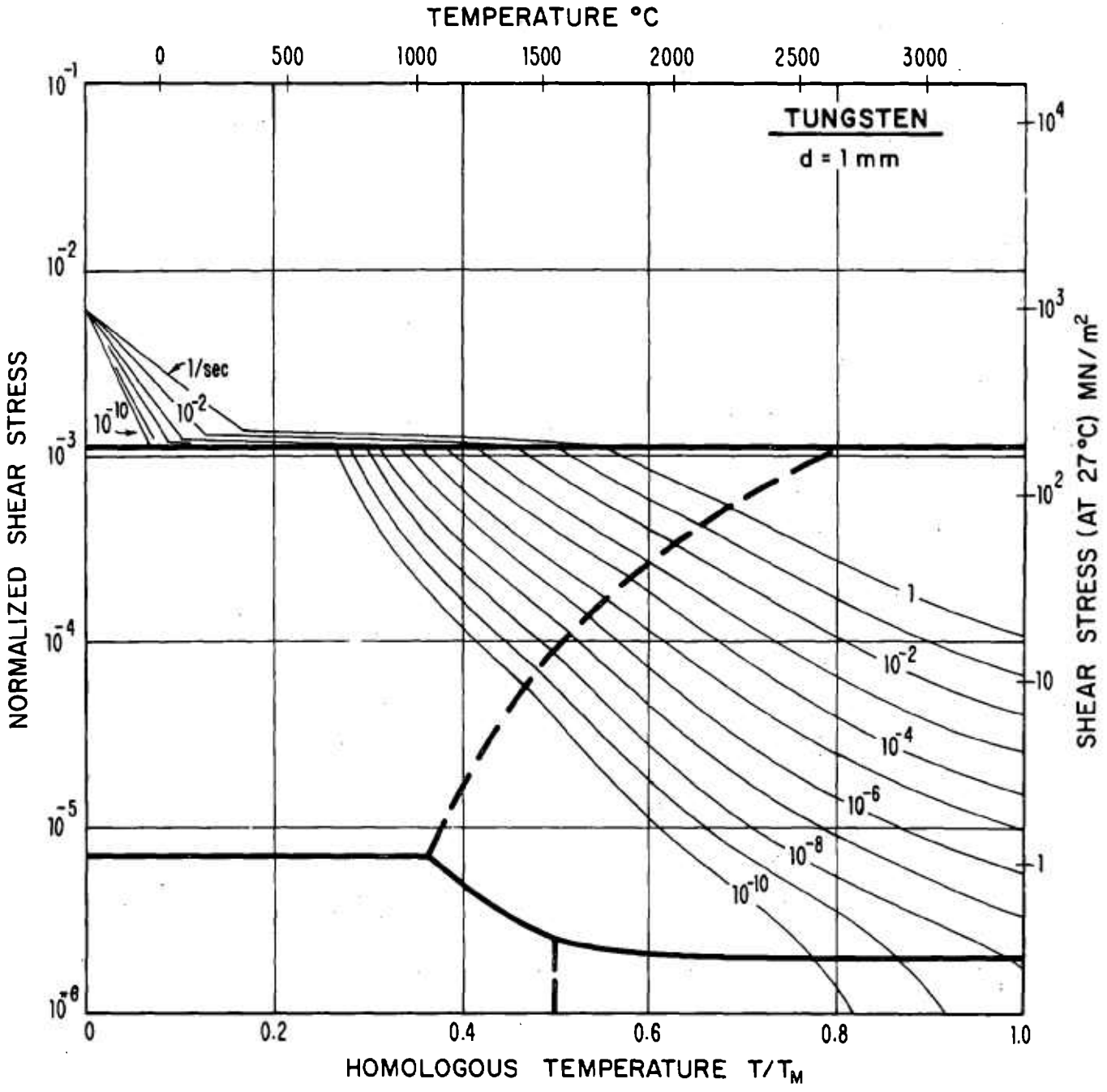

Fig. 14d) Tungsten of grain size 1mm.

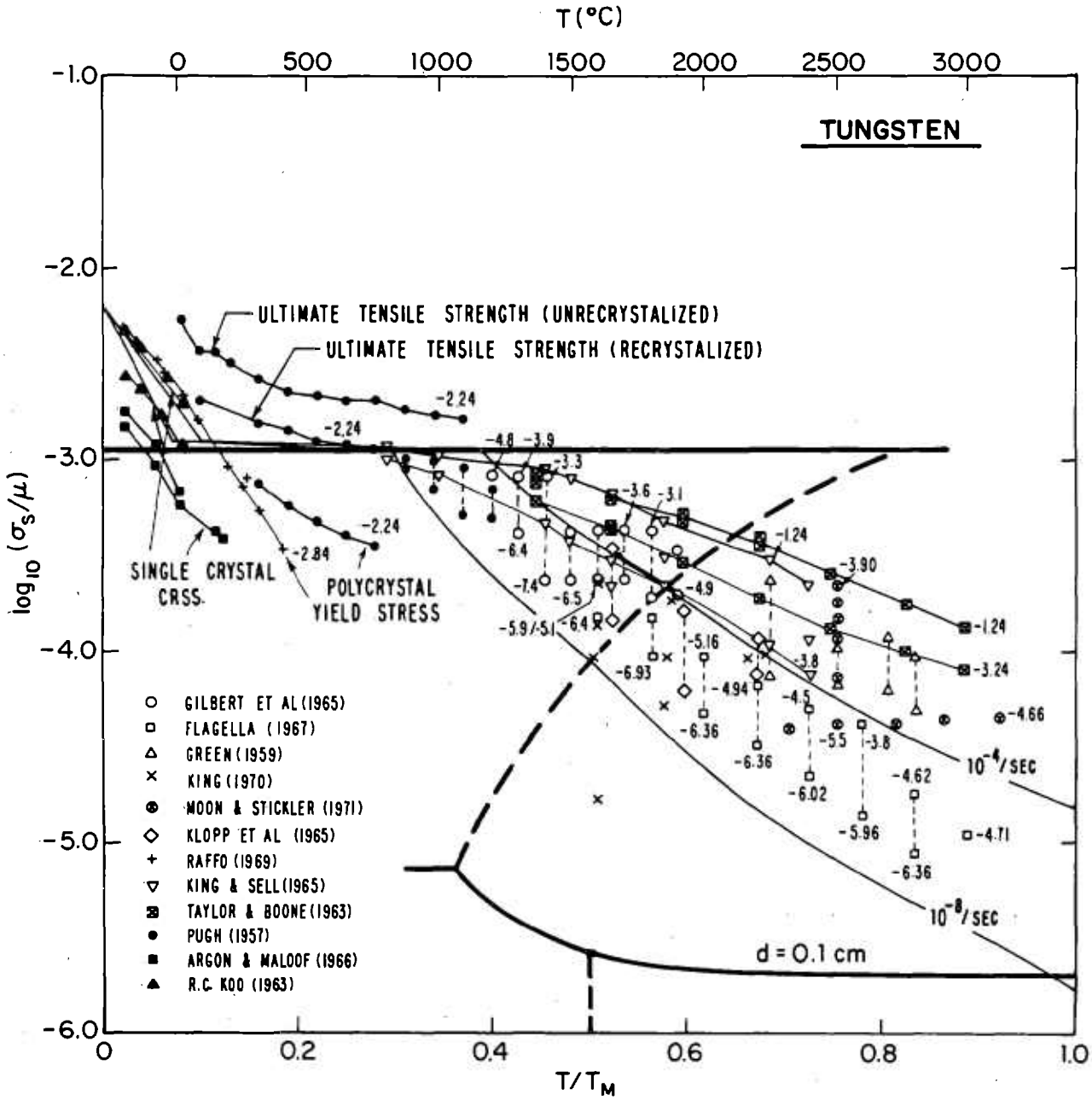

Fig. 14e) Tungsten experimental data.

5. DISCUSSION

Deformation mechanism maps have several important uses. First, they provide an excellent means by which the complicated relations between different deformation mechanisms can be presented and visualized. This depends, of course, on the accuracy with which the maps describe plastic behavior, which is, in turn, governed by the limitations imposed by the simplifications and assumptions that are required. Second, they provide a graphic means for the direct and easy comparison of experiment with theory, of different experiments one with another, and of the behavior of different materials or groups of materials. Finally, the maps provide a qualitative method for the selection of a material for engineering applications, the prediction of the mechanisms by which the sample or structure deforms, and the prediction of the effects of strengthening mechanisms. The following discussion will treat each of these points in turn.

5.1 General Accuracy

Within the limitations of steady-state or constant-structure formulations, the deformation maps in the major mechanism fields are as accurate as can be determined from available experimental data. There remain, however, several regions and mechanisms which are not presently well understood. Figure 15 shows qualitatively where some of these lie on a map for nickel. Some of the difficulties involved in describing twinning and the power-law (high stress) breakdown region have been discussed in section 2. The region

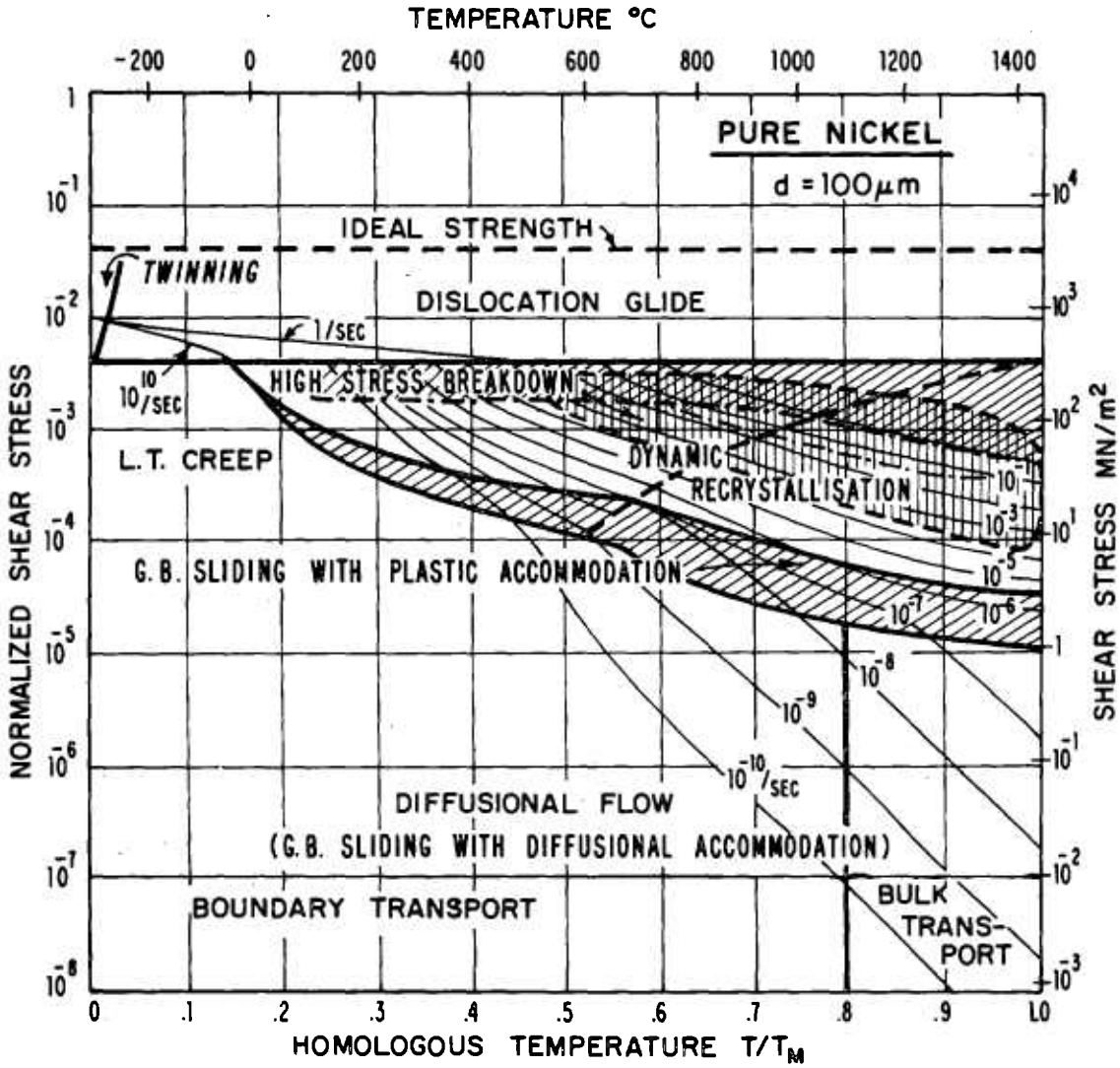

Fig. 15) Map for nickel with a grain size 100μm, showing the approximate regions in which twinning, grain-boundary sliding accommodated by power-law creep, the high stress power-law breakdown, and dynamic recrystallization occur.

of dynamic recrystallization is difficult to delineate because the ease of recrystallization depends on the purity. This may in fact account for much of the reported dependence on purity in the dislocation creep fields. Although recrystallization may provide an additional means of recovery to dislocations, we are uncertain whether the kinetics would be radically changed. The behavior may be that of repeated primary creep, similar to, but faster than, steady-state dislocation creep. The region of grain boundary sliding accommodated by plastic flow (dislocation creep within the grains) is definitely an expected coupled mechanism. We do not yet have a sufficiently accurate model to include on the maps, but the effect on the strain-rate should not be great.

The use of steady-state flow and constant-structure yield formulations is the major limitation on the maps in presenting a complete view of plastic deformation behavior. Steady-state flow is an accurate representation of diffusional creep (without grain growth or recrystallization). For dislocation creep, however, the steady-state formulation neglects primary and tertiary creep entirely. It also neglects logarithmic creep (which may be considered an extended primary creep). It would be possible to include primary creep by presenting a series of maps showing the cumulative strain at various times. The added dimension of time greatly increases the complexity. The parameters describing primary creep are known for only a few circumstances. In addition, the primary creep behavior depends on the initial dislocation structure; different studies will generally use material with different initial structures (different degrees of annealing). Within one

study, the initial structure may differ at different test temperatures because of recovery. For these reasons our maps are limited to the well known steady-state creep behavior.

Tertiary creep would also be difficult to characterize. The behavior of creep rupture from void growth and coalescence occurs in tension, but not in compression, and therefore does not represent general plastic behavior. The onset of tertiary creep also depends on void nucleation and growth, which would require the specification of additional parameters (e.g. the number and size of grain boundary second phase inclusions). Although we have neglected tertiary creep, it may often provide a problem in comparing experiments. A tensile creep experiment that shows no prolonged steady-state behavior may represent tertiary behavior starting before primary creep has ended. In this case, the reported minimum strain-rate may not be steady-state strain-rate.

For the dislocation glide field, the constant structure yield formulation does not allow a description of work-hardening behavior. Such behavior could be described by a series of maps showing the stress reached at various times for various constant strain-rates. This description differs from the one most appropriate for primary creep, providing further complications. We have, therefore, not included work-hardening.

5.2 Material Comparisons

Deformation mechanism maps provide a convenient method of making various comparisons: comparing experiment to theory, comparing materials

within a group of similar crystal structure and bonding, or comparing different groups of materials. The comparative use of various types of plots is certainly not original to this paper. The contribution of our approach is that experiment can easily be compared to a number of possible mechanisms if the data is specifically plotted according to its stress-temperature location. The important case for this study is within the dislocation creep field.

Many studies (though not all) have derived empirical creep parameters with little regard for the stress-temperature location of the data. With our method of plotting, we have found a generally consistent variation of parameters with stress and temperature that is consistent with the low/high temperature creep transition described in section 2.4a. In a similar manner, we expect that the power-law breakdown region will be described differently at high and low temperatures. Our experimental comparisons have also been useful in providing an understanding of how accurate our knowledge of material behavior actually is. Once we have formulated material behavior into accurate maps, we may make informative comparisons between materials within a group of similar crystal structure and bonding or between such groups. All the maps shown in section 4 are for two very similar groups: pure f.c.c. and pure b.c.c. metals. The mechanical properties of other groups, such as alkali halides, metal oxides, and carbides, is generally less well known. Although we may expect the same basic deformation mechanisms to operate, direct comparison is beyond the scope of this paper. From the maps we have presented, however, we may make the following informative conclusions.

5.2a F.C.C. comparisons

All maps shown thus far have a linear temperature scale normalized with respect to the melting temperature, and a logarithmic stress scale normalized with respect to the shear modulus. This permits a logical method of comparison. The f.c.c. maps should all be identical to the degree that the mechanical behavior can be described by crystal structure, the melting temperature and the shear modulus. This comparison can be demonstrated directly. Figure 16 shows the strain-rate contour for $\dot{\gamma} = 10^{-8}$/sec and grain size d = 100μm for the f.c.c. metals on un-normalized temperature and stress scales. Fig. 17 shows the same contours plotted on normalized scales. (These plots do not include Harper-Dorn creep or power-law breakdown). The great divergence is reduced but not eliminated.

In Fig. 18 we add three further normalizations. Because both dislocation creep and diffusional creep depend on self-diffusion, we compare strain-rate contours that are normalized with respect to melting point diffusivity. In dimensionless form, we use

$$\dot{\gamma} = \frac{10^{-14} D_v(T_M)}{b^2} .$$

The logical dimensionless normalization for the grain size is the Burgers' vector; we use $d = 4 \times 10^5 b$. For dislocation glide our important input parameter is the dislocation density (or obstacle spacing). This may also be normalized with respect to the Burgers' vector as:

$$\rho = \frac{2.5 \times 10^{-5}}{b^2} .$$

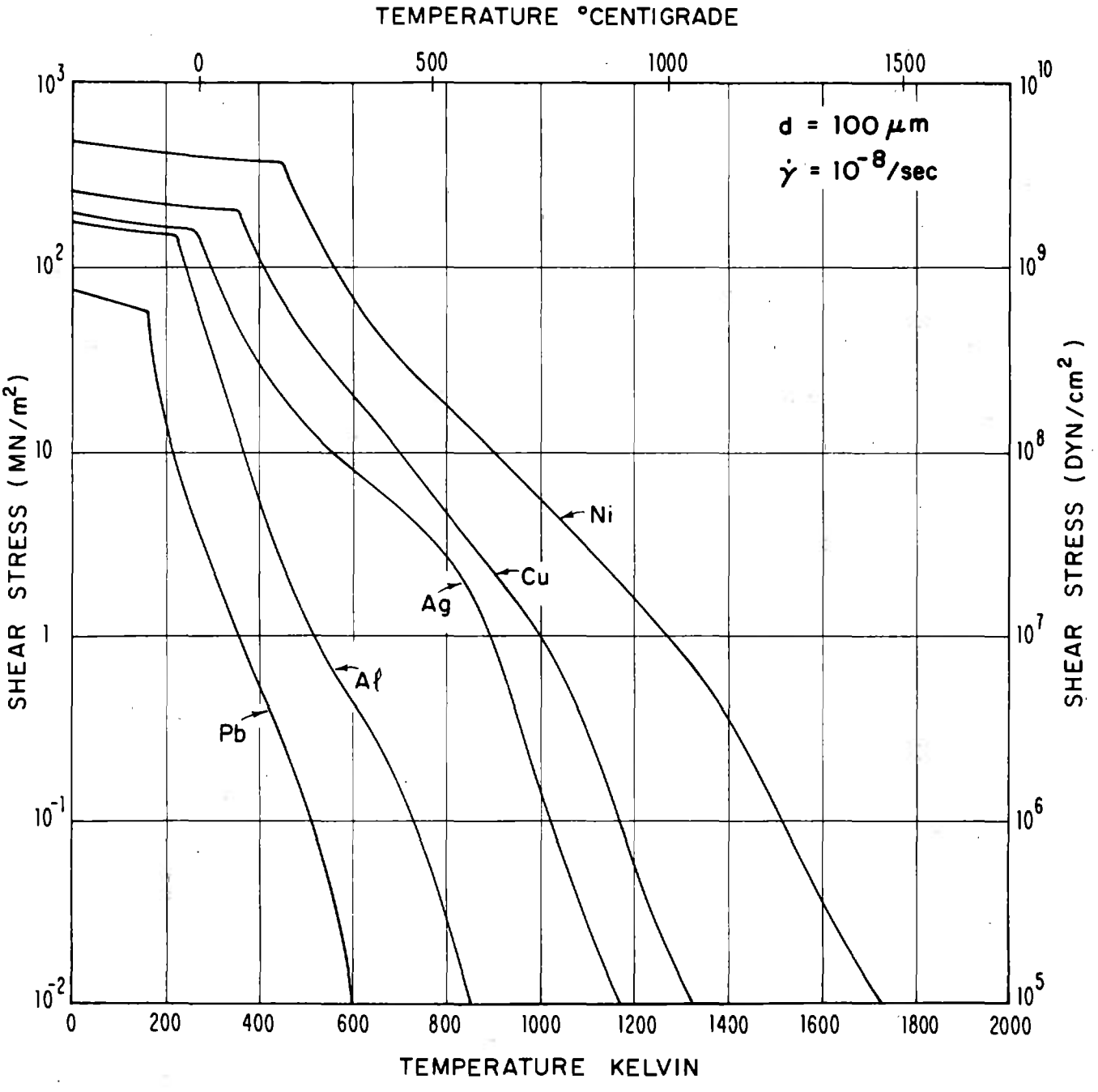

Fig. 16) Contours of $\dot{\gamma} = 10^{-8}$/sec for five f.c.c. metals on unnormalized stress and temperature scales; grain size = 100μm.

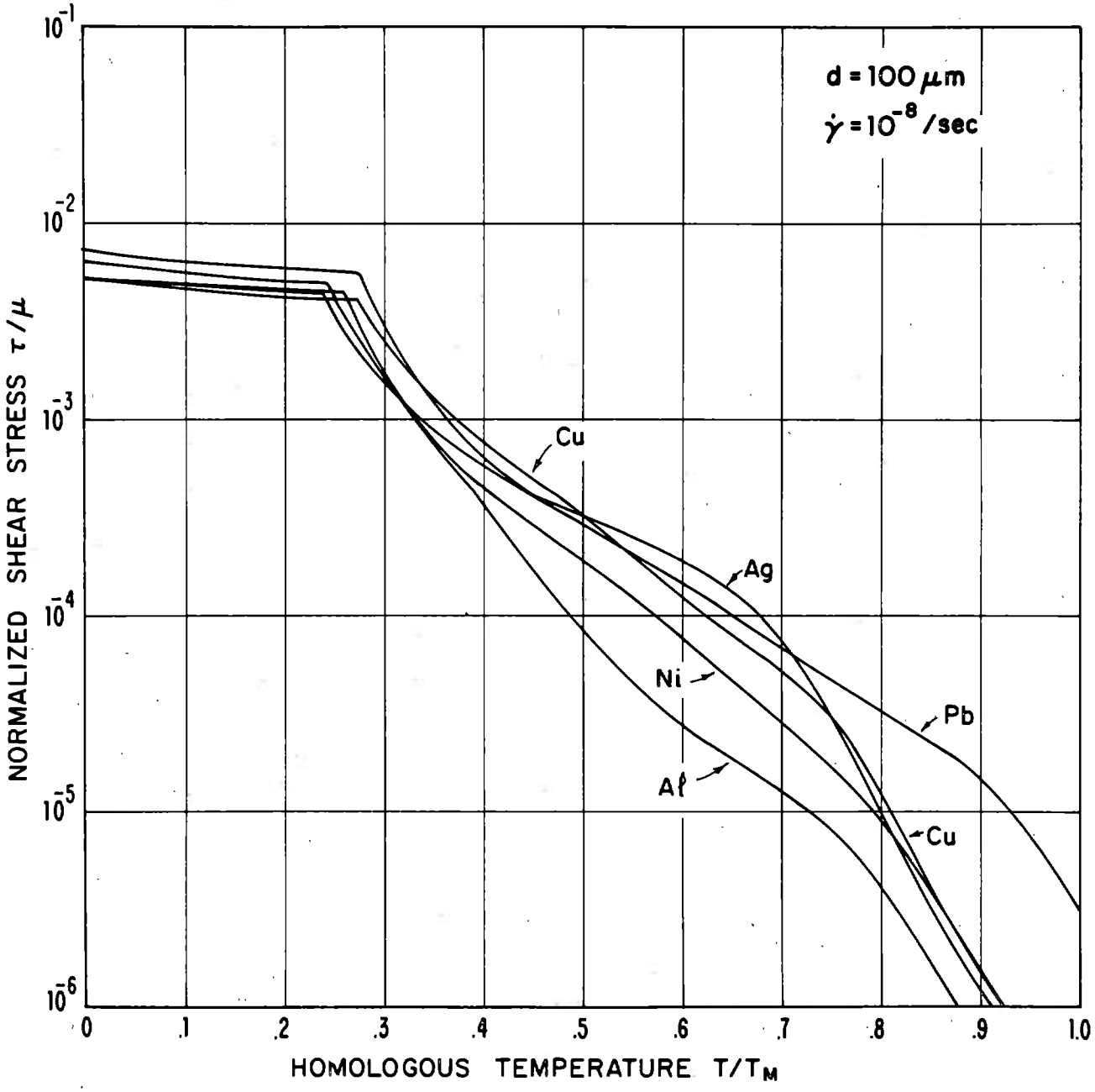

Fig. 17) Contours of $\dot{\gamma} = 10^{-8}$/sec for five f.c.c. metals on the usual normalized stress and temperature scales; grain size = 100μm.

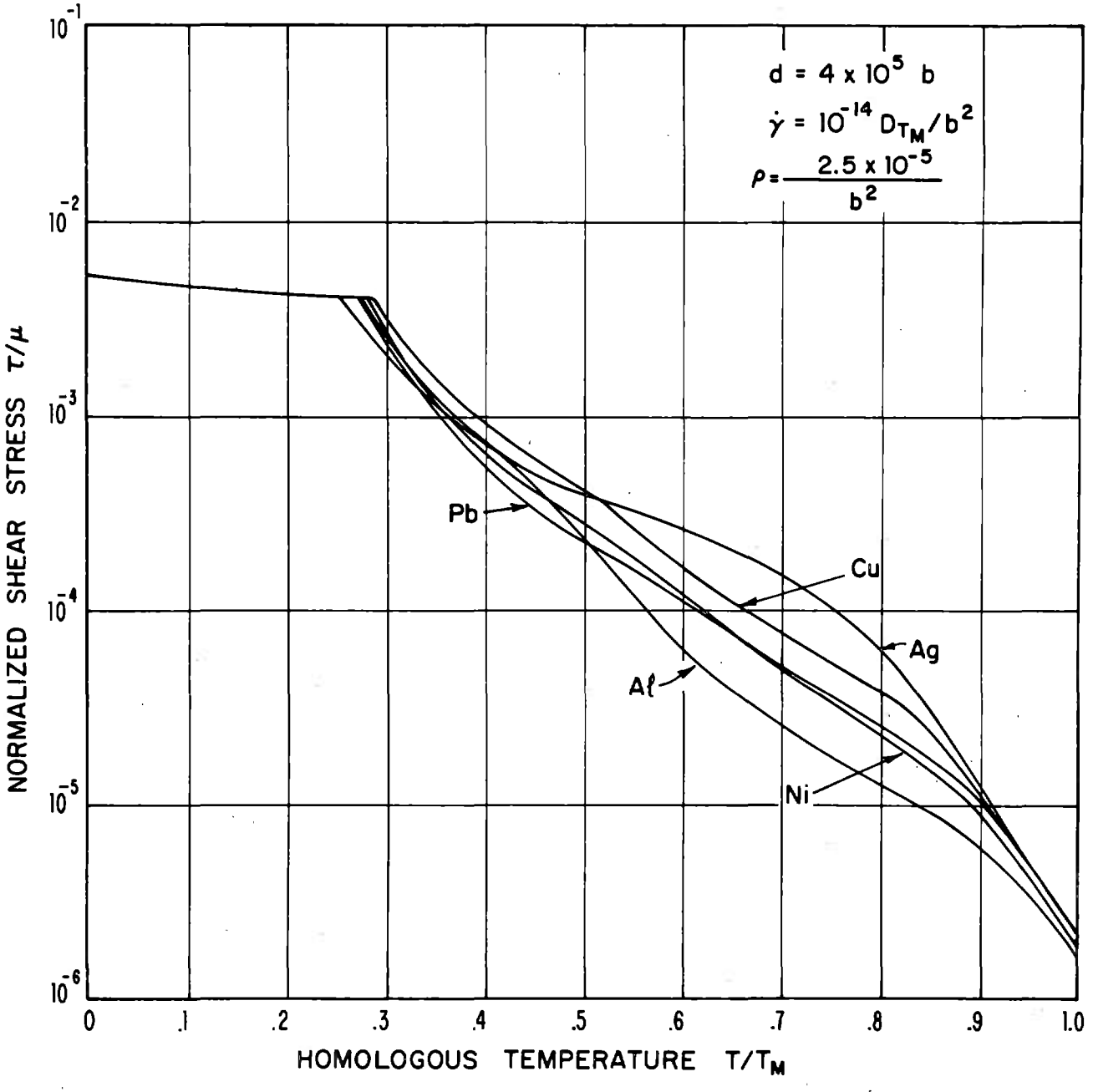

Fig. 18) Contours of $\dot{\gamma} = 10^{-14} D_{T_M}/b^2$ for five f.c.c. metals on the usual normalized scales, with the furteer normalizations of grain size = $4 \times 10^5 b$ and $\rho = 2.5 \times 10^{-5}/b^2$.

Using these normalizations, the contours for the dislocation glide region coincide: this is a direct result of our glide rate-equations. At the highest temperature in the Nabarro-Herring creep region, the contours are also closely bunched. The remaining divergence is in the power-law creep region.

It has been shown that the normalized high temperature creep strength of the f.c.c. metals increases as the stacking-fault energy decreases (see, for instance, Barrett and Sherby, 1965). This is exactly the effect shown in this figure: the order of contours (Al, Ni, Pb, Cu, Ag) matches the order of the stacking-fault energies. It may be added that this divergence of normalized contours is substantially greater than the experimental error involved in constructing the maps, and therefore represents a real material property.

Although the stacking-fault energy effect is well demonstrated, we do not believe that the accuracy of the maps justifies an independent determination of the exact form of this dependence. We can, however, point out that the stress exponent, n, does not correlate with the stacking-fault energy as has been suggested (see Bird et al, 1969). n is roughly adjustable between 4 and 5 for all pure f.c.c. metals, and will differ between different studies of each metal.

There are only a limited number of ways that we would expect normalized f.c.c. metals to differ. The primary one is, of course, the stacking-fault energy. The second difference is the dislocation core diffusion coefficient (as compared to volume diffusion). This should be related to stacking-fault energy through spacing of partials. The effect should

dominate in the low temperature creep field. The limited measurements of core diffusion do not really allow the effect to be investigated. Other properties, such as the degree of elastic anisotropy, probably have little effect.

5.2b B.C.C. comparisons

Figures 19 and 20 show comparative plots for the b.c.c. metals, similar to those shown for the f.c.c. metals. In this case the divergence found in the unnormalized plot (Fig. 19) is substantially eliminated in the stress and temperature normalized plot (Fig. 20). In the Peierls barrier-controlled yield region, there is a distinct difference between the group $\overline{V}$a metals (V, Nb and Ta) and the $\overline{VI}$b metals (Cr, Mo and W); the former show higher normalized Peierls stresses, and the lower values of ΔF_k (hence the steeper temperature dependence). This behavior has been pointed out previously by Bechtold et al (1960). In the creep region the correlation is very close for Cr, Mo and W: closer than the experimental error involved. The deviations of Ta, Nb and V are noticeable, but not great. Because the divergence in Fig. 20 is small (comparable to experimental error), we would not expect further normalizations to provide any better correspondence. This is especially true because the melting point diffusivities are approximately equal and not precisely known.

5.3 Design Applications

Deformation mechanism maps provide a means of demonstrating the effects of various changes in materials. This may be helpful in choosing

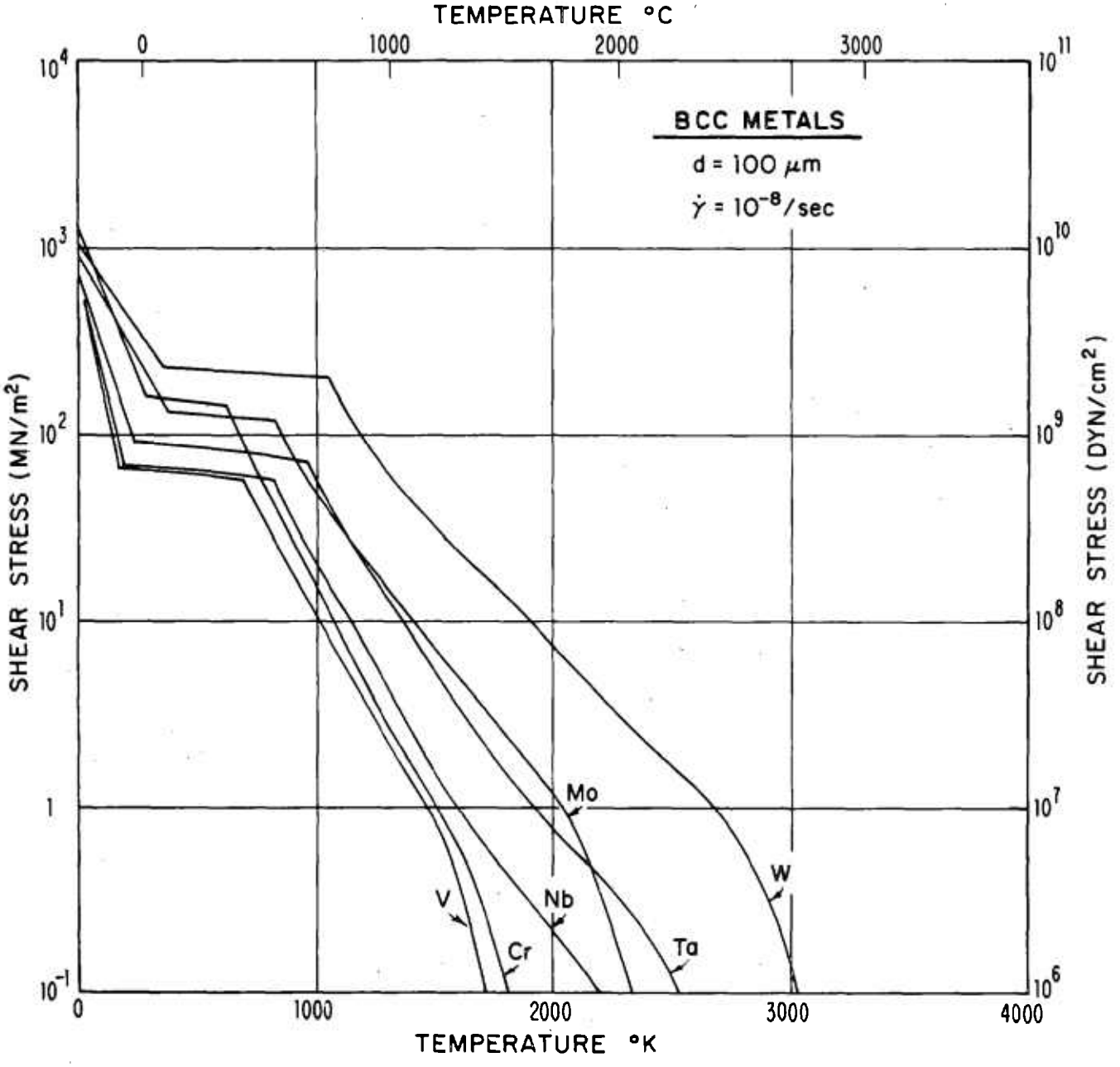

Fig. 19) Contours of $\dot{\gamma} = 10^{-8}$/sec for six b.c.c. metals on unnormalized stress and temperature scales; grain size = 100 m.

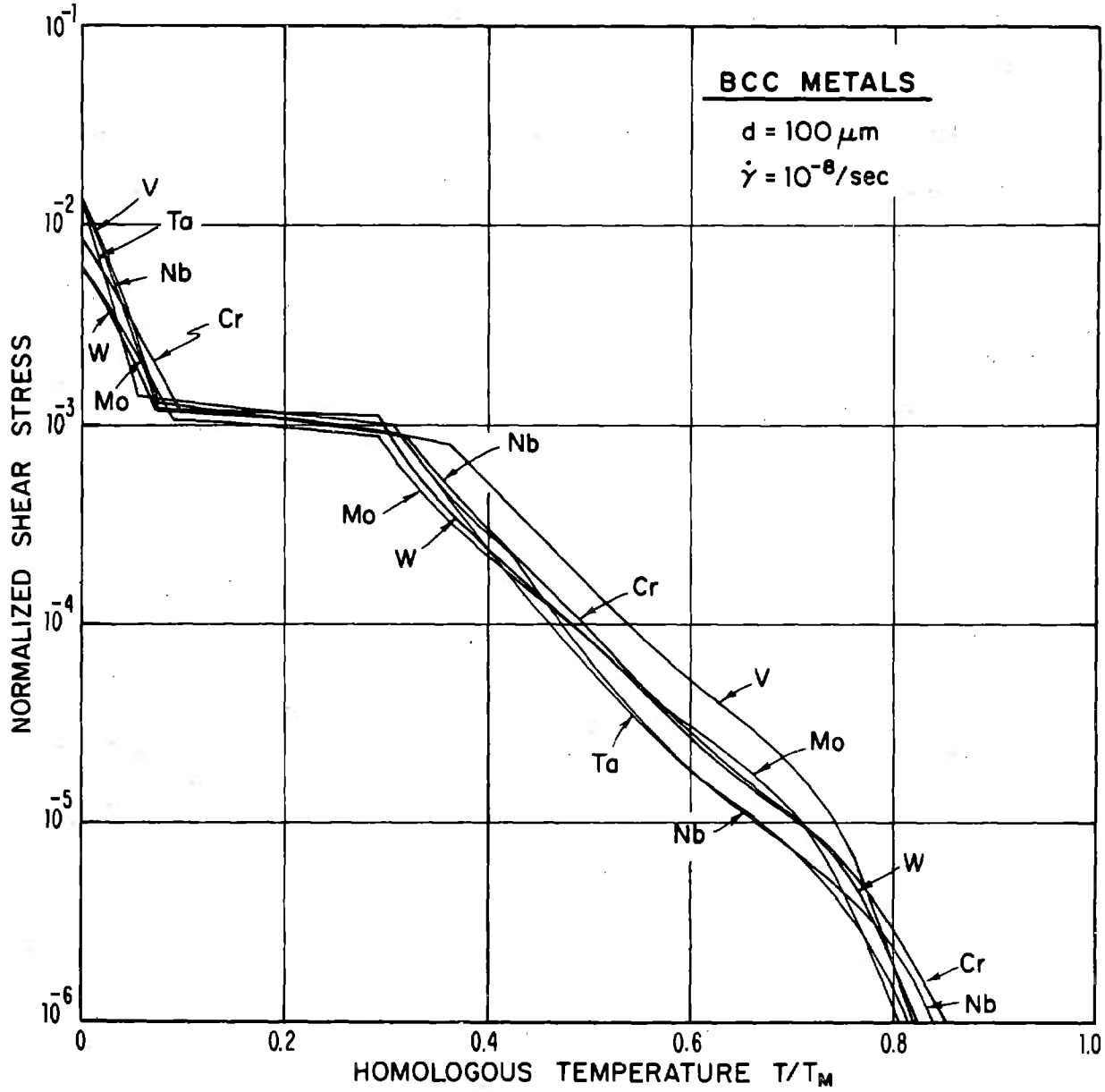

Fig. 20) Contours of $\dot{\gamma} = 10^{-8}$/sec for six b.c.c. metals on the usual normalized stress and temperature scales; grain size = 100 m.

materials for applications, even though the maps are not sufficiently accurate for engineering design. In this regard it is useful to have an idea of the areas of a map that are accessible to experiment, and the areas to which materials are exposed in practice. Fig. 21 shows these areas on a map for nickel, with shaded regions showing the actual scope of published creep and hot torsion tests. Also shown are regions of conventional cold and hot-working processes, the region in which a material is used for structural applications ($\dot{\gamma}$ < 1% per year), and, as a lower limit of interest, the region encountered in slow geophysical deformation processes ($\dot{\gamma} > 10^{-14}$/sec). This figure illustrates the important point that the areas of stress/temperature space which are most studied by laboratory experiments are often those which are least encountered in the forming, or in the applications, of materials. The mechanisms identified in the lab tests may not be those that are dominant in use. For this reason, our method of displaying the combined effects of many mechanisms is a useful one. Among the many desired design properties of materials, the maps describe only the resistance to yield or steady-state flow. This property is generally at its worst in pure metals (all maps of section 4) and various strengthening mechanisms are incorporated into almost all structural materials. To be useful, the strengthening mechanism must be effective against the deformation mechanism that dominates at the stress and temperature of service. For these purposes, the different deformation mechanisms are dislocation glide, dislocation creep, and diffusional creep. Strengthening mechanisms for one may have no effect on the others. For

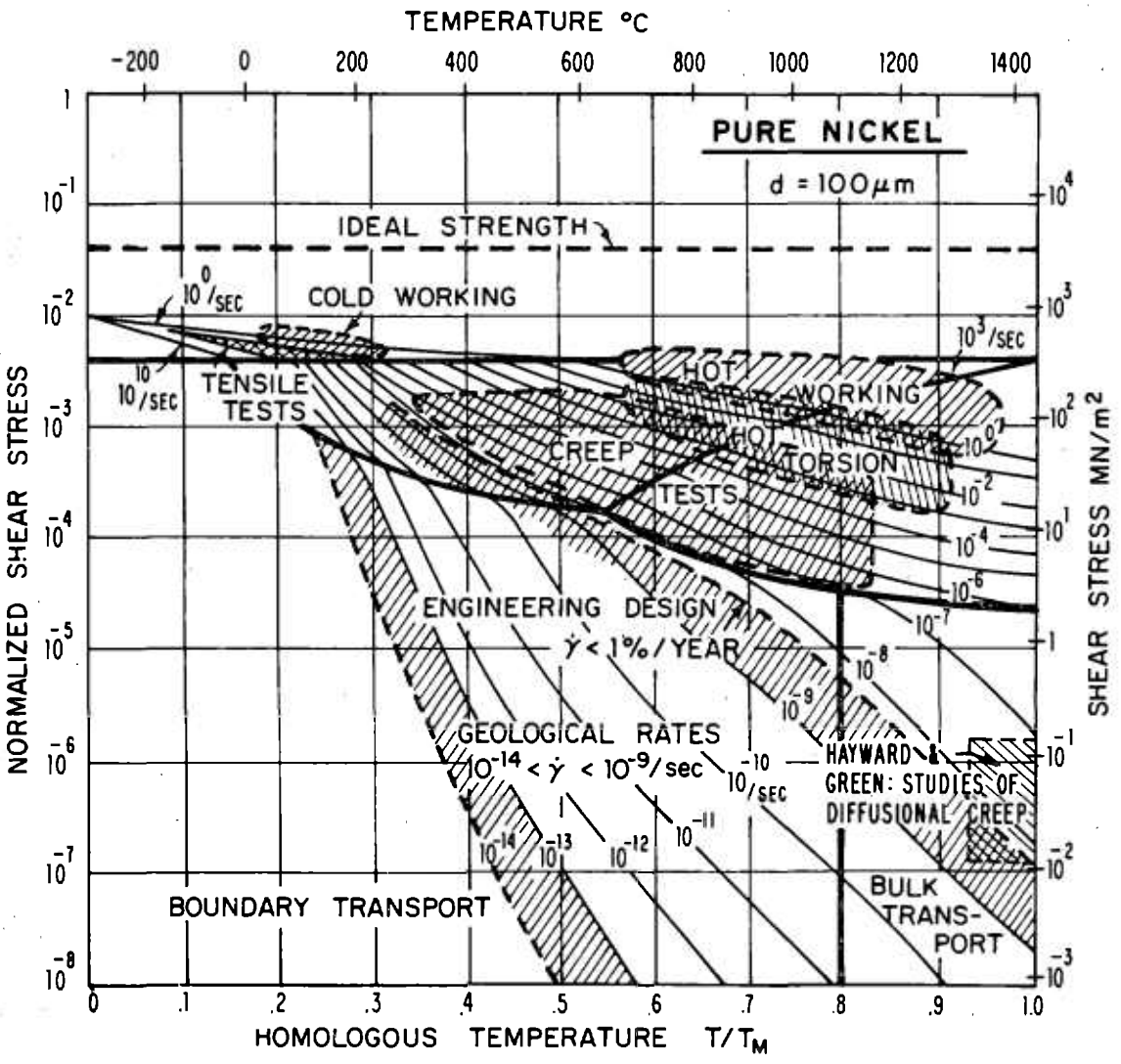

Fig. 21) Map for nickel of grain size 0.1mm, showing the areas in which creep and hot torsion tests have been carried out, and the areas in which materials are formed and used in engineering design.

example, the simplest means of strengthening against diffusional flow is to increase the grain size. This will have little effect on the steady-state dislocation creep, and will probably lower the low temperature dislocation glide flow stress. Similarly, increasing the dislocation density by work-hardening strengthens against dislocation glide, but will have little effect on high temperature creep because the dislocations will anneal out.

A full presentation of the different strengthening mechanisms available is beyond the scope of this paper. We have, however, prepared one simple example. Figure 22 shows a map for a recrystallized Ni — 1 vol% ThO_2 alloy, based on the creep data of Wilcox and Clauer (1969). The ThO_2 is a stable dispersion of average particle diameter 2.2×10^{-6}cm, and a mean planar center to center spacing 2.505×10^{-5}cm. (Grain size 0.1mm is assumed). Although we do not have an accurate theory for climb-controlled creep in such a structure, we can determine experimental parameters for our dislocation creep standard equation: $n = 8.0$, $A = 5.0 \times 10^{15}$. Diffusion coefficients, modulus, etc are assumed to be the same as for pure nickel. For the dislocation glide field, we have used the initial Orowan stress based on the particle spacing. This is lower than the yield stress for work-hardened pure nickel, but the alloy would work-harden very quickly when deformed. Diffusional creep is assumed to be the same as for pure nickel.

As can be seen by comparision with Fig. 4c, the dispersion greatly inhibits dislocation creep and contracts the field. At this assumed

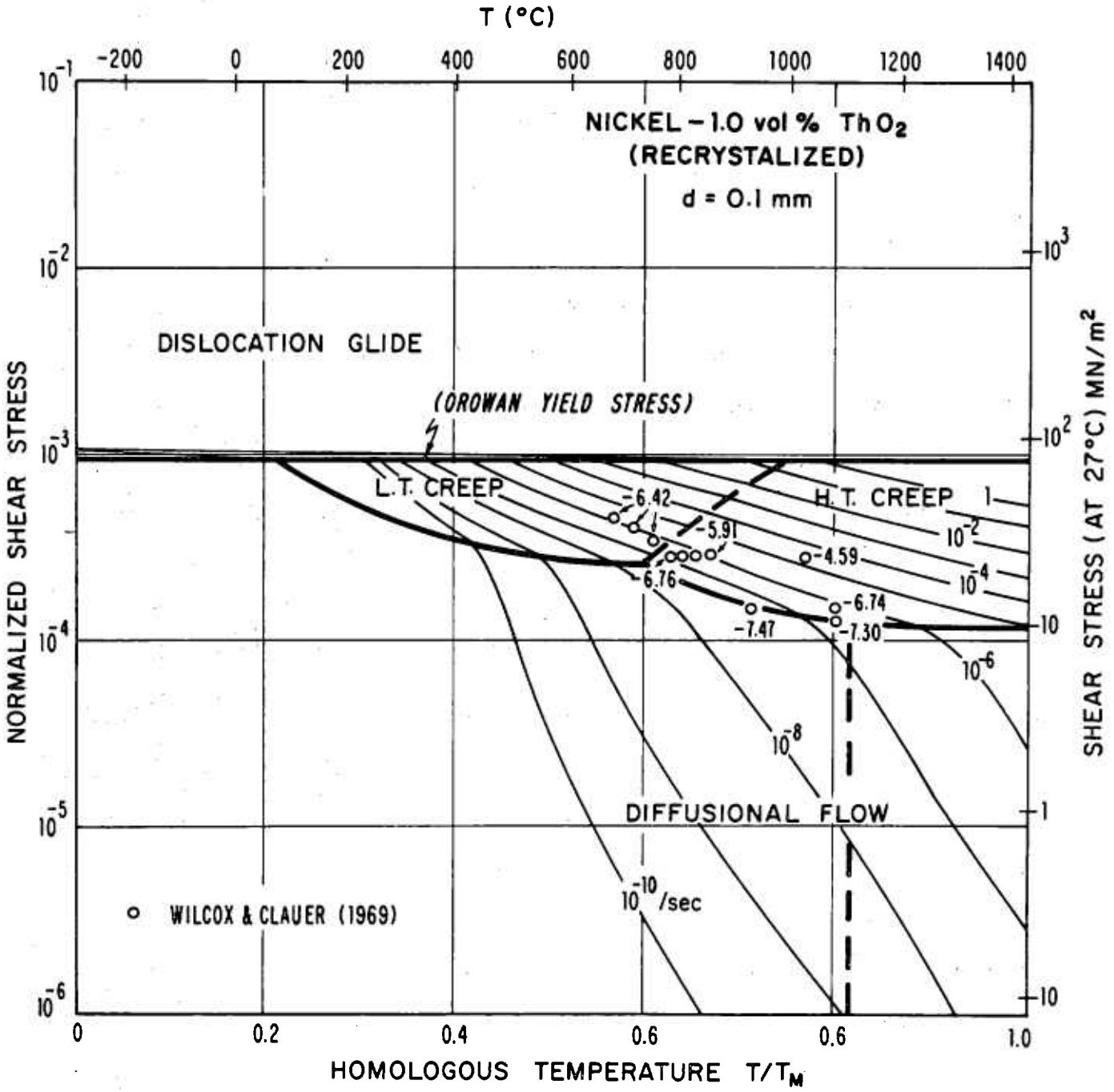

Fig. 22) Map for a nickel — 1.0 vol% ThO_2 alloy, recrystallized to a grain size of about 0.1mm. The dislocation creep field is based on the plotted data of Wilcox and Clauer (1969). The dislocation glide field is based on the Orowan yield stress for a mean planar particle spacing of 2.5×10^{-5}cm.

grain size, diffusional creep now becomes an important mechanism to consider, since it becomes dominant at stresses slightly lower than the plotted data. We can clearly see that extrapolation of the creep data to low stress at high temperatures would not be adequate for design purposes.

6. SUMMARY

1) Deformation maps can be constructed which show fields of stress and temperature in which several different deformation mechanisms are dominant. Strain-rate contours on these maps provide a representation of the stress—temperature—strain-rate relationship.

2) We have constructed such maps for five f.c.c. and six b.c.c. metals, arriving at an optimized set of input data by careful comparison with a mass of experimental data. By this procedure, maps can be constructed which depict farily accurately the steady-state mechanical behavior of the metal in question.

3) Maps for pure metals of similar structure (on normalized stress and temperature scales) are strikingly similar. Further normalizations can be used to make them almost superimpose. For f.c.c. metals, the residual differences are predominantly due to the stacking-fault energy. For the b.c.c. metals studied, the residual differences are of the general order of magnitude of the experimental uncertainty.

4) Maps for engineering materials can be constructed. As an example, one for a recrystallized Ni — 1 vol% ThO_2 alloy is presented in the text. The maps are useful for design under certain conditions, particularly when

they indicate that a change of mechanism may occur between the region of experimental observation and the region of design application.

ACKNOWLEDGEMENTS

This work was supported in part by the Office of Naval Research under Contract N00014-67-A-0298-0020, in part by the National Science Foundation under Contract NSF-GH-33576, and by the Division of Engineering and Applied Physics, Harvard University. We wish to acknowledge the valuable contribution of Dr. U.F. Kocks and Prof. A. Argon, who made a number of their unpublished results and ideas available to us, and the advice and help of Prof. B. Chalmers and Prof. D. Turnbull.

TABLE 1: MATERIAL PARAMETERS

Metal	Ω (10^{-23} cm)	b (10^{-8} cm)	T_M (°K)	μ_0* ($\frac{10^{11}\text{dynes}}{\text{cm}^2}$)	$\frac{1}{\mu_0}\frac{\partial\mu}{\partial T}$* ($10^{-4}$/°K)	D_{o_v}† (cm^2/sec)	Q_v† ($\frac{\text{kcal}}{\text{mole}}$)	δD_{o_B}† (cm^3/sec)	Q_B† $\frac{\text{kcal}}{\text{mole}}$
Ni	1.09	2.49	1726	7.89 (1)	3.7 (1)	1.9 (2)	68.0 (2)	3.5×10^{-9} (3)	27.4 (3)
Cu	1.18	2.56	1356	4.21 (5)	3.97 (5)	0.2 (6)	47.12 (6)	$5.0\times10^{-}$ (10)	24.8 (7)
Ag	1.71	2.89	1234	2.64 (8)	4.75 (8) 4.36 (8')	0.44 (9)	44.3 (9)	4.5×10^{-9} (10)	21.5 (10)
Al	1.66	2.86	933	2.54 (12)	5.4 (12)	1.71 (13)	34.0 (13)	5×10^{-8} (7)	20.1 (7)
Pb	3.03	3.49	600	0.732 (15)	12.64 (15)	1.37 (16)	26.1 (16)	8×10^{-8} (17)	15.7 (17)
V	1.403	2.632	2173	5.01 (18)	1.75 (19)	$\left(\frac{0.36}{214.0}\right)$	$\left(\frac{73.65}{94.14}\right)$ (20)	5×10^{-8} (7)	50. (7)
Cr	1.201	2.498	2163	12.6 (21)	2.3 (19)	0.28 (22)	73.2 (22)	5×10^{-9} (7)	46 (7)
Nb	1.798	2.86	2741	4.43 (18)	0 (7)	1.1 (24)	96.0 (24)	5×10^{-8} (7)	63 (7)
Mo	1.53	2.73	2883	13.4 (25)	1.5 (25)	0.5 (26)	96.9 (26)	5.46×10^{-8} (7)	63 (7)
Ta	1.80	2.86	3271	6.12 (18)	1.35 (27)	0.124 (28)	98.7 (28)	5.72×10^{-8} (7)	67 (7)
W	1.59	2.74	3683	16.0 (24)	1.04 (27)	5.6 (29)	140. (29)	3.33×10^{-7} (30)	92.0 (30)

	$a_c D_{o_c}$† (cm^4/sec)	Q_c† ($\frac{\text{kcal}}{\text{mole}}$)	A††	n (31)	τ_p (31) ($\frac{10^9\text{dynes}}{\text{cm}^2}$)	ΔF_k (31) (10^{-13} ergs)	ℓ (cm)
Ni	3.1×10^{-15} (4)	40.6 (4)	3.0×10^{6} §	4.6			4×10^{-6}
Cu	10^{-16} (31)	28.0 (31)	7.4×10^{5}	4.8			4×10^{-6}
Ag	2.8×10^{-16}	19.7 (11)	3.157×10^{2}	4.3			4×10^{-6}
Al	7×10^{-17} (14)	19.6 (14)	3.4×10^{6}	4.4			4×10^{-6}
Pb	10^{-14}	15.7 (7)	2.5×10^{8}	5.0			4×10^{-6}
V	10^{-15}	50. (7)	1×10^{8}	5.0	8.36	8.0	2×10^{-5}
Cr	10^{-15} (7)	46. (23)	1.3336×10^{6}	4.3	12.3	11.5	2×10^{-5}
Nb	1.3×10^{-15} (7)	63. (7)	4×10^{7}	4.4	7.35	9.0	2×10^{-5}
Mo	10^{-14} (7)	63. (7)	1.0×10^{8}	4.85	8.84	15.5	2.73×10^{-5}
Ta	10^{-15} (7)	67 (7)	7.55×10^{5}	4.2	8.02	9.5	2×10^{-5}
W	7.854×10^{-14} (30)	90.5 (30)	1.1×10^{8}	4.7	10.41	17.0	2×10^{-5}

* $\mu = \mu_0[1 - (T - 300)\frac{1}{\mu_0}\frac{\partial\mu}{\partial T}]$

† $D_v = D_{o_v}\exp(-\frac{Q_v}{RT})$; $D_B = D_{c_8}\exp(-\frac{Q_B}{RT})$; $D_c = D_{o_c}\exp(-\frac{Q_c}{RT})$

†† These values are given for the tensile stress-tensile strain-rate. For the shear equation, we use:

$$A_2 = (\sqrt{3})^{n+1}A$$

§ This value is used for Fig. 4; a slightly smaller value is used for Figs. 1, 15 and 21.

References for Table 1

1. G.A. Alers, J.R. Neighbours and H. Sato, J. Phys. Chem. Solids 13, 40 (1960).
2. K. Monma, H. Suto and H. Oikawa, J. Japan Inst. Metals 28, 188 (1964).
3. A.R. Wazzan, J. Appl. Phys. 36, 3596 (1965).
4. R.F. Canon and J.P. Stark, J. Appl. Phys. 40, 4361 (1969); 40, 4366 (1969).
5. Y.A. Chang and L. Himmel, J. Appl. Phys. 37, 3567 (1966); W.C. Overton and J. Gaffney, Phys. Rev. 98, 969 (1955).
6. A. Kuper, H. Letaw, L. Slifkin, E. Sonder and C.T. Tomizuka, Phys. Rev. 96, 1224 (1954); ibid, errata 98, 1870 (1956).
7. Estimated.
8. Y.A. Chang and L. Himmel, J. Appl. Phys. 37, 3567 (1966) (preferred value).

8'. J.R. Neighbours and G.A. Alers, Phys. Rev. 111, 707 (1958) (value used on map).

9. C.T. Tomizuka and E. Sonder, Phys. Rev. 103, 1192 (1956) taken from N.L. Peterson, Solid State Physics 22, 409 (1968).
10. R.E. Hoffman and D. Turnbull, J. Appl. Phys. 22, 634 (1951).
11. D. Turnbull and R.E. Hoffman, Acta Met. 2, 419 (1954).
12. P.M. Sutton, Phys. Rev. 91, 816 (1953); D. Lazarus, Phys. Rev. 76, 545 (1959).
13. T.S. Lundy and J.F. Murdock, J. Appl. Phys. 33, 1671 (1962).
14. R.W. Balluffi, Phys. Stat. Sol. 42, 11 (1970).
15. H.B. Huntington, Solid State Physics 7, 213 (1958).
16. H.A. Resing and N.H. Nachtrieb, J. Phys. Chem. Solids 21, 40 (1961).
17. B. Okkerse, Acta Met. 2, 551 (1954).
18. D.I. Bolef, J. Appl. Phys. 32, 100 (1961).
19. P.E. Armstrong and H.L. Brown, Trans. AIME 230, 962 (1964).
20. R.F. Peart, J. Phys. Chem. Solids 26, 1853 (1965).
21. D.I. Bolef and J. de Klerk, Phys. Rev. 129, 1063 (1963).
22. W.C. Hagel, Trans. AIME 224, 430 (1962).
23. H. Gleiter and B. Chalmers, Prog. in Mat. Sci. 16, p. 93 (1972).
24. T.S. Lundy, F.R. Winslow, R.E. Pawel and C.J. McHargue, Trans. AIME 233, 1533 (1965).
25. D.I. Bolef and J. de Klerk, J. Appl. Phys. 33, 2311 (1962).
26. J. Askill and D.H. Tomlin, Phil. Mag. 8, 997 (1963).
27. W. Koster, Z. Metallk. 39, 1 (1948).
28. R.E. Pawel and T.S. Lundy, J. Phys. Chem. Solids 26, 937 (1965).
29. S.L. Robinson and O.D. Sherby, Acta Met. 17, 109 (1969).
30. K.G. Kreider and G. Bruggeman, Trans. AIME 239, 1222 (1967).
31. Derived from comparison with experiment as described in text.

FIGURE REFERENCES

NICKEL

1) J. Weertman and P. Shahinian, Trans. AIME 206, 1223 (1956).

2) J.P. Dennison, R.J. Llewellyn and B. Wilshire, J. Inst. Met. 94, 130 (1966).

3) W.D. Jenkins, T.G. Digges and L.R. Johnson, J. Res. N.B.S. 53, 329 (1954).

4) P.W. Davies and J.P. Dennison, J. Inst. Met. 88, 471 (1959-60).

5) E.C. Norman and S.A. Duran, Acta Met. 18, 723 (1970).

6) S. Karashima, H. Oikawa and T. Motomiya, Trans. Jap. Inst. Met. 10, 205 (1969).

7) C.M. Sellars and A.G. Quarrell, J. Inst. Met. 90, 329 (1961-62).

8) W.D. Jenkins and T.G. Digges, J. Res. N.B.S. 48, 313 (1952).

9) P. Shahinian and M.R. Achter, Trans. AIME 215, 37 (1959).

10) W.M. Yim and N.J. Grant, Trans. AIME 227, 868 (1963).

11) C.R. Barrett and O.D. Sharby, Trans. AIME 233, 1116 (1965).

12) J.E. Cannaday, R.J. Austin and R.K. Saxer, Trans. AIME 236, 595 (1966).

13) M.J. Luton and C.M. Sellars, Acta Met. 17, 1033 (1969).

14) C.M. Sellars and W.J. McG. Tegart, Mem. Sci. Rev. Met. 63, 731 (1966).

15) P. Haasen, Phil. Mag. 3, 384 (1958).

16) D. Hardwick, C.M. Sellars and W.J. McG Tegart, J. Inst. Met. 90, 21 (1961-62).

17) E.R. Hayward and A.P. Greenough, J. Inst. Met. 88, 217 (1959-60).

18) G.J. Richardson, C.M. Sellars and W.J. McG. Tegart, Acta Met. 14, 1225 (1966).

19) V.M. Rozenberg, Fiz. Metal. Metalloved. 14(1), 114 (1962).

20) H.P. Stuwe, Acta Met. 13, 1337 (1965).

21) R.W. Guard, J.H. Keeler and S.F. Reiter, Trans. AIME 200, 226 (1954).

COPPER

1) D.J. Lloyd and J.D. Embury, Met. Sci. J. 4, 6 (1970).

2) C.R. Barrett and O.D. Sherby, Trans. AIME 230, 1322 (1964).

3) C.R. Barrett, J.L. Lytton and O.D. Sherby, Trans. AIME 239, 170 (1967).

4) E.C. Muehleisen, C.R. Barrett and W.D. Nix, Scripta Met. 4, 995 (1970).

5) B. Burton, Met. Sci. J. 5, 11 (1971).

6) P. Feltham and J.D. Meakin, Acta Met. 7, 614 (1959).

7) W.D. Jenkins and T.G. Digges, J. Res. N.B.S. 47, 272 (1951).

8) W.D. Jenkins and C.R. Johnson, J. Res. N.B.S. 60, 173 (1958).

9) T.E. Tietz and J.E. Dorn, Trans. AIME 206, 156 (1956).

10) J.F. Alder and V.A. Phillips, J. Inst. Met. 83, 80 (1954-55).

11) S.K. Samanta, Int. J. of Mech. Sci. 11, 433 (1969); J. Mech. Phys. Solids 19, 117 (1971).

12) G.I. Taylor and H. Quinney, Proc. Roy. Soc. A143, 307 (1933).

13) K. Schröder, A.J. Giannuzzi and G. Gorscha, Acta Met. 16, 469 (1968).

14) E.R. Gilbert and D.E. Munson, Trans. AIME 233, 429 (1965).

15) B. Burton and G.W. Greenwood, Acta Met. 18, 1237 (1970).

16) P.R. Thornton and T.E. Mitchell, Phil. Mag. 7, 361 (1962).

17) C.R. Barrett and O.D. Sherby, Trans. AIME 233, 1116 (1965).

18) R.P. Carreker, Jr. and W.R. Hibbard, Jr., Acta Met. 1, 654 (1953).

19) H.P. Stuwe, Acta Met. 13, 1337 (1965).

20) K. Monma, H. Suto and H. Oikawa, J. Japan Inst. Met. 28, 253 (1964).

21) B.Y. Pines and A.F. Sirenko, Fiz. Metal. Metalloved 15(4), 584 (1963).

22) D. Hardwick and W.J. McG. Tegart, J. Inst. Met. 90, 17 (1961-62).

23) B. Drube and H.P. Stuwe, Z. Metallkde. 58, 799 (1967).

SILVER

1) K. Schröder, A.J. Giannuzzi and G. Gorsha, Acta Met. 16, 469 (1968).

2) G.R. Leverant, F.V. Lenel and G.S. Ansell, Trans. A.S.M. 59, 890 (1966).

3) D.E. Munson and R.A. Huggins, DMS Report No. 63-4, Standord, Univ., Feb. 1963.

4) C.R. Barrett and O.D. Sherby, Trans. AIME 233, 1116 (1965).

5) R.P. Carreker, Jr., Trans. AIME 209, 112 (1957).

6) R.P. Carreker, Jr. and R.W. Guard, Report No. 55-R1-1414, General Electric Co., Schenectady, N.Y. (1955); data taken from: K.E. Amin, A.K. Mukherjee and J.E. Dorn, J. Mech. Phys. Solids 18, 413 (1970).

7) H. Suzuki and C.S. Barrett, Acta Met. 6, 156 (1958).

ALUMINUM

1) O.D. Sherby and J.E. Dorn, Trans. AIME 197, 324 (1953).

2) J.G. Harper, L.A. Shepard and J.E. Dorn, Acta Met. 6, 509 (1958).

3) I.S. Servi and N.J. Grant, Trans. AIME 191, 909 (1951).

4) J. Weertman, J. Mech. Phys. Solids 4, 230 (1956).

5) B. Burton, Phil. Mag. 27, 645 (1972).

6) C.R. Barrett, E.C. Muehleisen and W.D. Nix, Mater. Sci. Eng. 10, 33 (1972).

7) W.A. Wong and J.J. Jonas, Trans. AIME 242, 2271 (1968).

8) S.K. Samanta, Int. J. of Mech. Sci. 11, 433 (1969); J. Mech. Phys. Solids 19, 117 (1971).

9) J.F. Alder and V.A. Phillips, J. Inst. Met. 83, 80 (1954-55).

10) C.M. Sellars and W.J. McG. Tegart, Mem. Sci. Rev. Met. 63, 731 (1966).

11) J.E. Hockett, Trans. AIME 239, 969 (1967).

12) H.P. Stuwe, Acta Met. 13, 1337 (1965).

13) C.R. Barrett and O.D. Sherby, Trans. AIME 233, 1116 (1965).

14) G.V. Vladimirova, V.A. Likhachev, M.M. Myshlyayev, and S.S. Olevskiy, Fiz. Metal. Metalloved. 31(1), 177 (1971).

15) J.R. Cotner and W.J. McG. Tegart, J. Inst. Met. 97, 73 (1969).

16) O.D. Sherby, T.A. Trozera and J.E. Dorn, Proc. ASTM 56, 789 (1956).

17) O.D. Sherby, J.L. Lytton and J.E. Dorn, Acta Met. 5, 219 (1957).

18) D. Hardwick and W.J. McG. Tegart, J. Inst. Met. 90, 17 (1961-62).

19) R.P. Carreker, Jr. and W.R. Hibbard, Jr., Trans. AIME 209, 1157 (1957)

20) U.F. Kocks, Met. Trans. 1, 1121 (1970).

LEAD

1) J. Weertman, Trans. AIME 218, 207 (1960).

2) K. Hanffstengel and H. Hanemann, Z. Metallk. 30, 41 (1938).

3) A.A. Smith, Trans. AIME 143, 165 (1941).

4) P. Feltham, Proc. Phys. Soc. (B) 69, 1173 (1956).

5) R.C. Gifkins, J. Inst. Met. 81, 417 (1952-53); Trans. AIME 215, 1015 (1959).

6. J.H. Nicholls and P.G. McCormick, Met. Trans. 1, 3469 (1970).

7) C.D. Michalopoulos and F.R. Brotzen, J. Inst. Met. 96, 156 (1968).

8) V.A. Stepanov and V.V. Shpeyzman, Fiz. Metal. Metalloved. 29(2), 375 (1970).

9) J. McKeown, J. Inst. Met. 60, 201 (1937).

10) C.D. Wiseman, O.D. Sherby, and J.E. Dorn, Trans. AIME 209, 57 (1957).

11) F.A. Mohamed, K.L. Murty and J.W. Morris, Jr., Met. Trans. 4, 935 (1973).

12) E.N. da C. Andrade and K.H. Jolliffe, Proc. Roy. Soc. (A) 254, 291 (1960).

VANADIUM

1) K.R. Wheeler, E.R. Gilbert, F.L. Yaggee, and S.A. Duran, Acta Met. 19, 21 (1971).

2) C.T. Wang and D.W. Bainbridge, Met. Trans. 3, 3161 (1972).

3) W.R. Clough and A.S. Pavlovic, Trans. ASM 52, 948 (1960).

4) T.E. Mitchell, R.J. Fields and R.L. Smialek, J. Less-Common Metals 20, 167 (1970).

CHROMIUM

1) J.R. Stepehens and W.D. Klopp, J. Less-Common Metals 27, 87 (1972).

2) C.S. Landau, H.T. Greenaway and A.R. Edwards, J. Inst. Met. 89, 97 (1960-61).

3) J.W. Pugh, Trans. ASM 50, 1072 (1958).

4) M.J. Marcinkowski and H.A. Lipsitt, Acta Met. 10, 95 (1962).

NIOBIUM

1) G. Brinson and B.B. Argent, J. Inst. Met. 91, 293 (1962-63).

2) E.L. Francis, UKAEA Reprot IGR R/R 304, Risley, Library and Information Dept., Warrington, Lancashire, 1958.

3) R.T. Begley, WADC TR-57-344, Part II, Dec. 1958.

4) D.J. Maykuth and R.I. Jaffee, Columbium Metallurgy, Proc. of AIME Symposium, Bolton Landing, N.Y., June 9-10, 1960; Interscience Publishers, pp. 223-256, N.Y. (1961).

5) D.P. Gregory and G.H. Rowe, Ibid, pp. 309-340.

6) T.L. Briggs and J.D. Campbell, Acta Met. 20, 711 (1972).

7) E.T. Wessel, LL. France, and R.T. Begley, Columbium Metallurgy, op. cit., pp. 459-502.

8) E.A. Abramyan, L.I. Ivanov and V.A. Yanushkevich, Fiz. Metal. Metalloved 28(3), 496 (1969).

9) R.R. Vandervoort, Trans. AIME 245, 2269 (1969).

10) J. Stoop and P. Shahinian, High Temperature Refractory Metals, Part 2, AIME Symposium, Gordon and Breach Science Publishers, N.Y. pp. 407-432 (1966).

MOLYBDENUM

1) J.W. Pugh, Trans. ASM 47, 984 (1955).

2) J.B. Conway and P.N. Flagella, 'Seventh Annual Report - AEC Fuels and Materials Development Program', GE - NMPO, GEMP - 1004, March 29, 1968; also, Creep Rupture Data for the Refractory Metals to High Temperatures, Gordon and Breach, p. 610-612 (1971).

3) M. Semchyshen and R.Q. Barr, Summary Report NR 039-002 to Office of Naval Research, Climax Molybdenum Co. (1955).

4) H. Carvalhinhos and B.B. Argent, J. Inst. Met. 95, 364 (1967).

5) W.V. Green, M.C. Smith and D.M. Olson, Trans. AIME 215, 1061 (1959).

6) T.L. Briggs and J.D. Campbell, Acta Met. 20, 711 (1972).

7) G.A. Alers, R.W. Armstrong and J.H. Bechtold, Trans. AIME 212, 523 (1958).

8) A. Lawley, J. Van den Sype and R. Maddin, J. Inst. Met. 91, 23 (1962-63).

TANTALUM

1) W.V. Green, Trans. AIME 233, 1818 (1965).

2) R.L. Stephenson, Technical Report ORNL-TM-1994, Dec. 1967.

3) F.F. Schmidt, W.D. Klopp, W.M. Albrecht, F.L. Holden, H.R. Ogden and R.I. Jaffee, Battelle Memorial Inst. Report WADD TR 59-13, March 1960.

4) D.C. Drennan, M.E. Lanston, C.J. Slunder and J.G. Dunleavy, BMI Rept. 1326, Battelle Memorial Inst., March 2, 1959.

5) J.B. Preston, W.P. Roe and J.R. Kattus, Tech. Report, Southern Research Inst., WADC TR 57-649, Part I, Jan. 1958.

6) T.E. Mitchell and W.A. Spitzig, Acta Met. 13, 1169 (1965).

7) J.H. Bechtold, Acta Met. 3, 249 (1955).

8) J.W. Pugh, Trans. ASM 48, 677 (1966).

9) R.R. Vandervoort, Trans. AIME 245, 2269 (1969).

10) E.T. Wessel, as reported by J.H. Bechtold, E.T. Wessel and L.L. France in Refractory Metals and Alloys, edited by M. Semchyshen and J.J. Harwood, AIME, p. 49 (1961).

TUNGSTEN

1) E.R. Gilbert, J.E. Flinn and F.L. Yaggee, paper presented at the Fourth Syoposium on Refractory Metals, The Met. Soc. of AIME, Oct. 3-5, 1965.

2) P.N. Flagella, GE-NMPO, GEMP-543, Aug. 31, 1967, presented at Third International Symposium - High Temperature Technology, Asilomar, Calif., Sept. 1967.

3) W.V. Green, Trans. AIME 215, 1057 (1959).

4) G.W. King, Westinghouse Report BLR # 90284-2, Sept. 14, 1970.

5) D.M. Moon and R. Stickler, Phil. Mag. 24, 1087 (1971).

6) W.D. Klopp, W.R. Witzke and P.L. RAffo, Trans. AIME 233, 1860 (1965).

7) P.L. Raffo, J. Less-Common Metals 17, 133 (1969).

8) G.W. King and H.G. Sell, Trans. AIME 233, 1104 (1965).

9) J.L. Taylor and D.H. Boone, Trans. ASM 56, 643 (1963).

10) J.W. Pugh, Proc. ASTM 57, 906 (1957).

11) A.S. Argon and S.R. Maloof, Acta Met. 14, 1449 (1966).

12) R.C. Koo, Acta Met. 11, 1083 (1963).

References

1. E.A. Abramyan, L.I. Ivanov and V.A. Yanushkevich, Fiz. Metal. Metalloved 28(3), 496 (1969).
2. J.F. Alder and V.A. Phillips, J. Inst. Met. 83, 80 (1954-55).
3. A.S. Argon and S.R. Maloof, Acta Met. 14, 1449 (1966).
4. A.S. Argon, Scripta Met. 4, 1001 (1970).
5. P.E. Armstrong, J.M. Dickinson and H.L. Brown, Trans. AIME 236, 1404 (1966).
6. M.F. Ashby, Scripta Met. 3, 837 (1969).
7. M.F. Ashby, Acta Met. 20, 887 (1972a).
8. M.F. Ashby, Surface Science 31, 498 (1972b).
9. R.W. Balluffi, Phys. Stat. Sol. 42, 11 (1970).
10. C.R. Barrett and O.D. Sherby, Trans. AIME 230, 1322 (1964).
11. C.R. Barrett and O.D. Sherby, Trans. AIME 233, 1116 (1965).
12. J.E. Bechtold, E.T. Wessel and L.L. France, in Refractory Metals and Alloys, edited by M. Semchyshen and J.J. Harwood, AIME, pp. 25-81 (1961).
13. J.E. Bird, A.K. Mukherjee and J.E. Dorn, in Quantitative Relation between Properties and Microstructure, Israel Univ. Press, Jerusalem, pp. 255-342
14. G.F. Bolling and R.H. Richman, Acta Met. 13, 709, 723 (1965).
15. T.L. Briggs and J.D. Campbell, Acta Met. 20, 711 (1972).
16. G. Brinson and B.B. Argent, J. Inst. Met. 91, 293 (1962-63).
17. R.P. Carreker, Jr. and R.W. Guard, Report No. 55-R1-1414, General Electric Co., Schenectady, N.Y. (1955).
18. H. Carvalhinos and B.B. Argent, J. Inst. Met. 95, 364 (1967).
19. R.L. Coble, J. Appl. Phys. 34, 1679 (1963).
20. J.B. Conway and P.N. Flagella, 'Seventh Annual Report - AEC Fuels and Materials Development Program', GE-NMPO, GEMP-1004 (March 29, 1968).
21. B. de Meester, C. Yin, M. Doner and H. Conrad in "Rate Processes in Plastic Deformation", eds: J.C.M. Li and A.K. Mukherjee, A.S.M. (1973).
22. A.G. Evans and R.D. Rawlings, Phys. Stat. Sol. 34, 9 (1969).
23. P. Feltham, Proc. Phys. Soc. (B) 69, 1173 (1956).
24. P. Feltham and J.D. Meakin, Acta Met. 7, 614 (1959).
25. P.N. Flagella, GE-NMPO, GEMP-543, (Aug. 31, 1967), presented at Third International Symposium - High Temperature Technology, Asilomar
26. J.E. Flinn and E.R. Gilbert, Trans. AIME 236, 1512 (1966).
27. H.J. Frost and M.F. Ashby, J. Appl. Phys. 42, 5273 (1971).
28. G.B. Gibbs, Mem. Sci. Rev. Met. 62, 781 (1965).
29. R.C. Gifkins, J. Inst. Met. 81, 417 (1952-53); Trans. AIME 215, 1015 (1959).

30. E.R. Gilbert, J.E. Flinn and F.L. Yaggee, paper presented at the Fourth Symposium on Refractory Metals, The Met. Soc. of AIME (Oct. 3-5, 1965).

31. W.V. Green, M.C. Smith and D.M. Olson, Trans. AIME 215, 1061 (1959).

32. W.V. Green, Trans. AIME 215, 1057 (1959).

33. W.V. Green, Trans. AIME 233, 1818 (1965).

34. P. Guyot and J.E. Dorn, Can. J. Phys. 45, 983 (1967).

35. J.G. Harper and J.E. Dorn, Acta Met. 5, 654 (1957).

36. J.G. Harper, L.A. Shepard and J.E. Dorn, Acta Met. 6, 509 (1958).

37. E.W. Hart, Acta Met. 5, 597 (1957).

38. C. Herring, J. Appl. Phys. 21, 437 (1950).

39. J.P. Hirth and J. Lothe, Theory of Dislocations, McGraw Hill (1968).

40. K.M. Jassby and T. Vreeland, Phil. Mag. 21, 1147 (1970).

41. J.J. Jonas, C.M. Sellars and W.J. McG. Tegart, Met. Rev. 14, 1 (1969).

42. A. Kelly, Strong Solids, Oxford University Press (1966).

43. G.W. King and H.G. Sell, Trans. AIME 233, 1104 (1965).

44. D. Klahn, A.K. Mukherjee and J.E. Dorn, Second International Conference on the Strength of Metals and Alloys, ASM, p. 951, Asilomar, Calif. (1970).

45. U.F. Kocks, Met. Trans. 1, 1121 (1970).

46. U.F. Kocks, A.S. Argon and M.F. Ashby, to appear in Progress in Materials Science (1974).

47. R.C. Koo, Acta Met. 11, 1083 (1963).

48. A. Kumar, F.E. Hauser and J.E. Dorn, Acta Met. 16, 1189 (1968).

49. A. Kumar and R.G. Kumble, J. Appl. Phys. 40, 3475 (1969).

50. A. Lawley, J. Van den Sype and R. Maddin, J. Inst. Met. 91, 23 (1962-63).

51. G.R. Leverant, F.V. Lenel and G.S. Ansell, Trans. A.S.M. 59, 890 (1966).

52. L.M. Lifshitz, Soviet Phys. JETP 17, 909 (1963).

53. T. S. Lundy and J.F. Murdock, J. Appl. Phys. 33, 1671 (1962).

54. J.K. MacKenzie, Ph.D. Thesis, Bristol University (1959).

55. M.J. Marcinkowski and H.A. Lipsitt, Acta Met. 10, 95 (1962).

56. T.E. Mitchell, R.J. Fields and R.L. Smialek, J. Less-Common Metals 20, 167 (1970).

57. T.E. Mitchell and W.A. Spitzig, Acta Met. 13, 1169 (1965).

58. F.A. Mohamed, K.L. Murty and J.W. Morris, Jr., paper presented at John E. Dorn Memorial Sumposium, Cleveland, Ohio (Oct. 1972).

59. A.K. Mukherjee, J.E. Bird and J.E. Dorn, Trans. ASM 62, 155 (1969).

60. F.R.N. Nabarro, Report on a Conference on the Strength of Metals (Phys. Soc. London 1948).

61. J.H. Nichols and P.G. McCormick, Met. Trans. 1, 3469 (1970).

62. R.E. Pawel and T.S. Lundy, J. Phys. Chem. Solids 26, 937 (1965).

63. J.W. Pugh, Trans. ASM 47, 984 (1955).

64. P.L. Raffo, J. Less-Common Metals 17, 133 (1969).

65. R.Raj and M.F. Ashby, Met. Trans. 2, 1113 (1971).

66. H.A. Resing and N.H. Nachtrieb, J. Phys. Chem. Solids 21, 40 (1961).

67. S.L. Robinson and O.D. Sherby, Acta Met. 17, 109 (1969).

68. S.K. Samanta, Int. J. of Mech. Sci. 11, 433 (1969).

69. S.K. Samanta, J. Mech. Phys. Solids 19, 117 (1970).

70. F.F. Schmidt, W.D. Klopp, W.M. Albrecht, R.L. Holden, H.R. Ogden and R.I. Jaffee, Battelle Memorial Inst. Report WADD TR 59-13 (March 1960).

71. K. Schröder, A.J. Giannuzzi and G. Gorscha, Acta Met. 16, 469 (1968).

72. C.M. Sellars and W.J. McG. Tegart, Mem. Sci. Rev. Met. 63, 731 (1966).

73. M. Semchyshen and R.Q. Barr, Summary Report NR 039-002 to Office of Naval Research, Climax Molybdenum Co. (1955).

74. I.S. Servi and N.J. Grant, Trans. AIME 191, 909 (1951).

75. J.R. Stephens and W.D. Klopp, J. Less-Common Metals 27, 87 (1972).

76. R.L. Stocker and M.F. Ashby, Scripta Met. 7, 115 (1973).

77. J. Stoop and P. Shahinian, High Temperature Refractory Metals, Part 2, AIME sypposium, Gordon and Breach Science Publishers, N.Y., pp. 407-432 (1966).

78. D. Turnbull and R.E. Hoffman, Acta Met. 2, 419 (1954).

79. W.R. Tyson, Phil. Mag. 14, 925 (1966).

80. R.R. Vandervoort, Met. Trans. 1, 857 (1970).

81. C.T. Wang and D.W. Bainbridge, Met. Trans. 3, 3161 (1972).

82. J. Weertman, J. Mech. Phys. Solids 4, 230 (1956).

83. J. Weertman, Trans. AIME 218, 207 (1960).

84. J. Weertman, Trans. AIME 227, 1475 (1963).

85. E.T. Wessel, as reported by J.H. Bechtold, E.T. Wessel and L.L. France in Refractory Metals and Alloys, edited by M. Semchyshen and J.J. Harwood, AIME, p. 49 (1961).

86. K.R. Wheeler, E.R. Gilbert, F.L. Yaggee and S.A. Duran, Acta Met 19, 21 (1971).

87. B.A. Wilcox and A.H. Claver, Met. Sci. J. 3, 26 (1969).

88. B.A. Wilcox and A.H. Claver, Met. Sci. J. 3, 26 (1969).